Supplementary Materials for

High-throughput pathological markers for prognosis and molecular signatures based on pan-cancer tissue atlases

Yiping Jiao[*,1], Cong Xia[2], Chengfei Cai[3,1], Yacong Guo[4], Junhong Li[5],

Welong Ming[1], Xiangxue Wang[1], Shanshan Hong[1], Jun Xu[*,1]

Contents

Section 1 Pan-cancer tissue segmentation 2

1.1 Dataset and model training 2

1.2 TCGA internal validation 6

1.3 External validations 10

1.3.1 Tumor stroma segmentation in breast cancer 10

1.3.2 Comparison with pan-cancer TIL map 13

1.3.3 Comparison with CRCM 17

1.3.4 Independent validation in pancreas cancer dataset 18

Section 2 Generating tumor likelihood map 21

2.1 BRCA, COAD, STAD, UCEC and OV 21

2.2 PAAD 25

2.3 LUAD and LUSC 27

Section 3 Tissue feature analyses 28

3.1 Generating and quality control of tissue and tumor maps 28

3.2 Tissue feature definition 30

3.3 Survival analysis of tissue features 33

3.4 Correlation with molecular features 44

3.4.1 Spearman correlation 44

3.4.2 Mann-Whitney U Test for immune subtypes 47

3.4.3 Predict molecular feature by tissue features 52

References 55

SECTION 1 PAN-CANCER TISSUE SEGMENTATION

1.1 DATASET AND MODEL TRAINING

In order to establish a semantic segmentation model capable of identifying multiple tissue types, we extracted a total of 669 regions of interest (ROIs) from five TCGA (The Cancer Genome Atlas) cohorts, namely BRCA, LUAD, LUSC, PAAD, and STAD. The average area of these ROIs was 1.991mm^2 (std = 1.125mm^2). These ROIs were saved in TIF format at a fixed resolution of 0.5μm/pixel for ease of viewing. We defined a total of 15 categories, including Background, Lymphocytes, Necrosis, Adipose, Fiber, Muscle, Nerves, Alveolar, Cartilage, Blood cells, Micro-vessels, Mucus or sediment, Carbon, Epithelial-like tissue, and Artifacts. These categories cover the majority of situations encountered in real-world pathological sections of corresponding tumor types. The annotation of these ROIs was completed using the Automated Slide Analysis Platform (ASAP) software (https://computationalpathologygroup.github.io/ASAP/) and saved in XML format. We completed annotations for over 10,000 polygons. Some examples of the patches are shown in Figure S1-1.

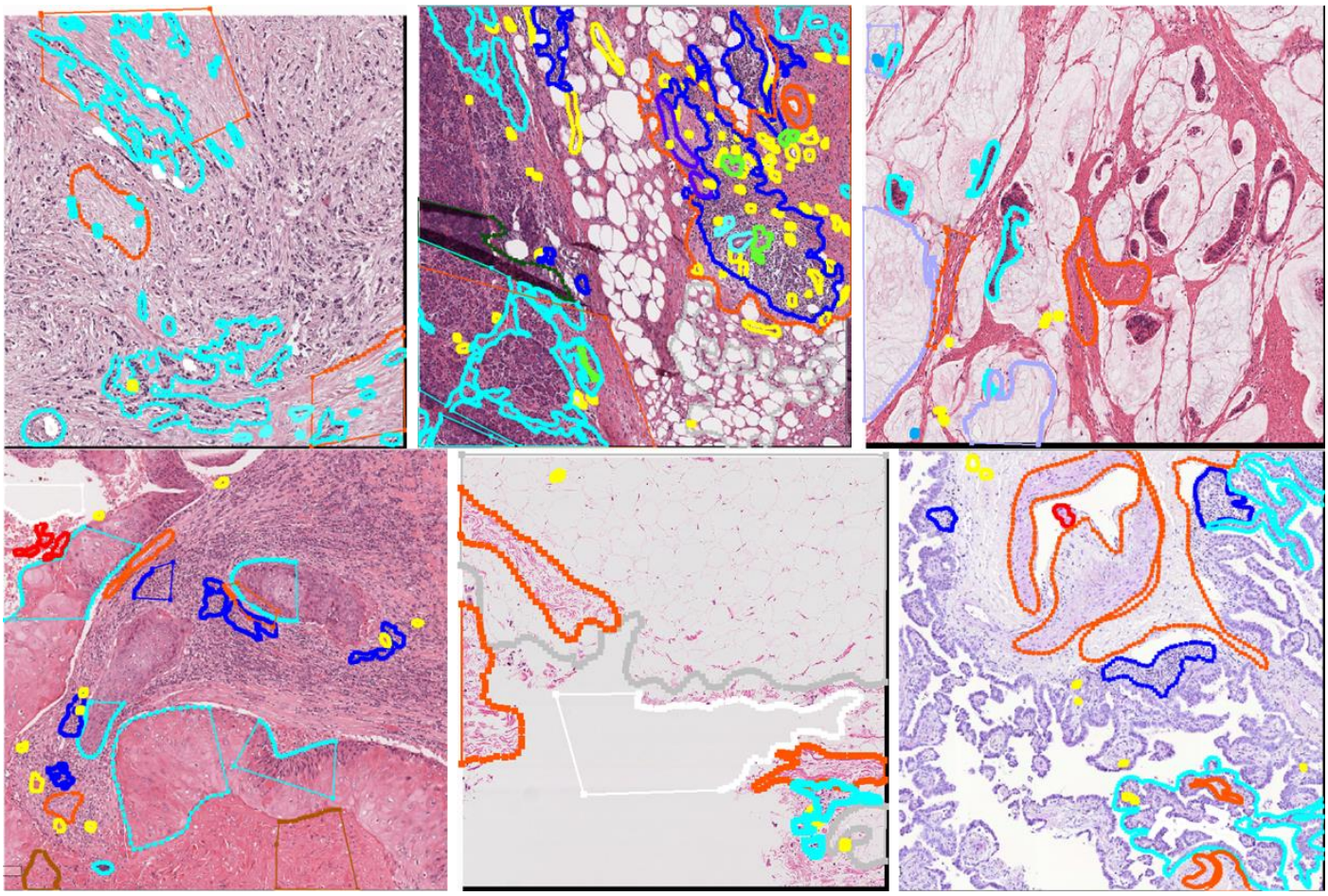

Figure S1-1. Examples of ROIs and annotations. The main categories depicted in the figure include epithelial-like tissue (in cyan), stroma (in orange), immune infiltration (in blue), and micro-vessels (in yellow).

After the annotation phase, the XML files were converted into TIF masks using the Python interface of ASAP (multiresolutionimageinterface, mir[1]). The source of ROI and pixel-level mask information is summarized in Table S1-1. The ROIs were then aligned with masked, and jointly cropped into patches for model training and validation. Specifically, we utilized a sliding window approach to extract 512x512 pixel patches from tissue images and masks with a stride of 448 pixels. Overlapping sampling was employed to avoid insufficient training of pixels located at the edges. A total of 17,159 patches were generated through image cropping, which were subsequently randomly divided into training and validation sets at a ratio of 7:3.

Table S1-1. Training data for the tissue segmentation model.

n_patient		121	96	71	78	25	391
n_ROI		182	164	107	182	34	669
Class		**BRCA**	**LUAD**	**LUSC**	**PAAD**	**STAD**	**Σ**
Backg	Area (pixel)	22080723	18571152	18771500	21604650	6476438	87504463
	Count	330	495	125	571	24	1545
Lymph	Area (pixel)	10619386	22159854	6143948	10307564	1088307	50319059
	Count	785	802	336	532	129	2584
Necro	Area (pixel)	6776984	10762868	6728587	3387531	349015	28004985
	Count	55	178	110	119	18	480
Adipo	Area (pixel)	35795882	188031	621741	11837724	-	48443378
	Count	117	2	2	35	-	156
Fiber	Area (pixel)	86623736	69172245	25989908	159070018	7118849	347974756
	Count	839	792	298	622	96	2647
Muscl	Area (pixel)	2465125	6167099	3450627	46769980	17291799	76144630
	Count	33	44	41	234	66	418
Nerve	Area (pixel)	186746	479706	1431690	10057681	366331	12522154
	Count	4	14	15	196	13	242
Alveo	Area (pixel)	-	23489026	17796638	-	-	41285664
	Count	-	149	104	-	-	253
Cartl	Area (pixel)	-	6269759	26639151	-	-	32908910
	Count	-	4	17	-	-	21
Blood	Area (pixel)	2113942	3057825	1325690	778671	83481	7359609
	Count	172	233	125	72	7	609
Micve	Area (pixel)	4142034	4901501	1787571	4927921	947427	16706454
	Count	1668	1703	638	1580	363	5952
Mucus	Area (pixel)	3886231	10726853	1658772	2080745	1109432	19462033
	Count	96	342	76	162	40	716
Carbo	Area (pixel)	904049	613056	137992	147184	371	1802652
	Count	20	162	82	19	1	284
Epith	Area (pixel)	91143971	73857068	33649196	88524205	9151049	296325489
	Count	1517	1560	678	1288	358	5401
Artfc	Area (pixel)	10815243	921225	22824109	5885755	4503016	44949348
	Count	65	71	44	48	13	241

The generated patches were used to train a semantic segmentation model that can recognize 15 different types of tissue or region. The model is a U-Net[2] with a VGG-19[3] encoding branch, the setting allowed us to leverage the prior knowledge obtained from natural images using transfer learning. Due to the difference in the channel number between VGG and the original U-Net, we adjusted the channels in the decoder pathway accordingly. Additionally, a lightweight coordinate attention mechanism [4] was introduced in the skip connections. The output size of the model is (H, W, 15), corresponding to the probability likelihood of the 15 different categories in pixel-level. During training, the input size of the model was set to H=W=480 pixels, which is slightly smaller than raw sample size (512 pixel). This introduces more translational diversity through random cropping. Mild color augmentation[5] was also introduced to improve model generalization. The batch size was set as 4, which can be trained in commonly available GPU like 1080Ti using Pytorch framework (https://pytorch.org/).

The loss function is a 1:1 mixture of cross-entropy and dice loss. The losses were aggregated per class first, enabling being weighted inversely of pixel count to deal with class imbalance. During the first 5 epochs of training, the VGG backbone is frozen, and only the decoding pathway and segmentation task head are trained. This may help to stabilize the backbone, and free from being affected by random initialization of the head layers[6]. We use an Adam optimizer[7] with an initial learning rate of 1e-5. The learning rate is multiplied by 0.9 every 10 epochs after 60 epochs. The training stops after 160 epochs. We record the loss and average dice score on both the training and validation sets every epoch and save the model weights with the lowest validation set loss for subsequent analysis. The changes in the loss, overall dice, and dice for each class in the training and validation sets are shown in Figure S2 and Figure S3. We did not observe overfitting phenomena of the validation loss, which may be due to the fact that the training set and validation set are homogenous at the slide level. We have set up independent test sets and external test sets, so we did not use separately validation set. This can avoid inappropriate termination of training due to domain shift between the training set and validation set. It can be seen that the validation dice for most classes can exceed 0.8, while the small vessels are a more challenging, with a dice score exceeding 0.6 in the later stages of training.

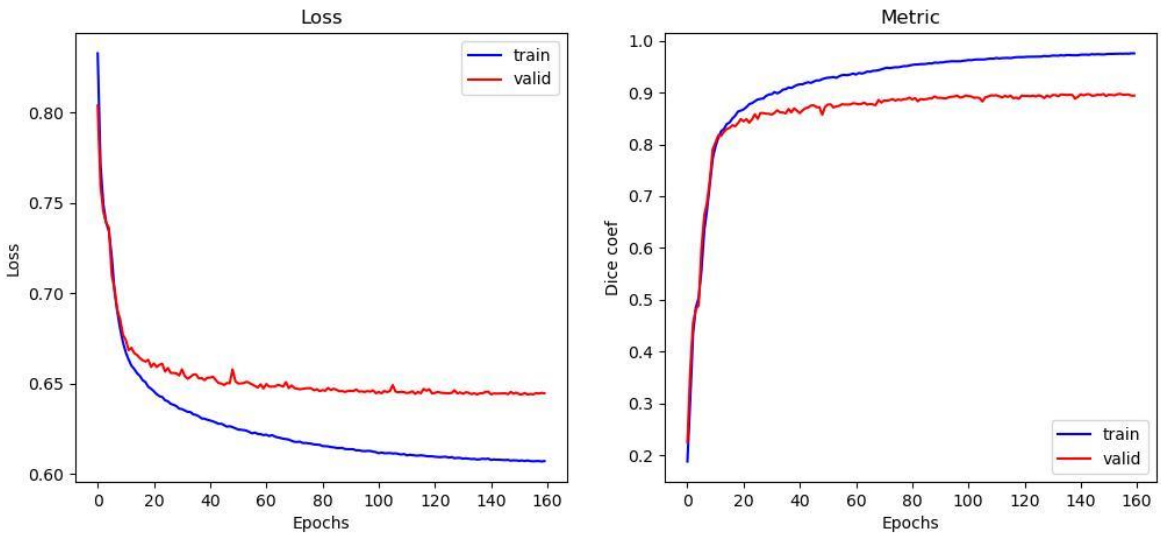

Figure S1-2. Overall training loss and dice coefficient.

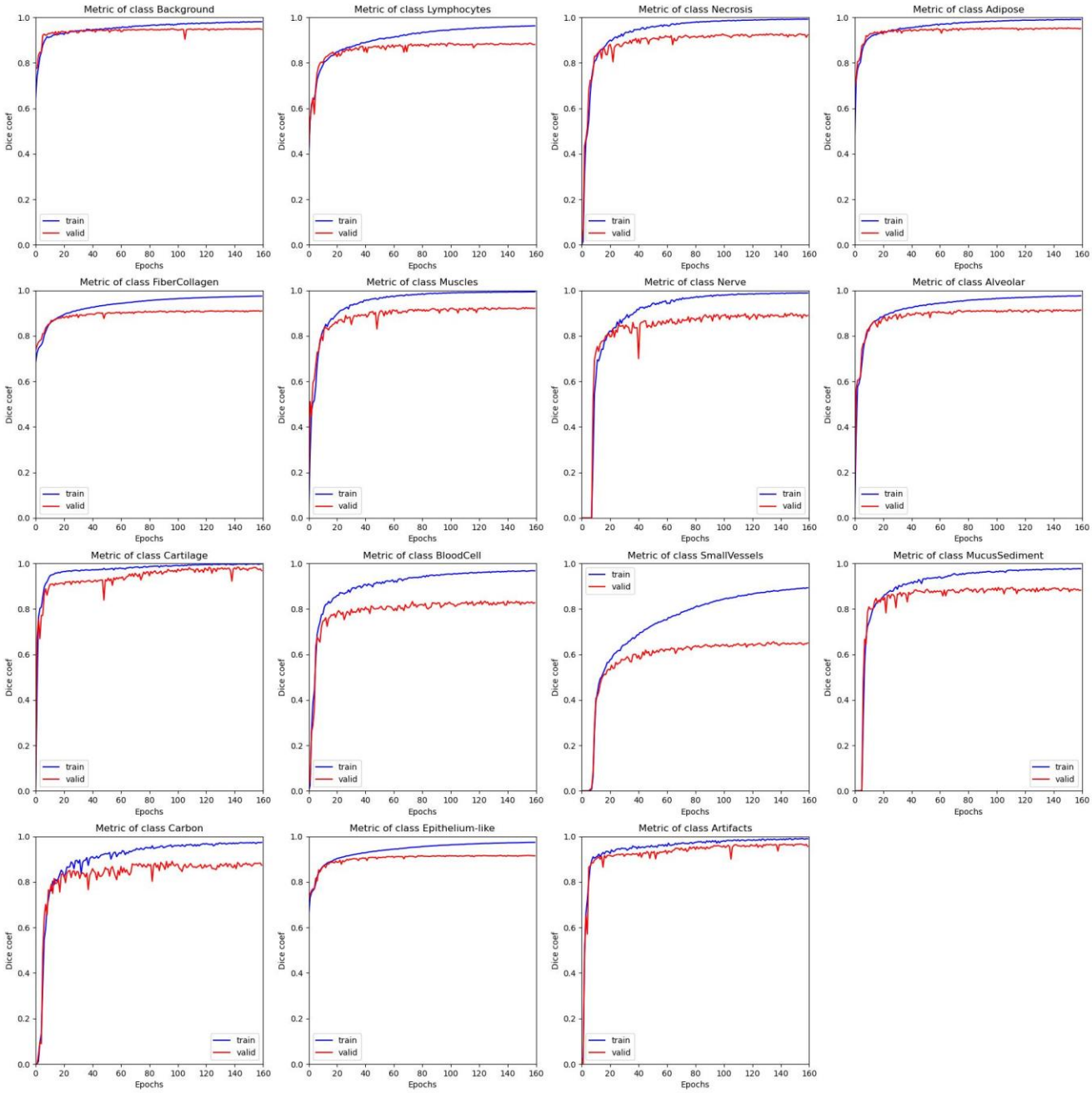

Figure S1-3. Training and validation dice of each class. The subfigures are arranged with the order of 'Background', 'Lymphocytes', 'Necrosis', 'Adipose', 'FiberCollagen', 'Muscles', 'Nerve', 'Alveolar', 'Cartilage', 'BloodCell', 'SmallVessels', 'MucusSediment', 'Carbon', 'Epithelium-like', and 'Artifacts', from top to bottom and left to right.

1.2 TCGA INTERNAL VALIDATION

To validate the performance of the model, we selected 5 slides from each of the BRCA, COAD, LUAD, LUSC, PAAD, STAD, and UCEC cohorts. A representative region was chosen for each slide, resulting 35 regions of interest (ROI) with an average area of 2.069mm^2. It is worth noting that the 35 patients involved in this phase were not present in the training set to avoid potential data leakage. Subsequently, these annotations were converted into masks, following the similar process as described previously. Once this step was completed, we will able to compare it with model predictions. The pixel counts for each label in the masks, as well as the number of annotated regions, are shown in Table S1-2. The quantified model performance are presented in Table S1-3, Figure S1-4, and Figure S1-5.

Table S1-2. Annotated data of the internal test set of TCGA

Class	Area (pixels)	Count
Backg	3396355	79
Lymph	9373037	167
Necro	4406930	92
Adipo	2927732	14
Fiber	66678954	182
Muscl	6988922	27
Nerve	697036	22
Alveo	3844726	4
Cartl	4400132	3
Blood	473153	52
Micve	1590004	845
Mucus	3001042	61
Carbo	94921	15
Epith	63299107	1021
Artfc	705591	8
Sum	171877642	2592

Table S1-3. Model performance per cohort on the internal test set of TCGA.

Cohort	Accuracy	Precision	Recall	Specificity	F1	Jaccard
BRCA	0.698	0.465	0.704	0.958	0.513	0.394
COAD	0.631	0.456	0.687	0.957	0.504	0.384
LUAD	0.440	0.304	0.757	0.956	0.385	0.281
LUSC	0.351	0.302	0.783	0.945	0.397	0.280
PAAD	0.656	0.401	0.805	0.960	0.494	0.361
STAD	0.282	0.248	0.827	0.936	0.355	0.237
UCEC	0.423	0.401	0.698	0.935	0.480	0.355
All	0.499	0.383	0.805	0.961	0.496	0.352

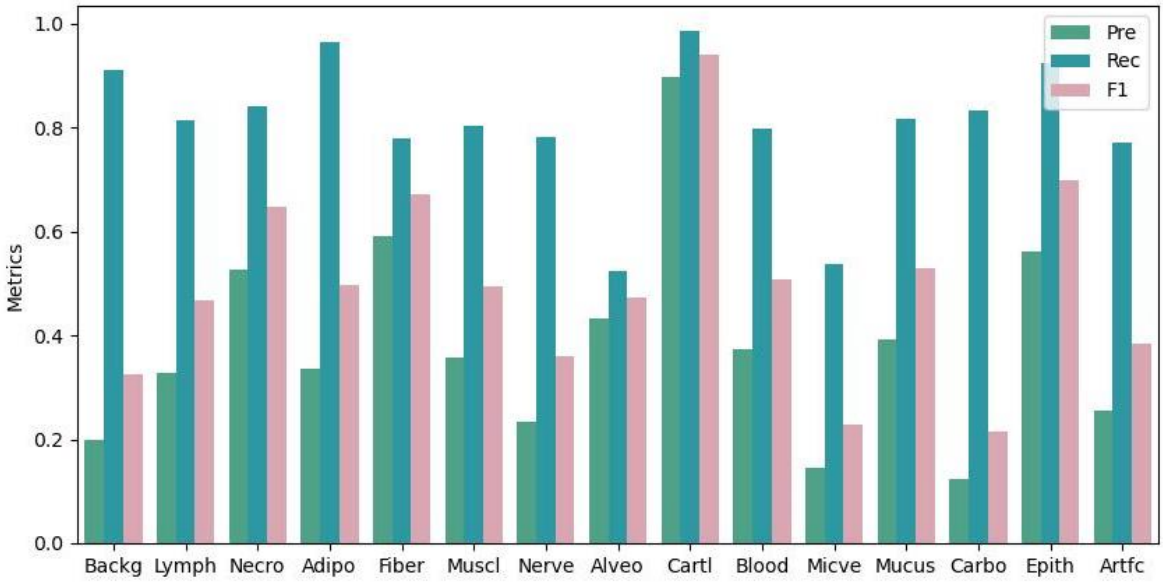

Figure 1-4. Performance of each class on the internal test set of TCGA

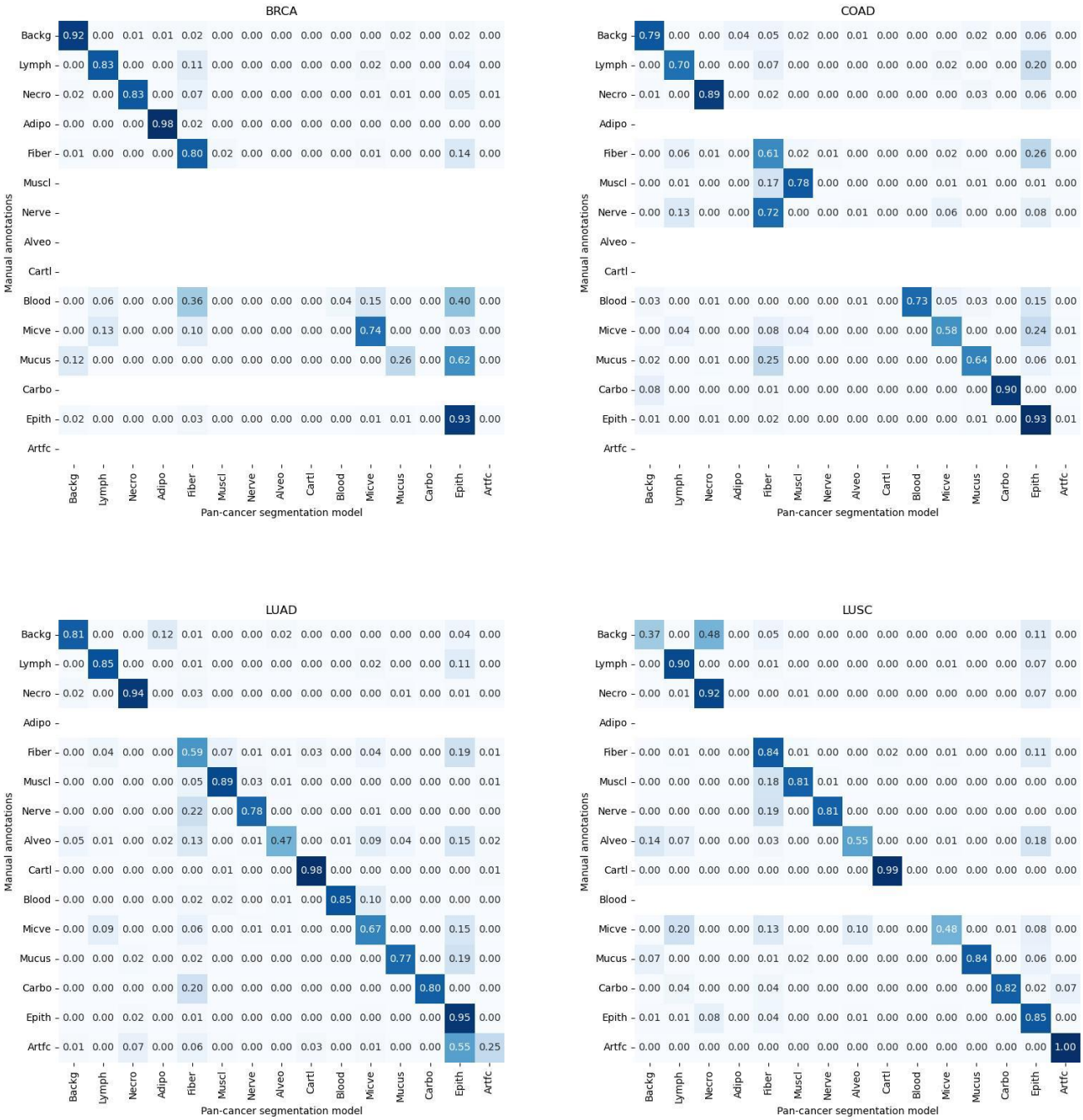

Figure S1-5. Confusion matrices for each cohort in internal TCGA test set. The category labels, in the order from top to bottom and left to right, are Background, Lymphocytes, Necrosis, Adipose, Fiber, Muscle, Nerves, Alveolar, Cartilage, Blood cells, Micro-vessels, Mucus or sediment, Carbon, Epithelial-like tissue, and Artifacts. Please note that some categories may not appear in specific cohorts, in which case the corresponding row in the confusion matrix will be blank.

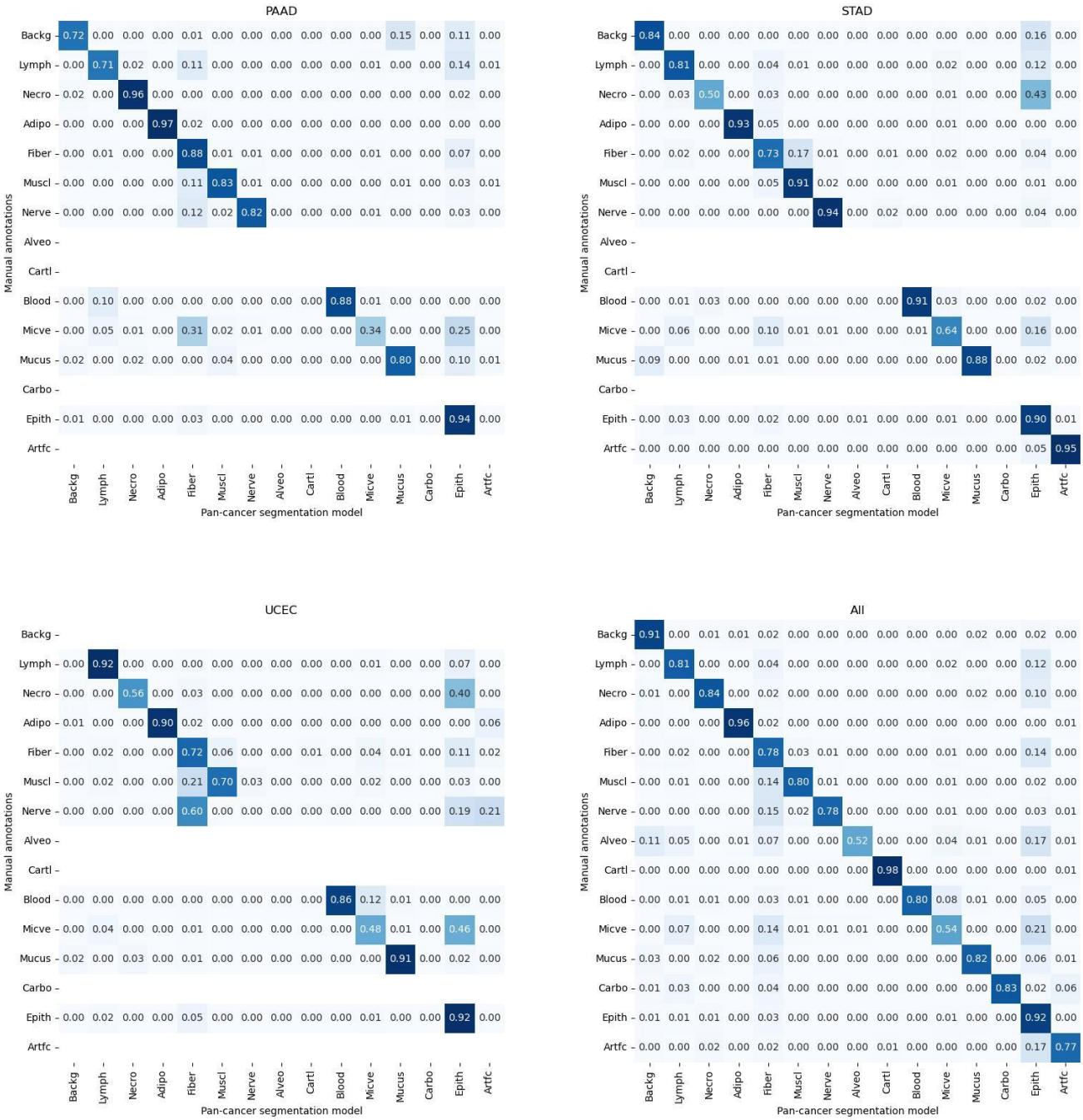

Figure S1-5. *(Continue)*

1.3 External validations

1.3.1 Tumor stroma segmentation in breast cancer

We obtained data from a previous work[8], which was used to train an epithelial-stromal classifier (ZIP file of "Epithelial-stromal classifier training images", available at https://tma.im/tma_portal/C-Path/supp.html). The data set contains 214 and 102 images from the so named NKI cohort and VGH cohort, respectively, corresponding to a total of 158 pairs of tissue images and masks. We manually inspected the samples and found one unmatched tissue image and mask (0.2_111_1_11.jpg and 2_111_1_11.jpg). For the remaining 157 pairs of samples, we determined the red (epithelial) and green (stromal) regions in the original masks using a simple RGB color threshold. There was an inconspicuous text box in the lower right corner of the mask image, which we also removed to avoid affecting subsequent analysis.

The pixel spacing of an image determines how the image should be scaled before being processed by a model; however, the information was not reported in the literature and dataset webpage. Therefore, we analyzed these TMA images using an in-house regression model trained on multiple TCGA cohorts with different resolutions. The results showed that the resolution of these images is likely to be between 0.475 and 0.525 (Figure S1-6), which is consistent with the estimation of pathologists. Therefore, we set a resolution of 0.5 μm/pixel for these images and applied our tissue segmentation model. Due to the differences in category setting, we categorized all non-epithelial-like class as 'stroma', and only considered the regions involved in the ground-truth annotations for quantitative metrics. The average F1-score can reach 0.846 in average (Table S1-4). Based on visual inspections, our model tends to include slightly more surrounding areas in the epithelial category, and misclassification is mainly due to factors such as isolated epithelial cells. Examples of predicted and misclassified samples of the tissue segmentation model are shown in Figure S1-7 and Figure S1-8, respectively.

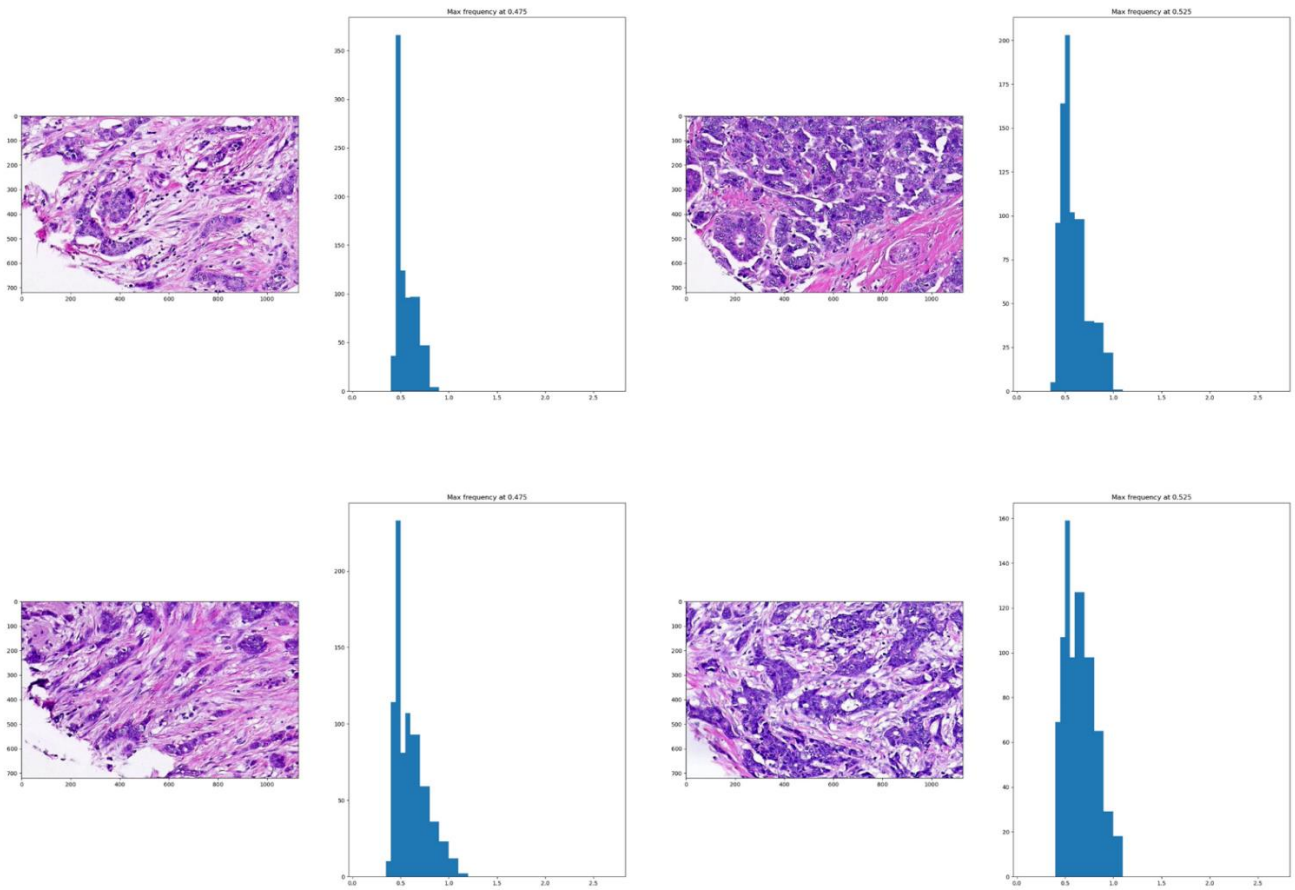

Figure S1-6. Estimating the pixel spacing of the breast epithelium-stroma segmentation dataset. TMA images are shown in the left, and the histogram of estimated pixel spading in slide-window manner are shown in the right.

Table S1-4. The performance on breast epithelium-stroma segmentation dataset.

Class	Accuracy	Precision	Recall	Specificity	F1	Jaccard
Stroma		0.864	0.811	0.811	0.837	0.719
Tumor	0.847	0.833	0.881	0.881	0.856	0.748
Average		0.848	0.846	0.846	0.846	0.734

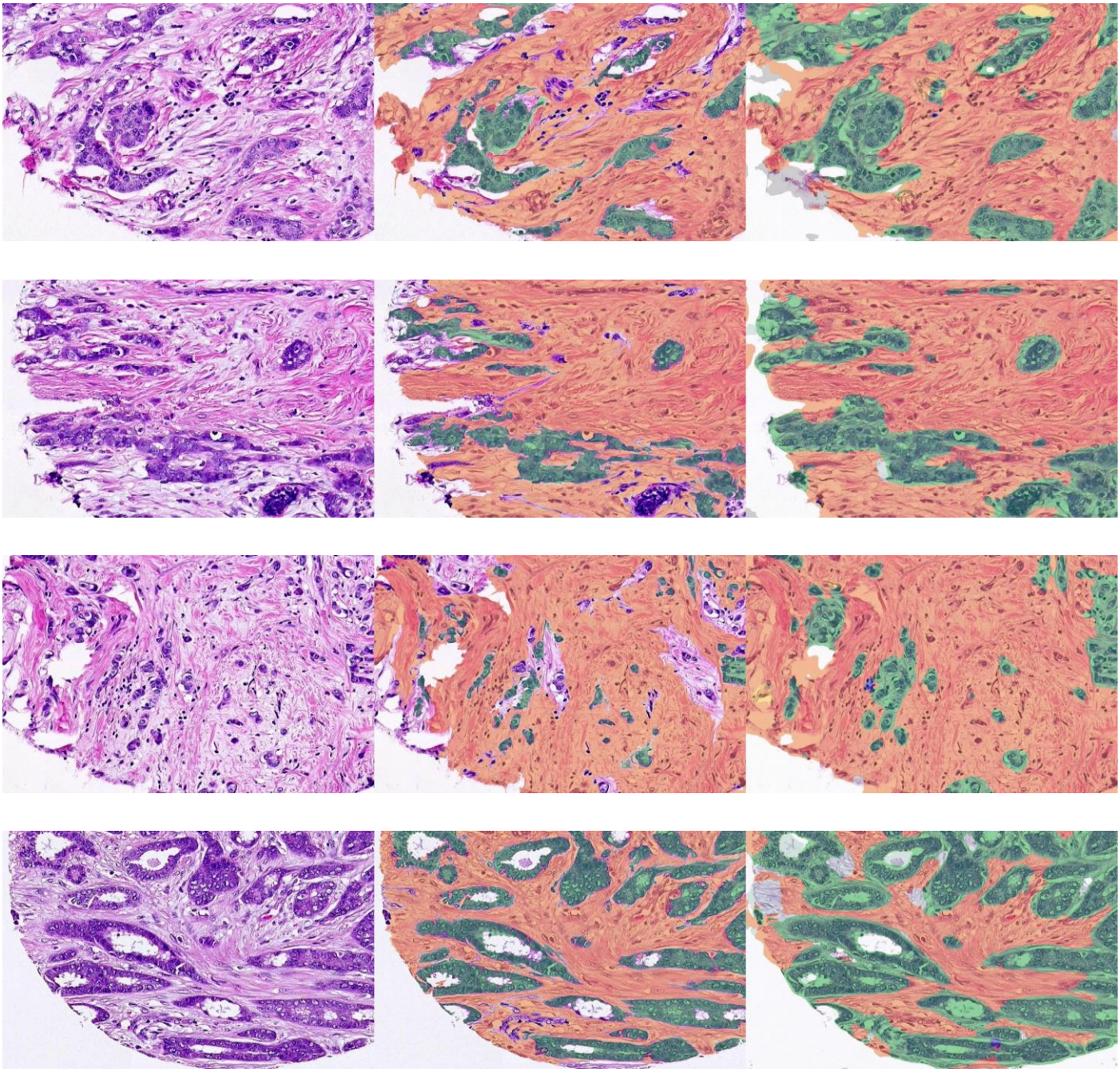

Figure S1-7. Visual examples of the model predictions on breast epithelium-stroma segmentation dataset. The raw histopathology TMA image, manual annotation (mask), and the segmentation results of our model are displayed from left to right.

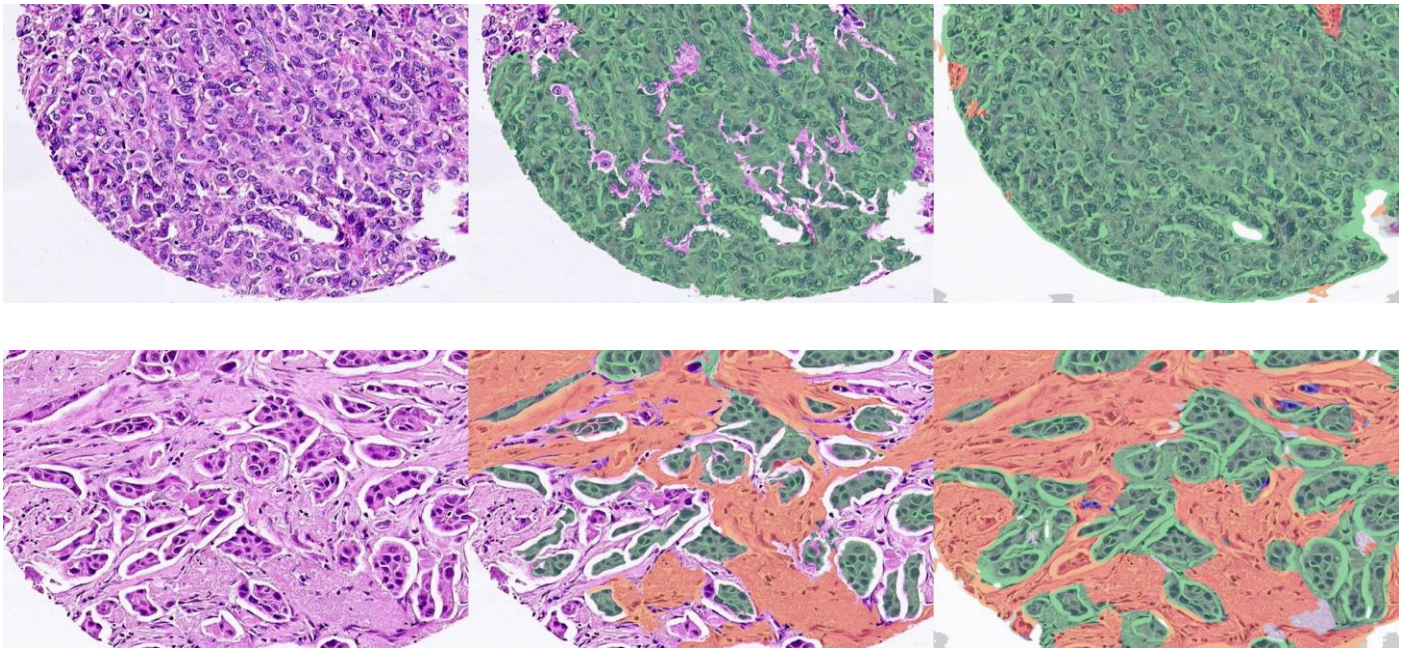

Figure S1-7. *(Continue)*

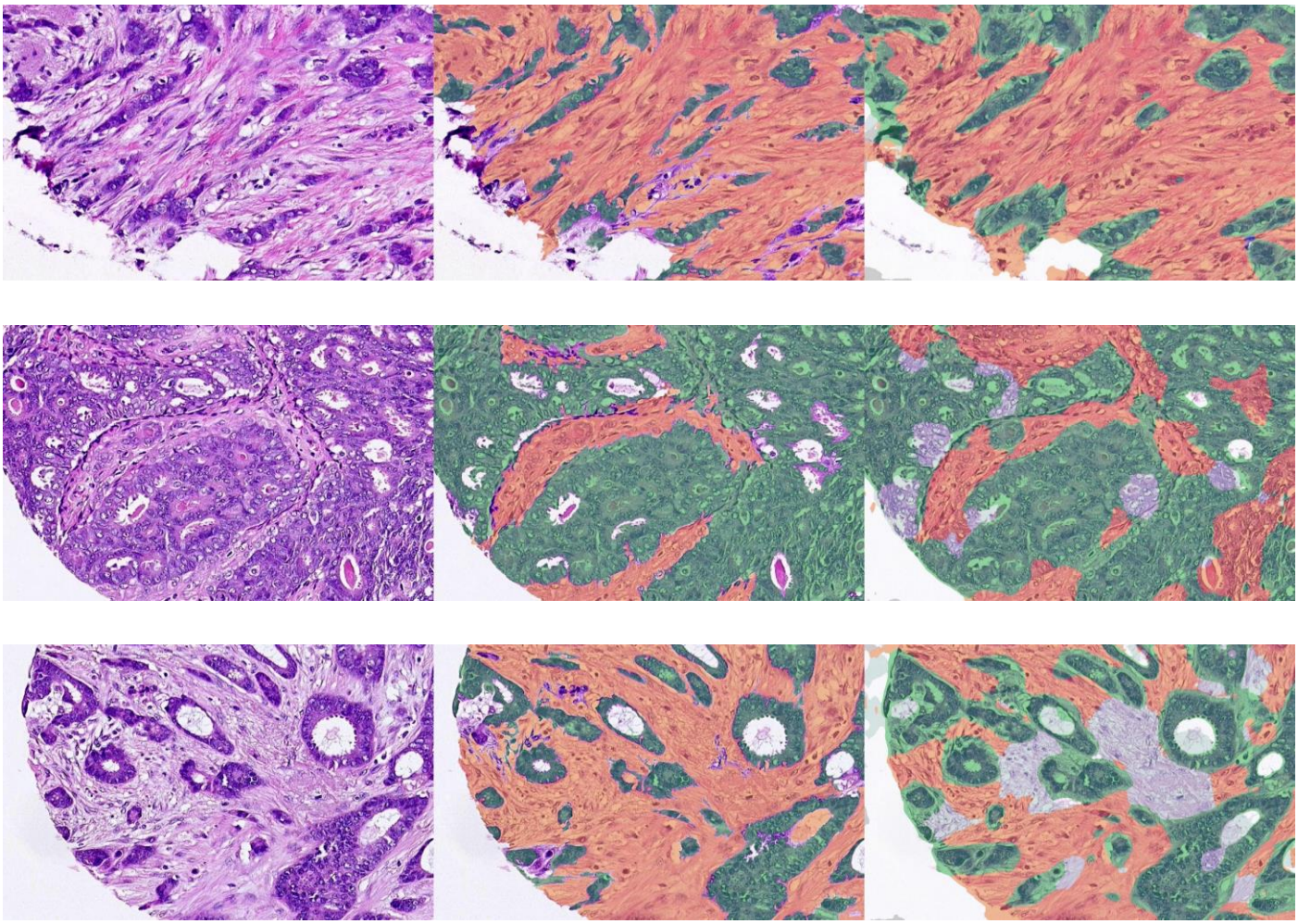

Figure S1-8. Example of misclassification on breast epithelium-stroma segmentation dataset. Misclassification is likely related to factors such as isolated epithelial cells, vacuolated epithelial nuclei, and color patterns that are not present in the training set.

1.3.2 Comparison with pan-cancer TIL map

Previous studies[9] provided TIL maps of multiple cohorts in TCGA (available at https://gdc.cancer.gov/about-data/publications/tilmap). We used the final results after thresholding by the authors (FOLDER TIL_maps_after_thres_v1) for our analysis. These TIL maps are uncompressed PNG images, which facilitated the extraction of masks based on color easily (red for lymphocyte regions, blue for other tissue regions, data not shown).

We down-sampled the whole-slide segmentation maps obtained from our model to match the resolution of the TIL map for comparison. The results showed that 21% of the lymphocyte areas marked by the TIL maps were labeled as 'Fibrous stroma' by our model, while 31% were labeled as 'Epithelial-like tissue'. For each of the seven available cohorts (except for OV, which is not included in the TIL map study), we visualized the most severe 'misclassification' region. Specifically, we find the slide with the highest frequency of 'misclassification' for each cohort, and generated a soft *misclassification map* by applying a Gaussian filter (sigma=10) on discrepancy prediction. The corresponding regions were then cropped and visualized as follows in Figure S1-9. In these examples, predictions of our model were generally accurate and had higher resolution for capturing the details of TIL patterns. Although there were some false-positive prediction in the dense muscle of UCEC, our model still outperformed the TIL maps.

BRCA：

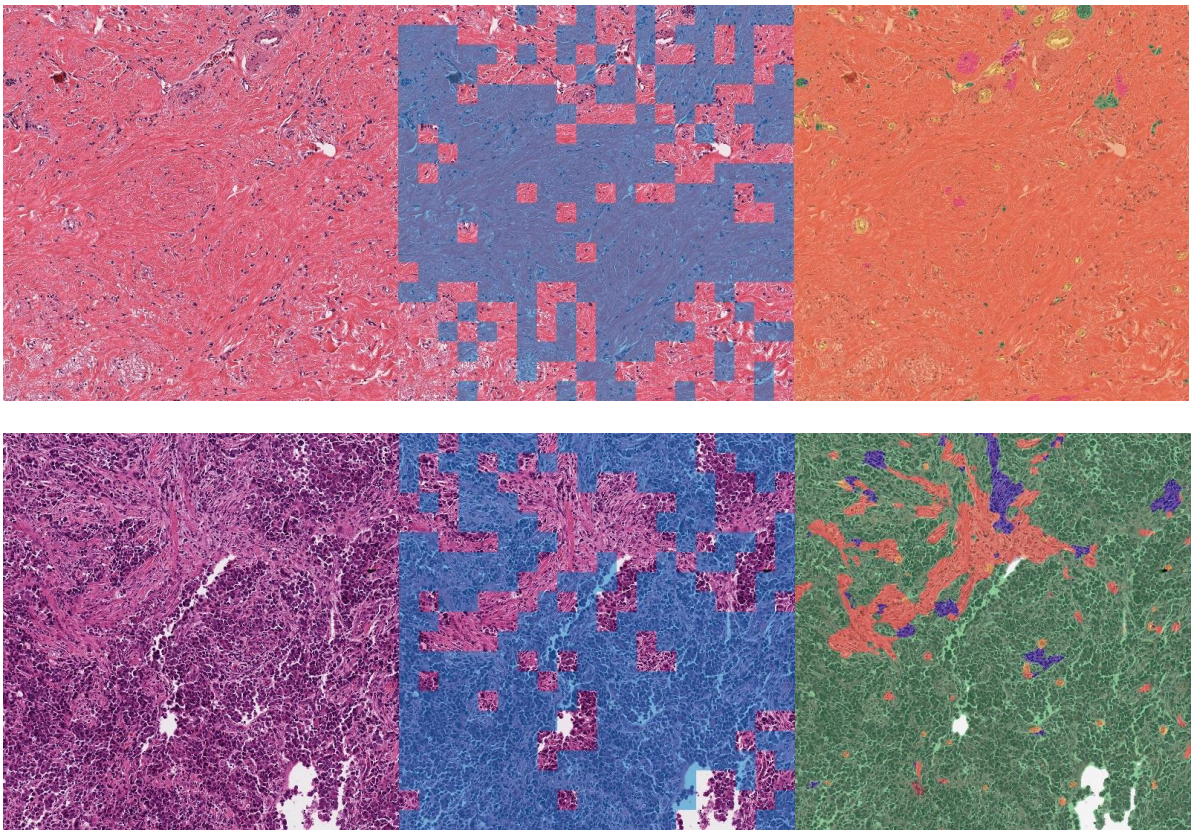

COAD:

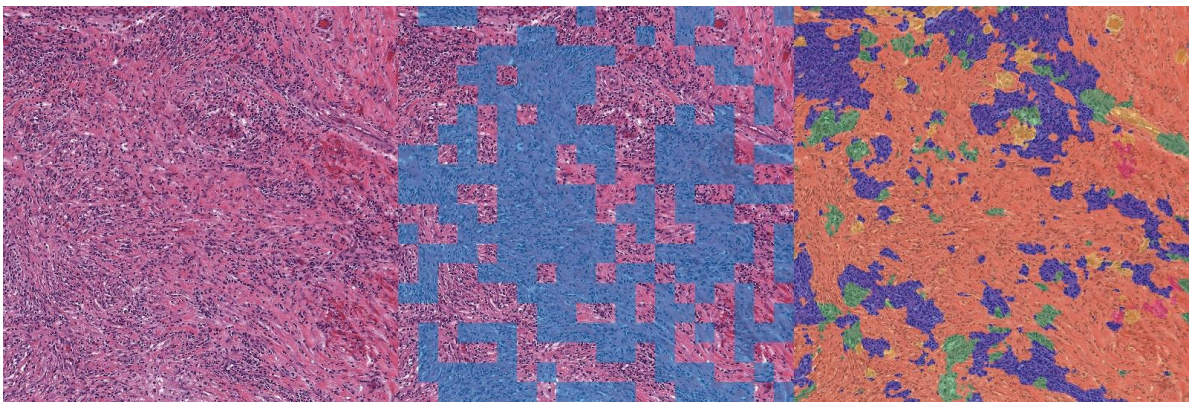

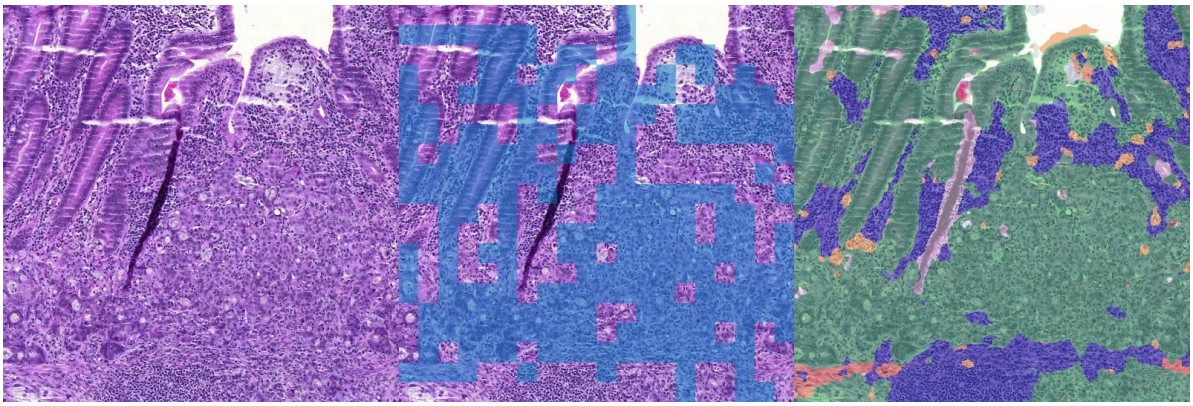

LUAD:

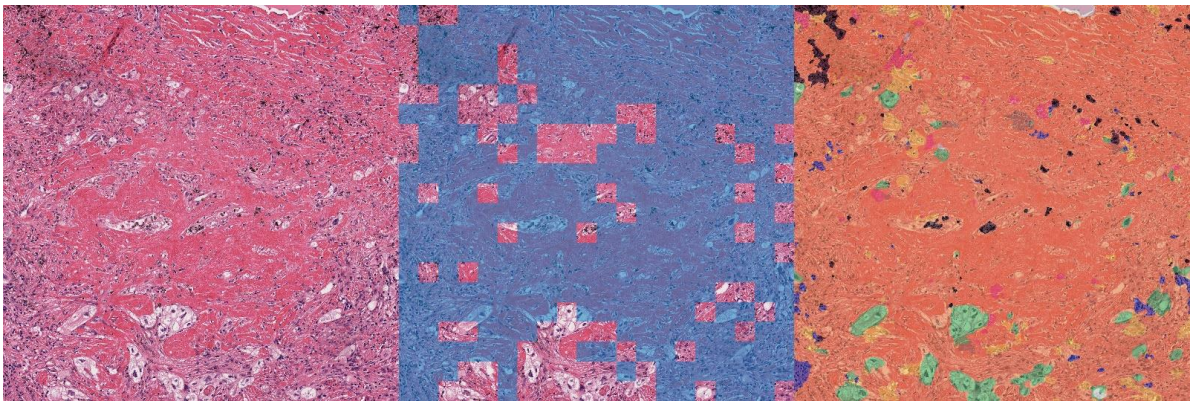

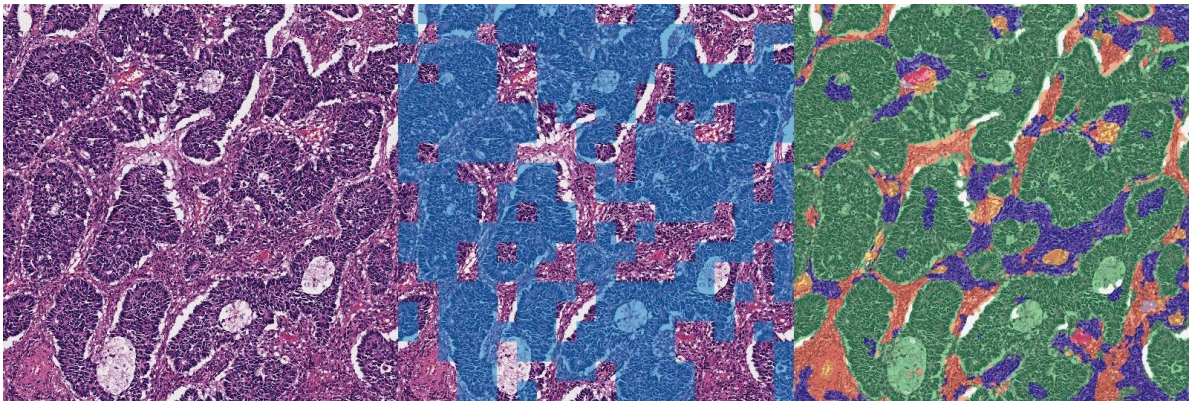

LUSC:

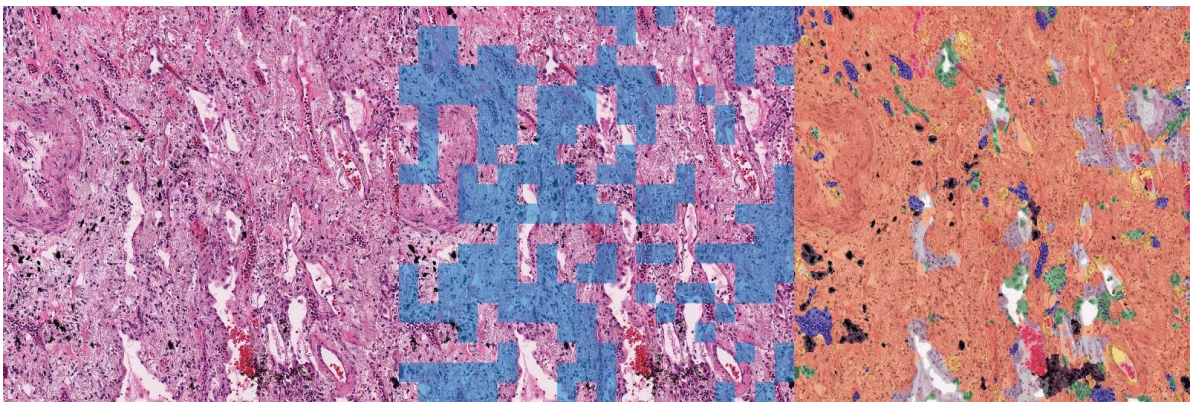

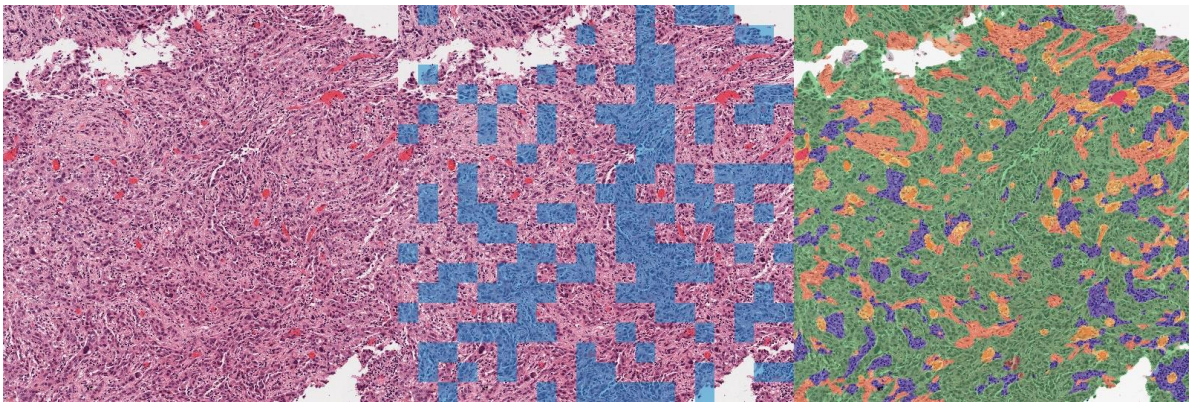

PAAD:

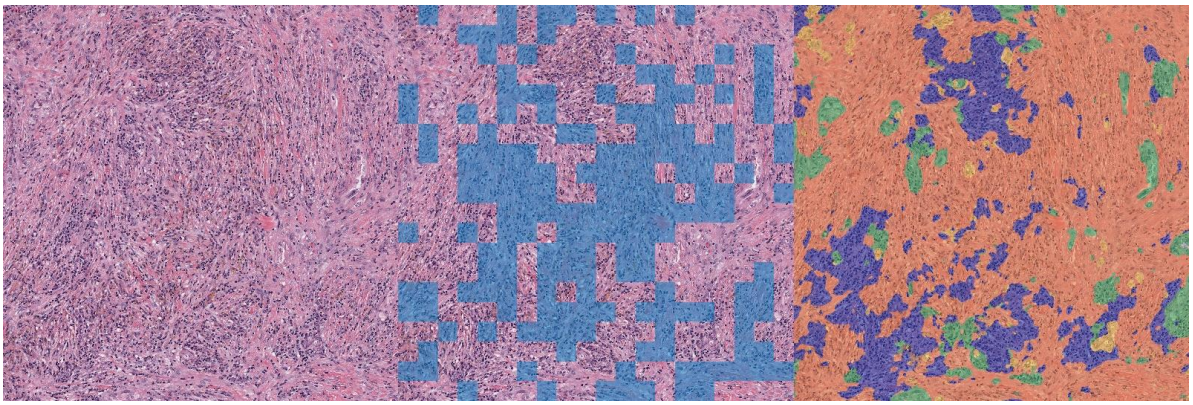

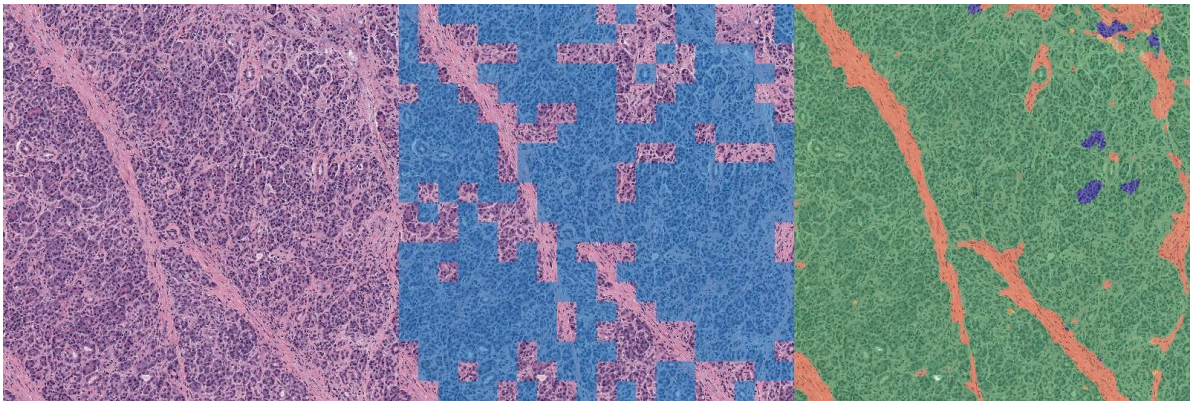

STAD:

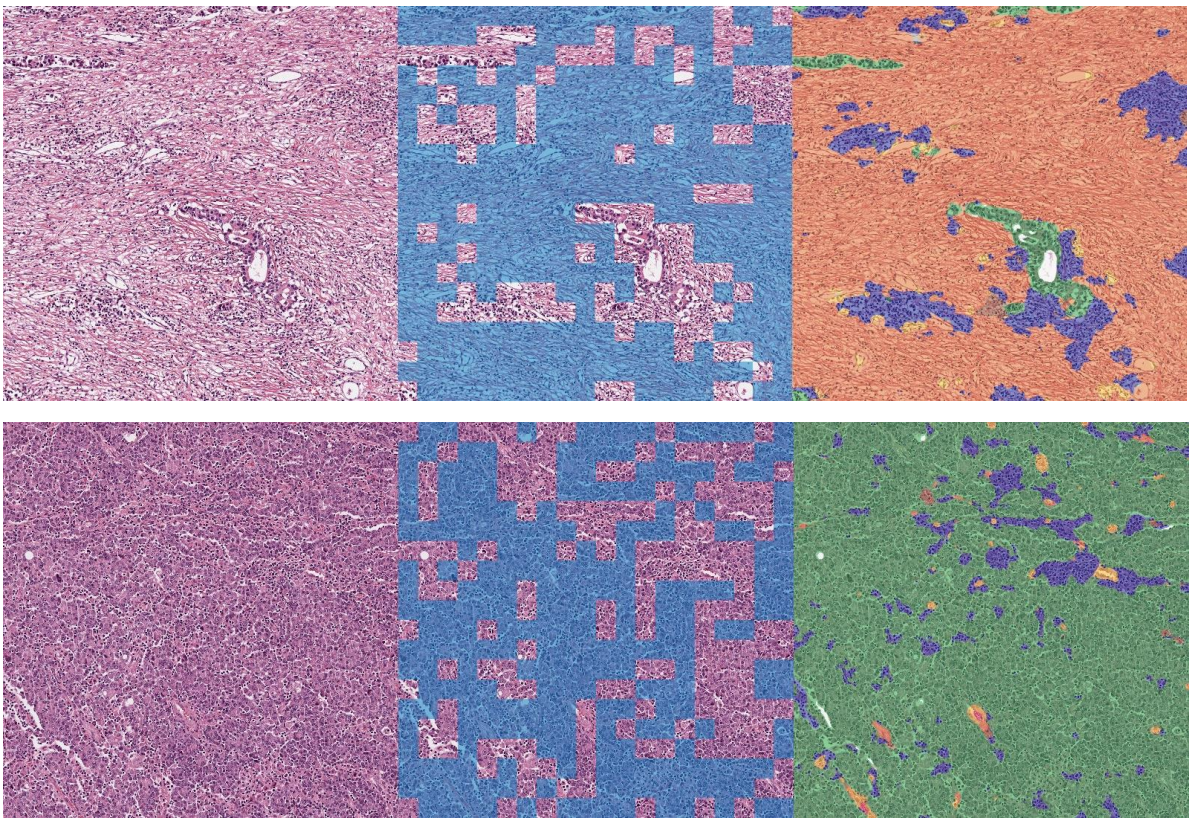

UCEC:

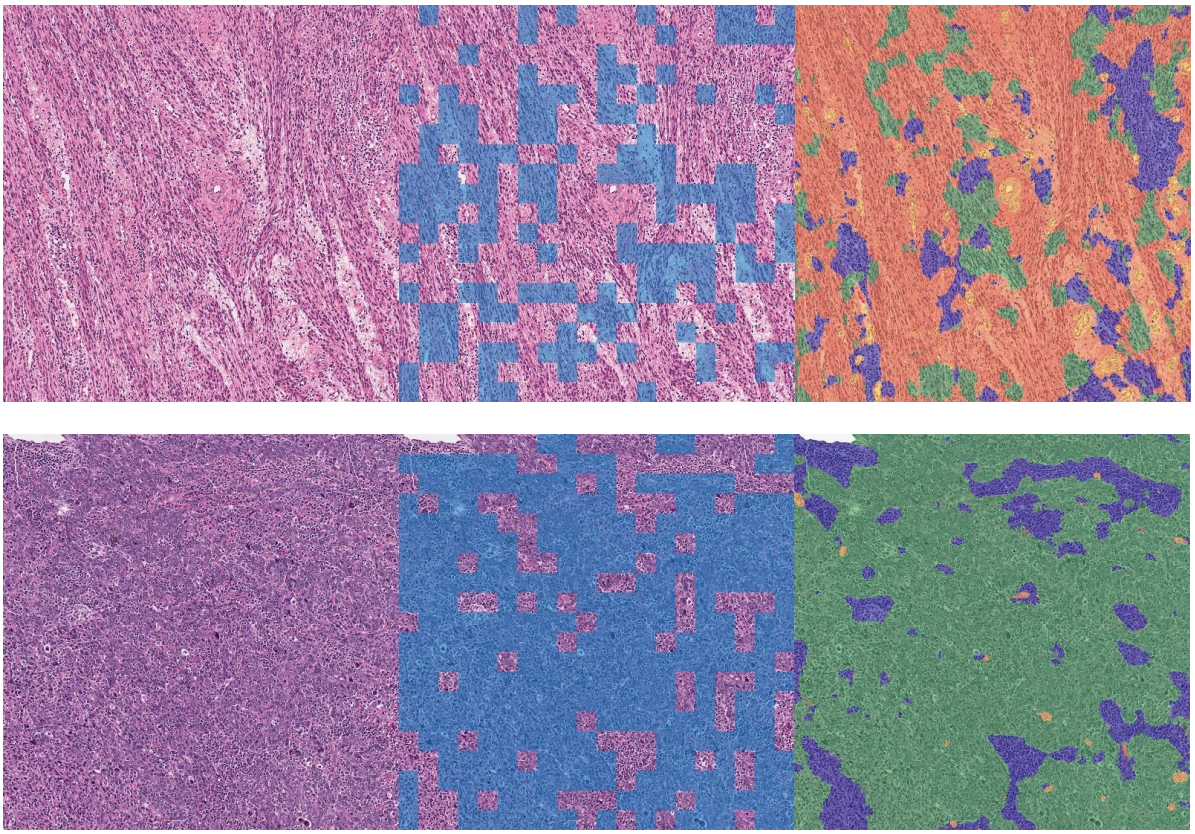

Figure S1-9. Comparison between TIL maps and the segmentation results of our model. The tissue image, discrepancy map (where TIL maps indicate lymphocytes, whereas our model output 'stroma' or 'epithelium-like tissue'), and our model predictions are shown from left to right.

1.3.3 Comparison with CRCM

In order to validate the tissue segmentation model, we reused a colorectal cancer tissue classification model (referred as CRCM) proposed in a previous study[10]. The CRCM was trained at a resolution of 0.5 μm/pixel, while the pixel resolution of the TCGA-COAD cohort ranged from 0.2325 to 0.2533 μm/pixel. Therefore, we extracted overlapping image patches of size 448x448 pixels with a stride of 224 pixels at the highest resolution and scaled them down to 224x224 pixels before processed by CRCM. The final whole-slide predictions were obtained by combining the predictions from individual patches, which have been used in our previous study on prognostic risk assessment in colon adenocarcinoma [11]. To qualitatively compare the differences between the CRCM and our model, we compared the predictions of the two models for each slide, the summarized results are as shown as the Sankey diagram in Figure S1-10. The vast majority of samples have the correct corresponding relationships. Some representative discrepancies are shown in Figure S1-11. It can be observed that our model, due to the advantages of semantic segmentation over patch classification, produces more precise segmentation boundaries for epithelial, lymphocyte, and necrotic regions. The last row of Figure S1-11 shows some imperfect segmentation of our model, where some part of epithelium and muscle are misclassified as mucus and epithelium.

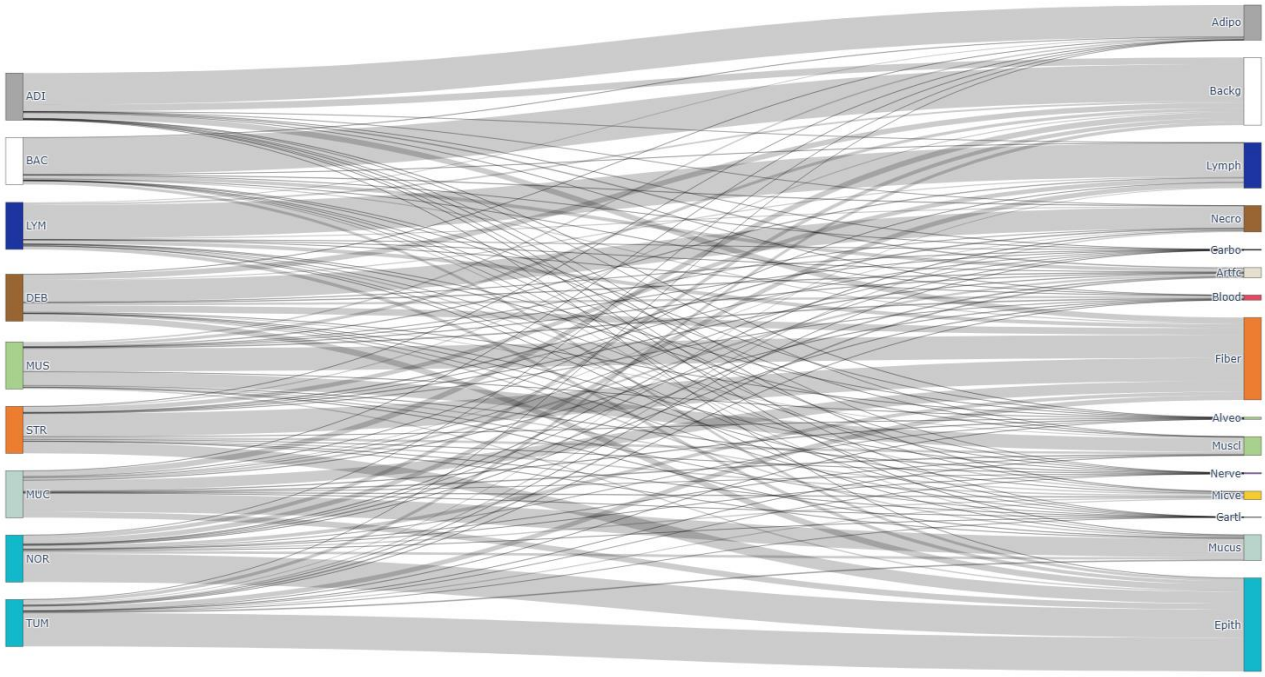

Figure S1-10. Sankey diagram of CRCM predictions and our model. The categories of CRCM are displayed on the left side, while the predicted categories of our model are shown on the right side.

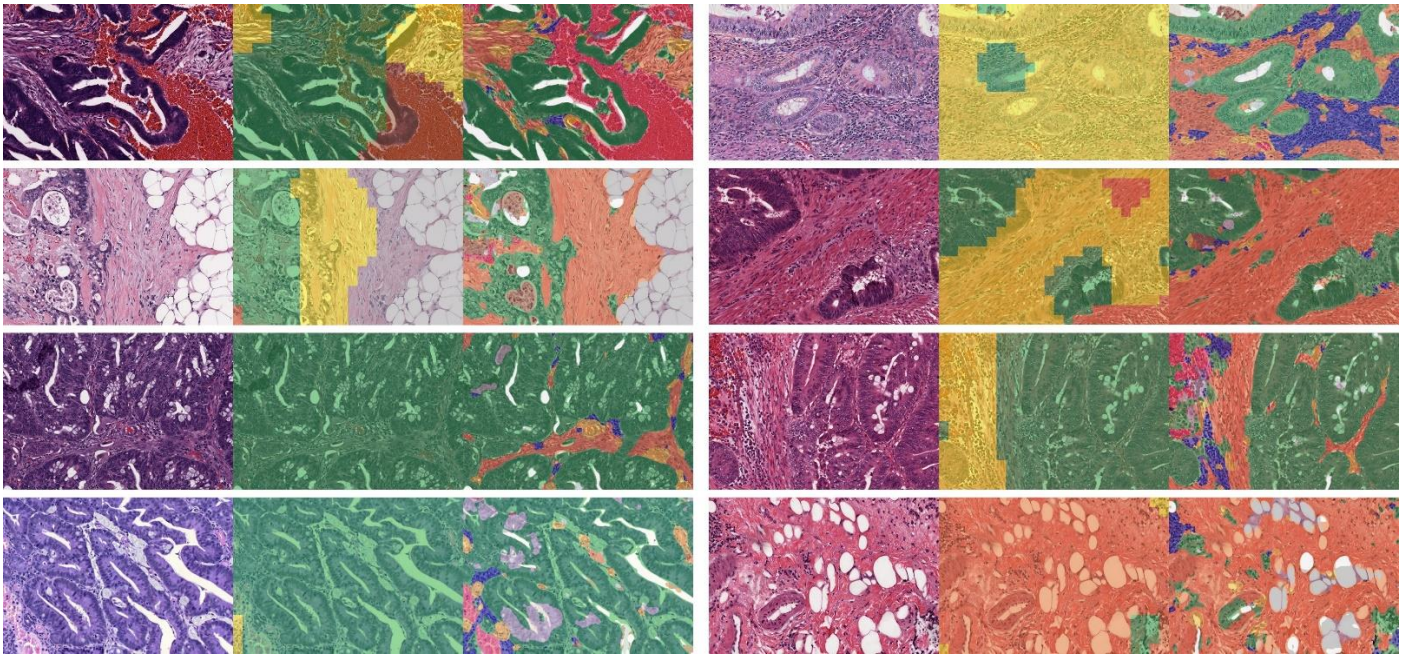

Figure S1-11 Representative discrepancies between CRCM and our model. Tissue images, CRCM predictions, and our high-resolution segmentation results are shown from left to right in each block. The mask color may slightly differ due to category setting (stroma and orange stands for stroma and muscle, respectively in CRCM, whereas the two class is aggregated as orange in our model).

1.3.4 Independent validation in pancreas cancer dataset

This dataset consists of a cohort of pancreatic ductal adenocarcinoma patients admitted to a hospital in central China from June 2015 to December 2021. Fifty representative histopathology slides were selected by pathologists and digitized using the 3DHISTECH PANNORAMIC SCAN II scanner (3DHistech, Hungary) after staining with hematoxylin and eosin. The pixel resolution of all slides was 0.275μm/pixel. Sparse annotations were made by pathologists for categories including background, lymphocytes, necrosis, adipose, fibrous stroma, muscle, nerves, micro-vessel, mucus and sediment, and epithelia-like tissue. These annotations were subsequently converted into masks using similar methods described above, for comparison with model predictions. The pixel-level label information is shown in Table S1-5. We noticed that the color style of this validation cohort is significantly different from that of the TCGA cohort, therefore we trained and apply a CycleGAN model[12] (code available from https://github.com/junyanz/pytorch-CycleGAN-and-pix2pix) for stain style transfer before applying the tissue segmentation model. The final segmentation performance of the proposed model on this dataset is shown in Table S1-6, and more visual examples are shown in Figures S1-12. Quantitative performance metrics and qualitative visualizations indicate that the model has high segmentation accuracy on this dataset. Representative misclassifications are mainly related to complex regions of tissue composition, we also noted confusion between the nerves, fibrous stroma, and muscles categories.

Table S1-5 Annotation and pixel labels of the pancreas cancer dataset. Each pixel corresponds to an physical area of about 1.21μm^2.

Class	Area (pixel)	n_region
Backg	94697	53
Lymph	20195089	466
Necro	25261228	424
Adipo	55568912	428
Fiber	32815080	772
Muscl	12706548	608
Nerve	9980337	579

Micve	351561	875
Mucus	11588605	487
Epith	11720384	708
Sum	180282441	5400

Table S1-6. Performance of our model on the pancreas cancer dataset

Class	Backg	Lymph	Necro	Adipo	Fiber	Muscl	Nerve	Micve	Mucus	Epith	Mean
Accuracy	0.777										
Precision	0.008	0.974	0.994	0.997	0.643	0.712	0.934	0.328	0.711	0.712	0.701
Recall	0.711	0.931	0.465	0.842	0.980	0.571	0.315	0.854	0.746	0.949	0.736
Specificity	0.952	0.997	1.000	0.999	0.879	0.982	0.999	0.997	0.979	0.973	0.976
F1	0.015	0.952	0.634	0.913	0.776	0.634	0.471	0.474	0.728	0.814	0.641
Jaccard	0.008	0.909	0.464	0.840	0.635	0.464	0.308	0.310	0.572	0.686	0.520

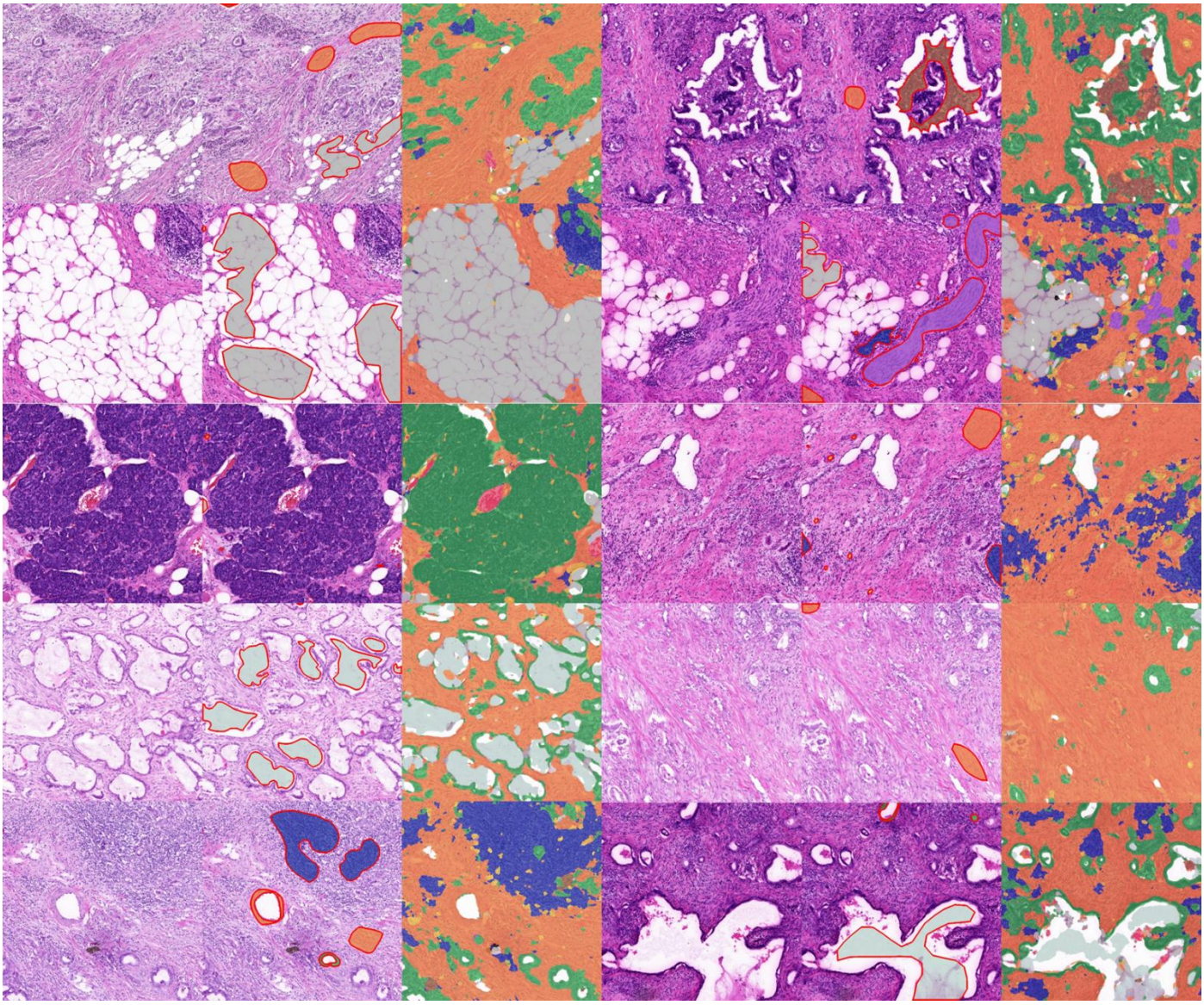

Figure S1-12. Visual example in pancreas cancer dataset. Tissue image, annotation(visualized with mask and red contour), and model predictions are shown from left to right in each block.

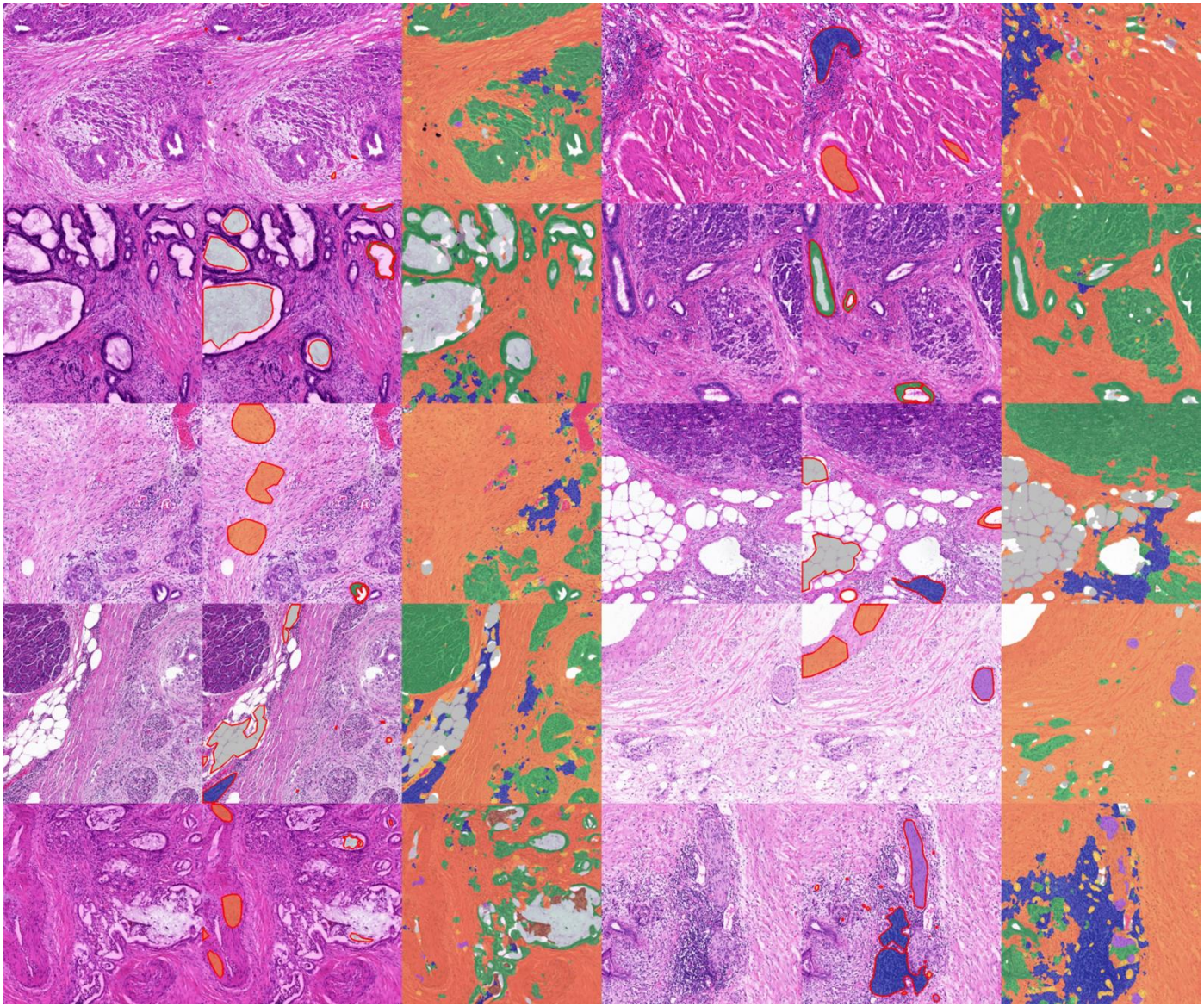

Figure S1-12 *(Continue)*

SECTION 2 GENERATING TUMOR LIKELIHOOD MAP

2.1 BRCA, COAD, STAD, UCEC AND OV

Considering the heterogeneity of tumors and the possibility of non-tumor components presented in tissue sections, it is necessary to identify the tumor regions in order to characterize the tumor features. Therefore, we obtained tumor masks through independent training or reusing existing models. In this study, we trained independent models for BRCA, COAD, STAD, UCEC, and OV in our research. Similar to the model development process for tissue segmentation, we established separate annotation categories for 'Tumor' and 'Non-tumor' for each cohort and used ASAP software for annotation. Note that the tumor localization only needs to capture the overall tumor extent without the need for precise delineation of epithelial. Therefore, we created rough tumor region annotations (for example, we allowed a small amount of stroma component adjacent to the tumor epithelium to be included). The annotation process was performed directly on whole-slide images. During the annotation process, we proactively included more challenging negative examples, especially normal epithelial components (such as terminal duct lobular unit structures in BRCA and normal glands in COAD). Some examples of annotation are shown in Figure S2-1, and the collected mask label is presented in Table S2-1.

Table S2-1. Data used for developing tumor detection models in BRCA, COAD, STAD, UCEC, and OV. Number of slides, polygons, and patches are given.

cohort	n_slide	non-tumor area (mm2)	tumor area (mm2)	non-tumor count	tumor count	non-tumor n_patch	tumor n_patch
BRCA	42	430.07	468.42	155	166	2226	2404
COAD	68	656.06	716.84	183	250	3584	3842
OV	57	408.31	601.39	211	267	1929	2960
STAD	50	606.73	445.01	108	170	3437	2265
UCEC	165	633.63	2124.75	290	927	3002	10032

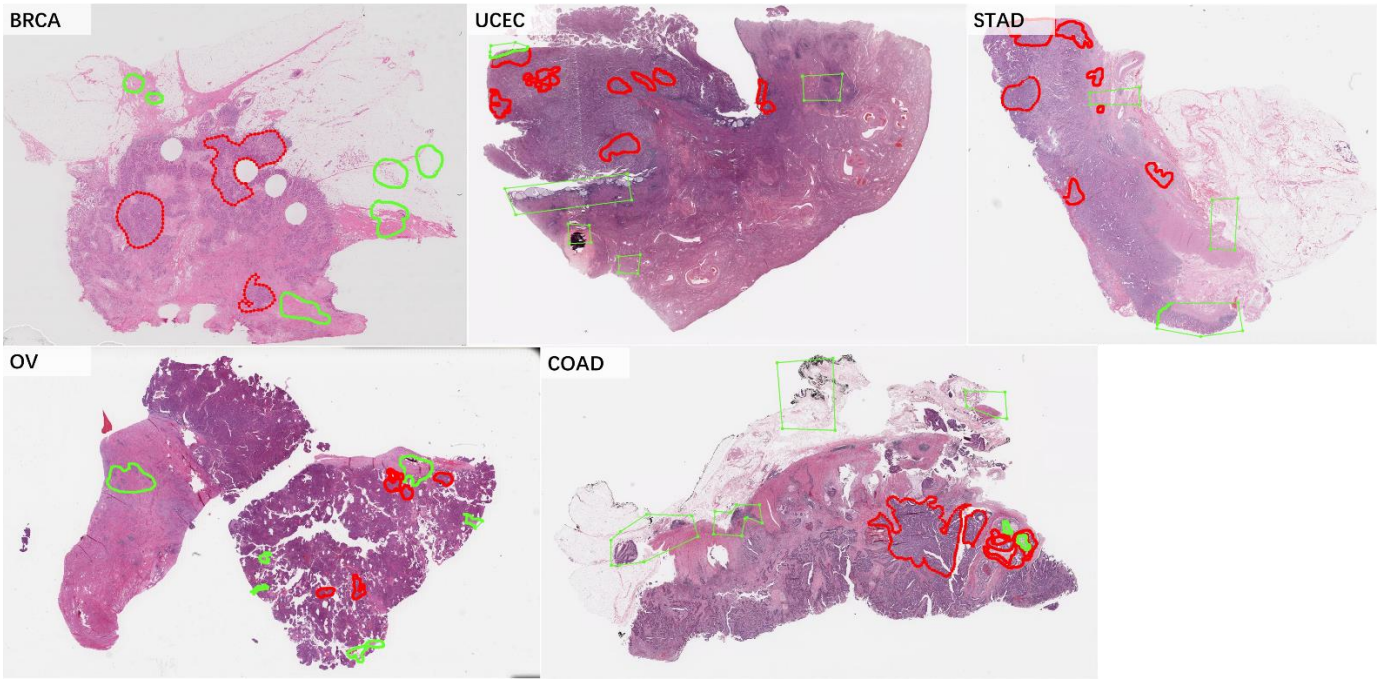

Figure S2-1. Example annotations of the 5 cohorts. Tumor region and non-tumor regions are contoured with red and green, respectively.

In order to obtain samples for training a tumor detection model, we cropped image patches of size 384x384 pixels with a stride of 192 pixels, using paired slides and tumor annotation masks at a resolution of 2.0μm/pixel. The patches were cropped with overlap and assigned labels based on the predominant label value within the patch region. For both tumor and non-tumor

categories, we required that the proportion of pixels corresponding to the masked category within a patch be greater than 50%, and that the proportion within the central 1/4 area of the patch be greater than 80%. This configuration helps avoid ambiguity in patch categorization in sparse annotation scenarios. The total number of cropped patches can be found in the last column of Table S2-1.

Subsequently, we randomly divided all patches into a training set and a validation set with a ratio of 8:2. The patches were further used to train a deep convolutional network to classify 'Tumor' and 'Non-tumor' patches. The model has VGG19 as its backbone, followed by a global average pooling layer to obtain 512-dimensional deep features. These features were then passed through a classification layer consisting of two neurons, which output the probability of a patch being tumor or not. During training, we followed the principle of class balancing and use 32 patches per batch. We defined an epoch as 128 batches and trained the network for maximum 50 epochs. Cross-entropy loss function and Adam optimizer[7] with an initial learning rate of 1e-4 were used. Learning rate decay strategy was also employed, which reduced the learning rate to 90% every 10 epochs starting from the 5th epoch. The backbone was initialized with ImageNet weights, while the classification layer was randomly initialized. To avoid interference from the randomly initialized classification layer, we initially froze the backbone and trained only the head for one epoch. Subsequently, we unfroze the backbone and trained the entire network. During training, we monitored the loss on the validation set and saved the best model with the lowest loss for subsequent inference. The training loss curves for the five tumor detection models are shown in Figure S2-2. It is important to note that these five tumor detection models were trained separately, and the corresponding model was used for subsequent whole-slide inference in each cohort.

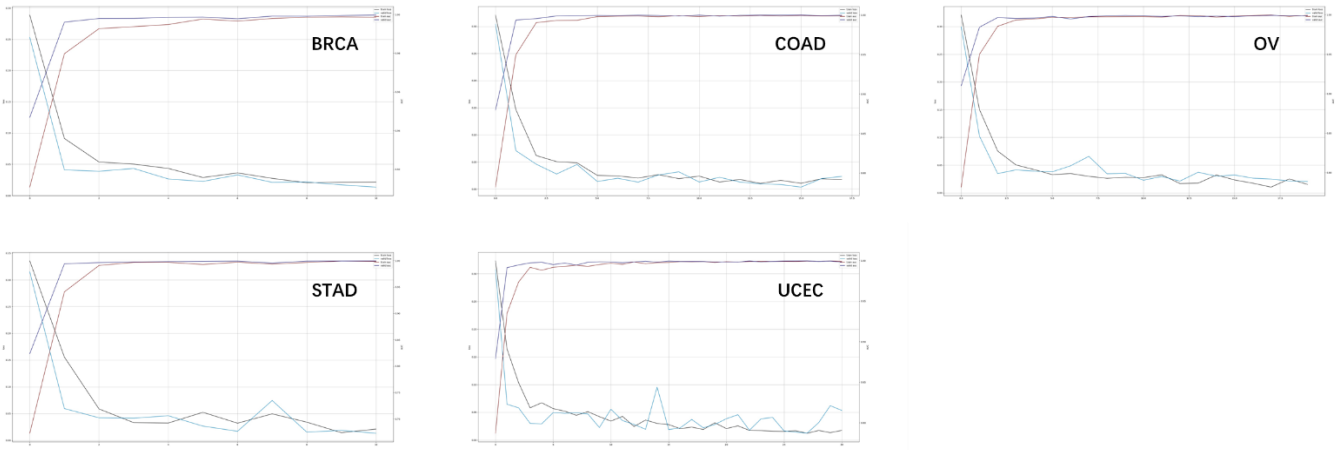

Figure S2-2. Training curves of tumor detection model in BRCA, COAD, STAD, UCEC, and OV cohorts.

In order to obtain a more detailed tumor detection mask, we didn't use non-overlapping patch classifier. Instead, we replaced the global average pooling layer of the VGG model with an average pooling layer of kernel size 12x12. Additionally, we replaced the fully connected layer for classification with an equivalent convolutional layer, thereby forming a fully convolutional semantic segmentation network[13]. This network can generate segmentation maps at a down-sampling rate of 32. To ensure both efficiency and quality for whole-slide evaluation, we enlarged the input image to 1024x1024 pixels and removed the 256-pixel region at the patch boarder for smoother results. We applied the aforementioned model at the same resolution as the training phase (2.0μm/pixel) and stitched local results seamlessly to obtain a tumor likelihood map.

During the model development process, we may start training with a few slides (around 50, for example). The initially developed model was then applied to the entire cohort for visual inspection. If notable prediction biases were recognized, we will supply more corresponding annotations to enhance the model. This process can be iterative used as needed, resulting more annotations. For instance, we found that the UCEC cohort is quite challenging, possibly due to the dense muscles. By combining this human-in-the-loop and semi-automatic segmentation approach, we obtained tumor likelihood maps for all diagnostic slides in the five cohort. Some examples are shown in Figure S2-3.

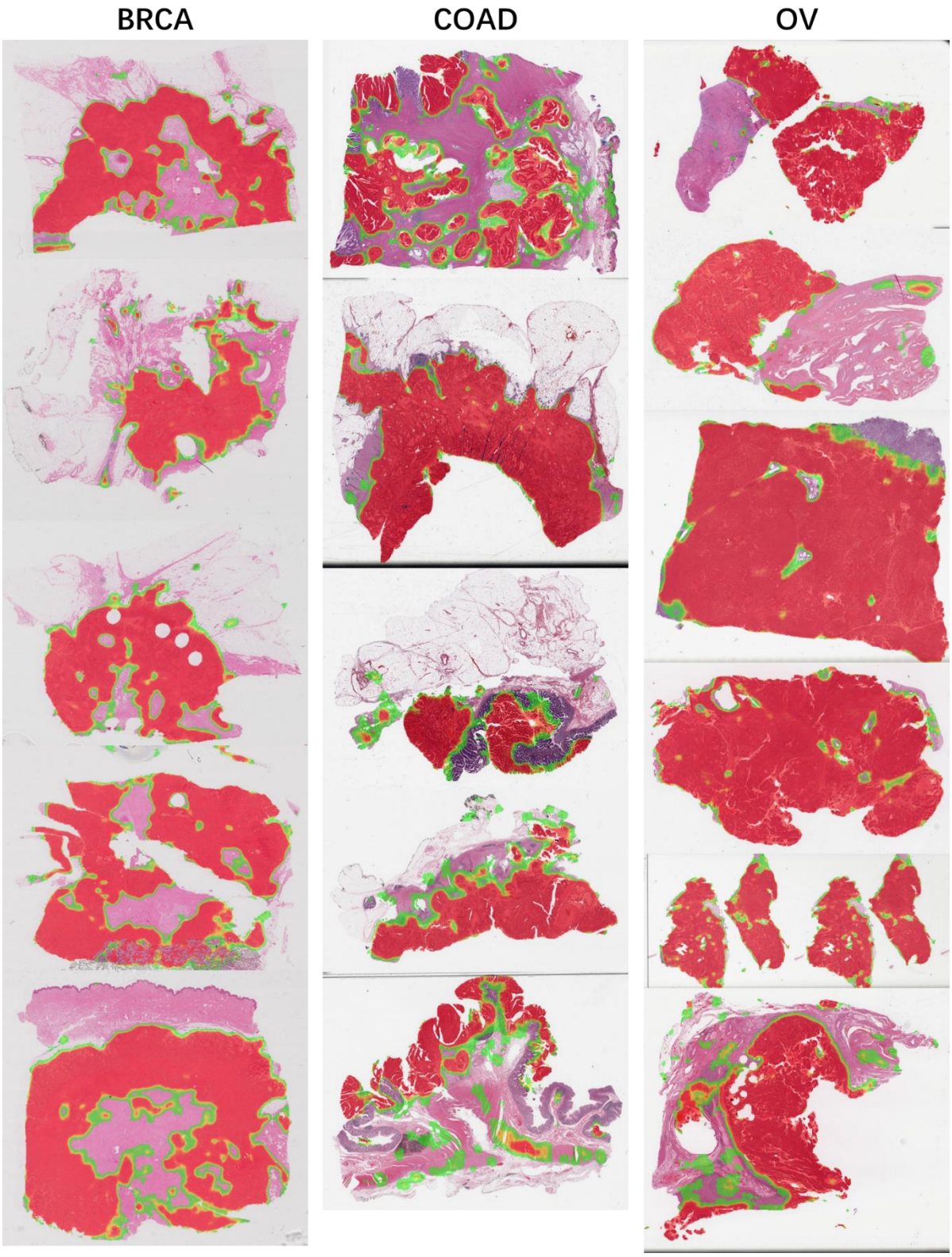

Figure S2-3. Examples of tumor detection in BRCA, COAD, STAD, UCEC, and OV. The predictions are visualized with heatmap overlay, where transparency and green indicate low likelihood, whereas red represent high tumor likelihood.

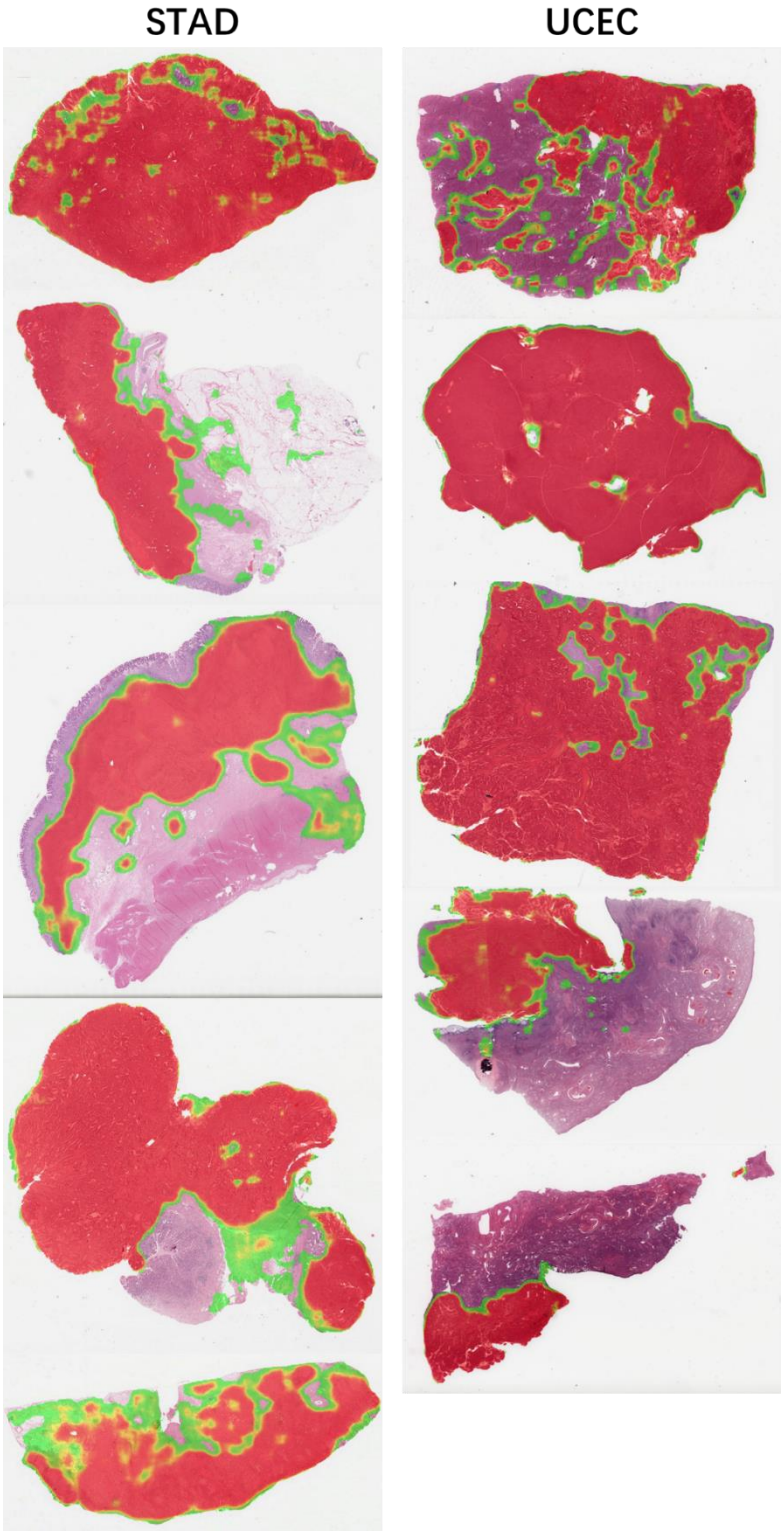

Figure S2-3. *(Continue)*

2.2 PAAD

The tumor segmentation for pancreas cancer is an independent project of our research group. The model development and whole-slide image inference process are similar to that in the aforementioned five cohorts. However, due to the widespread presence of difficult-to-distinguish structures such as pancreatitis, we adopted a different annotation category scheme, including 'Normal', 'Inflammatory', and 'Cancerous'. Pathologists draw representative rectangular ROIs for the three classes, as illustrated in Figure S2-4. The training and validation data consisted of 209 annotated slides from TCGA-PAAD and 244 slides from three private cohorts. These ROIs were subsequently cropped and saved at a resolution of 2.0μm/pixel. Then, patches of size 512x512 pixels were extracted with a stride of 256 pixels for model training. The patch information used to train the model development is shown in Table S2-2.

During the training process, the 'Normal' and 'Inflammatory' categories were merged as 'Non-tumor' category, with a sampling probability of 'Normal':'Inflammatory':'Cancerous'=1:1:2. Other parameters for model training included: batch-size=32, iteration-per-epoch=128, backbone-freeze-epoch=1, optimizer='adam', lr=1e-4, scheduler_plateau=8, scheduler_step=4, scheduler_gamma=0.9, max epochs=100. As the training phase used 512x512 pixel patches, we used a kernel size of 16x16 for the average pooling layer when converting the VGG classification network to equivalent fully convolutional neural network. Other inference strategies were consistent with the previous models. We applied the trained model to the TCGA-PAAD cohort. Despite only limited local annotations were provided, this semi-automated pipeline yielded a whole-slide tumor likelihood map. Visual examples of pancreas tumor detection are shown in Figure S2-5.

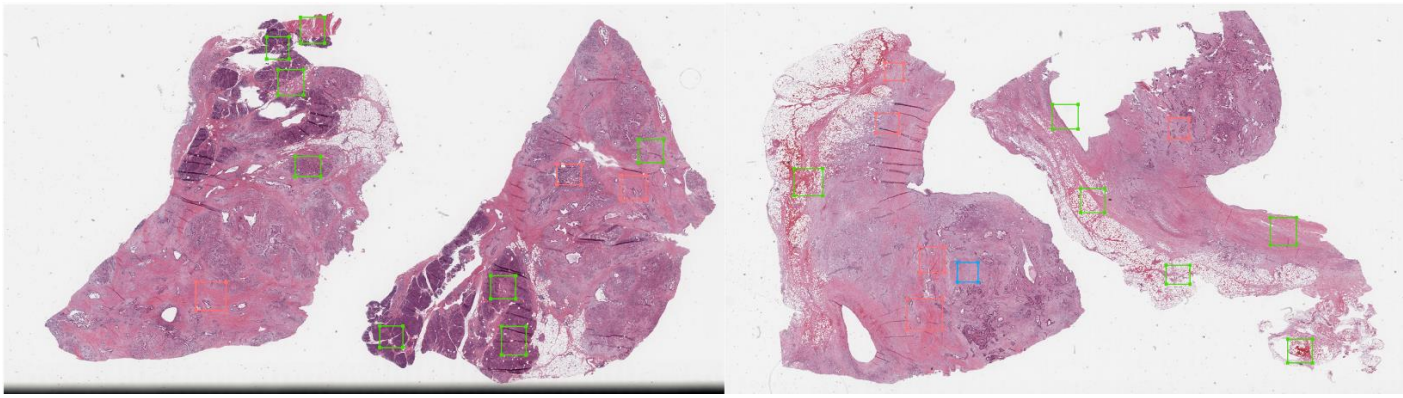

Figure S2-4. Data annotation examples of the pancreas tumor detection. The 'Normal', 'Inflammatory', and 'Cancerous' regions are marked with green, blue, and red rectangular, respectively.

Table S2-2. Data used for developing pancreas cancer detection model. The table gives patch number for all subsets.

	Cohort H		Cohort S		Cohort X		TCGA			Sum
Partition	Cancerous	Normal	Cancerous	Normal	Cancerous	Normal	Cancerous	Inflammatory	Normal	
train	1047	1921	1050	1735	1033	2436	433	86	440	10181
valid							1575	58	4247	5880
Sum	1047	1921	1050	1735	1033	2436	2008	144	4687	16061

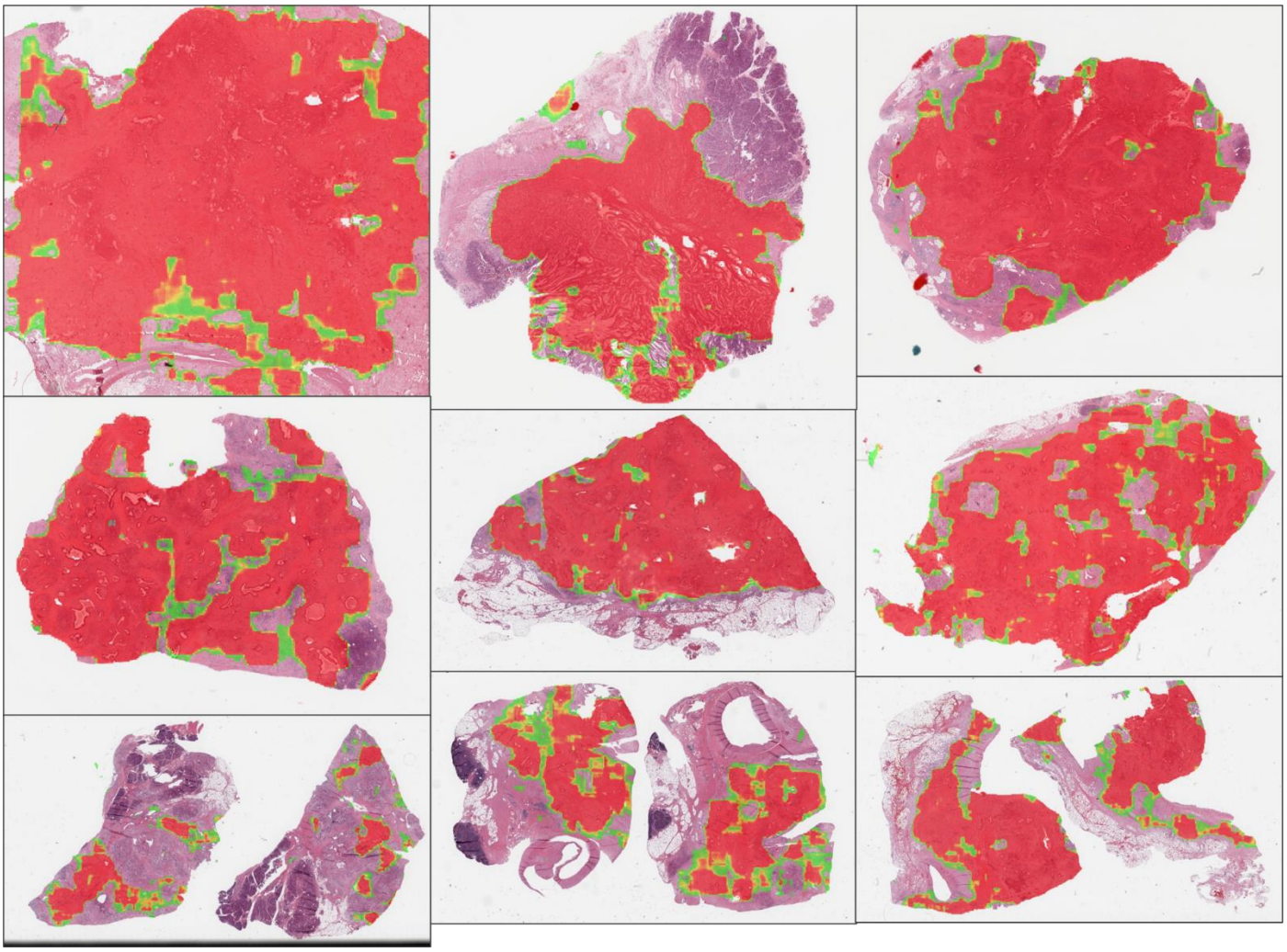

Figure S2-5. Tumor detection for pancreas cancer in TCGA-PAAD. The predictions are visualized with heatmap overlay, where transparency and green indicate low likelihood, whereas red represent high tumor likelihood.

2.3 LUAD AND LUSC

For the LUAD and LUSC cohorts, we utilized a previously published model available on the grand-challenge platform (accessible at https://grand-challenge.org/algorithms/lung-cancer-segmentation/). This model was jointly trained on the TCGA dataset and the ACDC@LUNGHP (Automatic Cancer Detection and Classification in Whole-slide Lung Histopathology) dataset[14]. It is capable of detecting lung adenocarcinoma, lung squamous cell carcinoma, and other type of lung cancer. The model achieved the third place in post-challenge leaderboard of the ACDC@LUNGHP challenge. Examples of the cancer lesion likelihood maps are shown in Figure S2-6 and Figure S2-7.

The model is a U-Net trained at a high resolution of 0.5μm/pixel, and can depict fine-grained tumor epithelium, this make it different from the previous six models. To maintain conceptual consistency, we performed post-processing on the segmentation results. Specifically, we obtained binary masks using a threshold of 0.5, followed by a distance transformation with a threshold of 250μm. Finally, we performed an intersection operation with a pre-extracted foreground mask [11] to exclude the misclassification in the background.

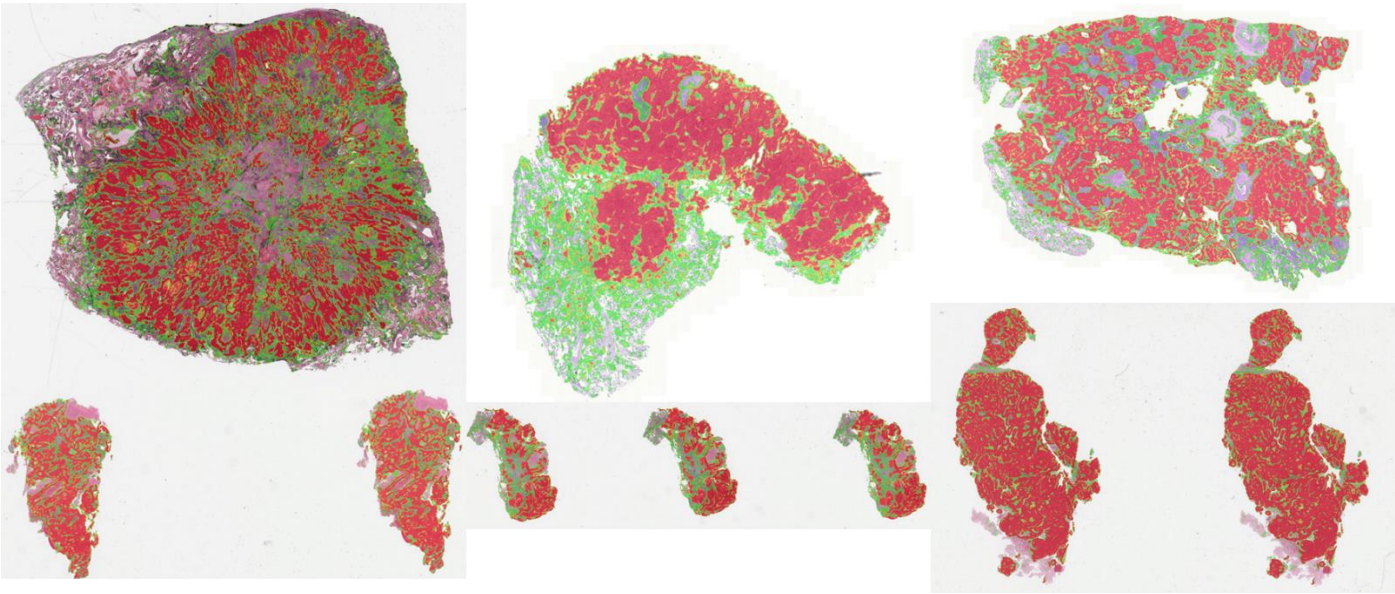

Figure S2-6. Tumor detection examples of the TCGA-LUAD cohort. Results visualized with heatmap.

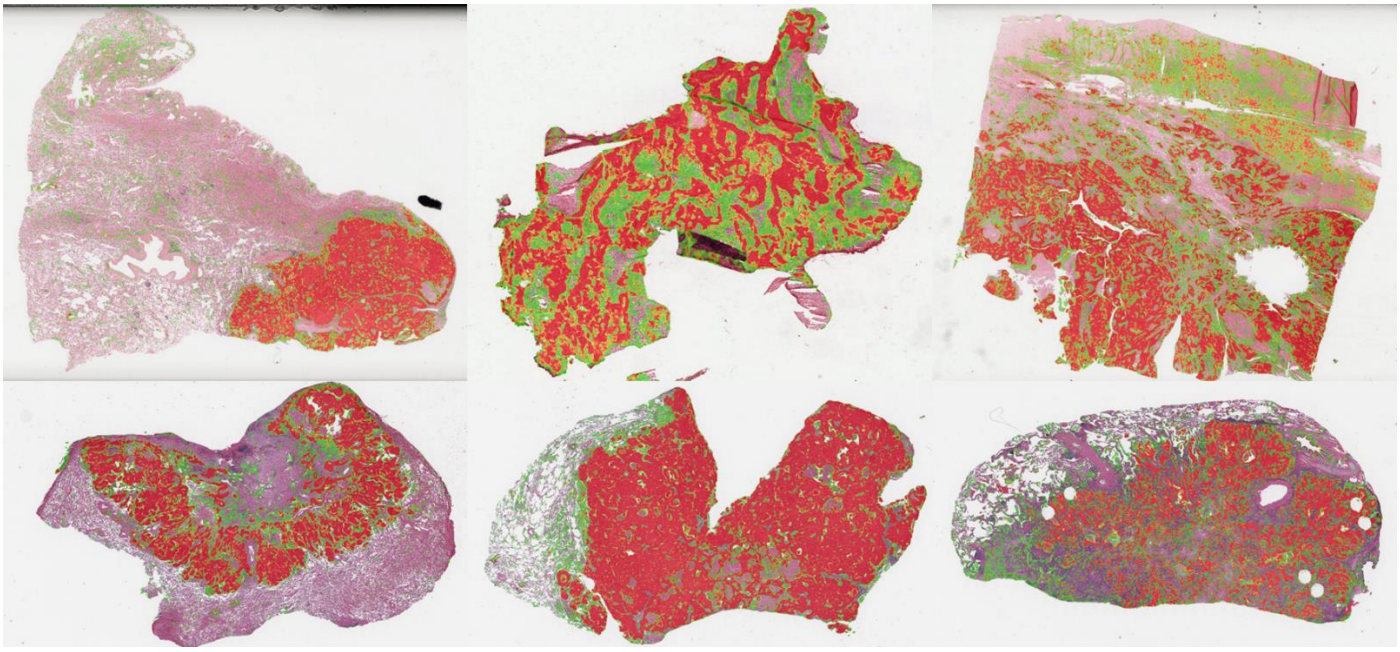

Figure S2-7. Tumor detection examples of the TCGA-LUSC cohort. Results visualized with heatmap.

SECTION 3 TISSUE FEATURE ANALYSES

3.1 GENERATING AND QUALITY CONTROL OF TISSUE AND TUMOR MAPS

The pipeline for generating tumor map has been described in Section 2. Similarly, we applied our tissue segmentation model on local views from giga-pixel whole-slide image with slide-window manner. Slightly different from tumor detection, we enlarge the input patch size to 1024x1024 pixel, and drop 128-pixel margin from the four side. All the local results are then re-organized as a high-resolution whole-slide tissue segmentation maps, which we referred as *Tissue Atlas*.

Before subsequent analysis, we acquire a quality control (QC) process considering factors including image quality, segmentation accuracy, and representativity of tissues. The QC consists of following steps:

1. We removed 23 slides from the STAD cohort, as these files only contained regions of interest with extremely small fields of view, with an uniform size of 1200 pixels by 1600 pixels. The file storage size ranging from 460-490KB. As these ROIs were unable to provide sufficient contextual information required for tumor microenvironment analysis, we excluded them and did not attempt to apply tumor detection and tissue segmentation models.
2. We excluded slides with unknown resolution, including 17, 10, and 19 slides from the COAD, LUAD, and STAD cohorts, respectively. These slides had a maximum edge length of 10,000 pixels and the resolution is too low to provide details.
3. We visually inspected all tumor maps at low resolution and performed high-resolution examination when the tumor contour or heatmap did not fit prior knowledge. The criteria for removal including: absence of tumor region, lymph nodes slide, entire slide necrotic, excessively small tumor regions, severe detection errors, and problematic results caused by quality issues (blurriness, non-H&E staining, non-FFPE slides, severe staining artifacts, etc.). Except for the already removed slides by resolution issue mentioned above, this criterion excluded 131 slides out of 3946.
4. Similarly, we examined all tissue atlas at low or/and high resolutions. Issues in specimen collection and slide preparation processes will also affect the accuracy of tissue atlas. Additionally, we removed cases where the segmentation of key components (tumor epithelium, lymphocytes, stroma) was inaccurate. These issues were predominantly observed in UCEC, mainly due to the complex muscular structure and misclassification of epithelium (which may resemble diffuse gastric cancer in some cases) and lymphocytes. This criterion resulted in the exclusion of 161 slides out of 3946. It is important to note that this exclusion process was independent to the QC of tumor maps. Ultimately, 3680 slides passed the QC for both tumor map and tissue map. Some examples that dropped by QC are shown in Figure S3-1.
5. A patient may have multiple slides with varying volumes of tumor tissue. In order to obtain the most representative results, we measured the area of the tumor map mask for the selected slides and chose the one with largest tumor area. In total, data from 3437 patients/slides were used for subsequent analysis (TCGA-BRCA, TCGA-COAD, TCGA-LUAD, TCGA-LUSC, TCGA-OV, TCGA-PAAD, TCGA-STAD, and TCGA-UCEC consists of 1010, 420, 455, 455, 101, 165, 356, and 475 patients respectively). It is important to note that QC was solely based on the quality of the tumor map and tissue map. In subsequent analyses, such as survival analysis, the patient number may be smaller than this value due to missing labels.

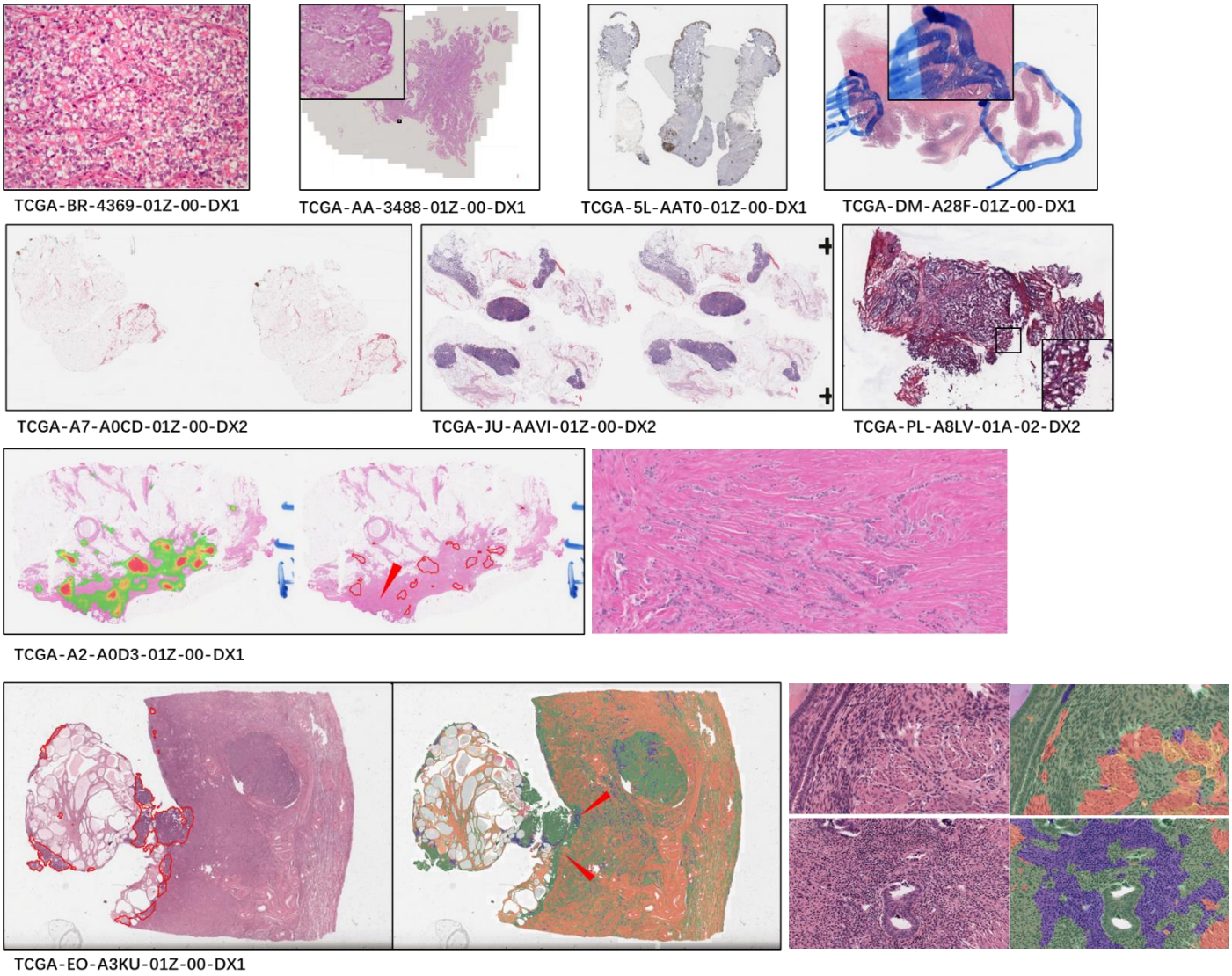

Figure S3-1. Quality control of tumor maps and tissue atlases. Examples slides that did not passed QC process are shown. The first two rows display small ROIs in STAD, slides with unknown resolution without details, None-H&E slides, cancerous region polluted by marker pen, slides without cancerous region, lymph node slide, and non-FFPE slides, respectively. The third row presents an excluded tumor map, where the breast cancer was not recognized by the tumor detection model due to the tiny scattered lesions (indicated by the red arrow). The fourth row displays an excluded tissue map, where the UCEC slide had dense muscle tissue (red arrows), which is misclassified as epithelial or lymphocytes.

3.2 Tissue feature definition

All histological features in this study were derived by combining tumor likelihood maps (being thresholded as binary maps, referred as tumor map hereafter) and tissue segmentation maps. Based on prior knowledge that features reflecting tumor characteristics may exist within the tumor, at the tumor periphery, and in adjacent areas, we defined these regions of interest (ROI) based on the tumor maps:

1. **Inside-tumor**: The main region of the tumor is defined by dividing the connected components based on the tumor map using four-connectivity, and selecting the subregions whose area exceeds 10% of the maximum connected component. This helps capture the main characteristics of the tumor, and similar concepts have been considered in previous literature, also referred to as significant regions[15,16].
2. **Invasive-margin-80**: Refers to the strip generated by the expansion of the main tumor region towards the surrounding area, with a distance threshold of 80μm. The distance was considered as threshold of cell-to-cell interactions[16].
3. **Invasive-margin-500**: We have noticed that the distance of 80 μm is actually very small. Since the tumor map is relatively rough, without precisely delineation of tumor epithelium, the 80 μm-definition may result in systematic biases in histological features. Therefore, we have set a wider range to obtain robust tumor microenvironment characteristics.
4. **Outside-tumor**: All regions that are not in tumor map.

In addition, when defining all the aforementioned regions of interest (ROIs), we utilized a foreground mask generated by an in-house model[11], which ensured that the ROIs were not affected by blank areas on the slide. Skipping blank and low-quality regions also accelerated the speed of whole-slide analysis and improved robustness.

The tissue atlas composed of 15 pixel-level labels. We obtained the area and connected components of each category for further analysis. For each of the aforementioned regions of interest (ROI), we generated tissue features as follows:

1. The area proportion of all categories. The most representative one is the proportion of lymphocyte within the tumor, reflecting the intensity of immune infiltration.
2. The ratio of connected components number and the total area per class, which reflects the average area of each object.
3. The area, number of components, and component number to area, of two selected categories. For example, the ratio between fibrous stroma and epithelial regions within the tumor area may serve as a potential measure of tumor-associated stroma.
4. In order to fully consider the spatial distribution, we examined the surrounding circular area within an 80μm range of a base tissue (typically focusing on epithelial-like tissue within tumors). We calculated the proportion of another component (such as lymphocytes) within the circular area, either in relation to the area of the base tissue or as a percentage of the base tissue area.

The metric definition is illustrated as Figure S3-2. We have noted that 'alveolar' should only exist in LUAD and LUSC, and its presence in other tumors is considered as noise. Therefore, the associated features will not be calculated. Similarly, cartilage typically appears in LUAD and LUSC. Carbon encompasses the deposition of carbon in the lungs as well as the ink-stained edges in the tissue. Artifacts are generated by factors such as tissue folding and defocus, and may not have diagnostic significance, so we exclude them in all tumor types. Additionally, due to confusion observed between fibrous stroma, muscles, and nerves in the validation sets, we merged them into a single 'stroma' category in subsequent steps. Finally, to ensure numerical stability, we use area as the denominator and add a small value (1e-6) to avoid zero division errors.

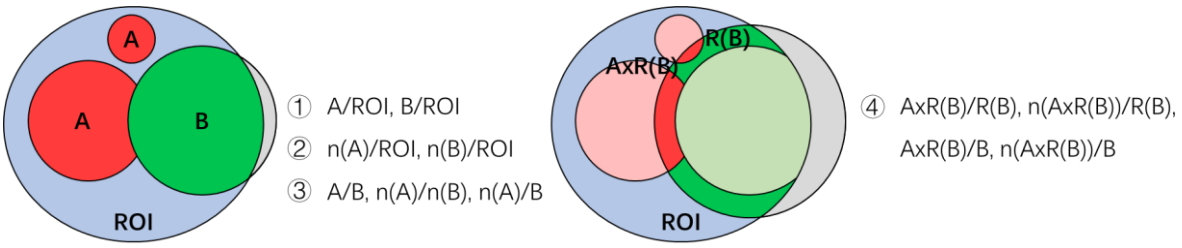

Figure S3-2. Definition of tissue features.

According to the rules above, up to 3168 tissue features were generated (with more features in the LUAD and LUSC cohorts, due to the presence of cartilage and alveolar categories). The original data that produced these features, such as area and number of connected domains, were also recorded and labeled with the prefix "NOFEATURE". The tissue map, tumor map, as well as quantified tissue features, will be made publicly available on our GitHub repository (https://github.com/jiaoyiping630/Pancancer-tissue-atlas). Boxplots of some representative features are shown in Figure S3-3.

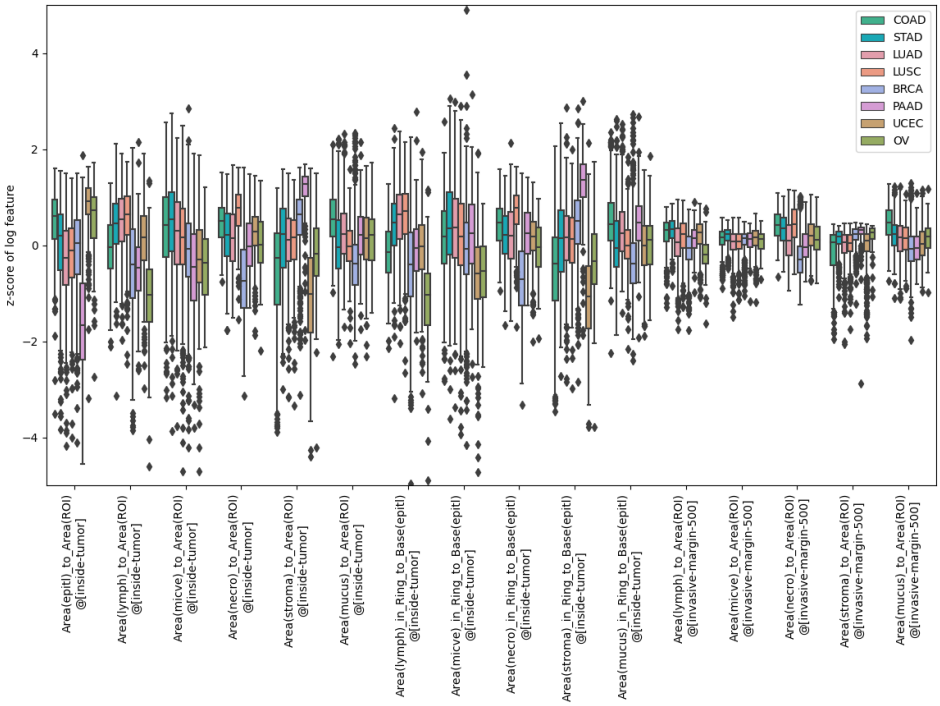

Figure S3-3. Boxplot of 16 representative features. This plot corresponds to Figure 3(A) in the main manuscript. Each sample represent a patient. The TME features are arranged in horizontal axis, with subgrouping by cohort inside.

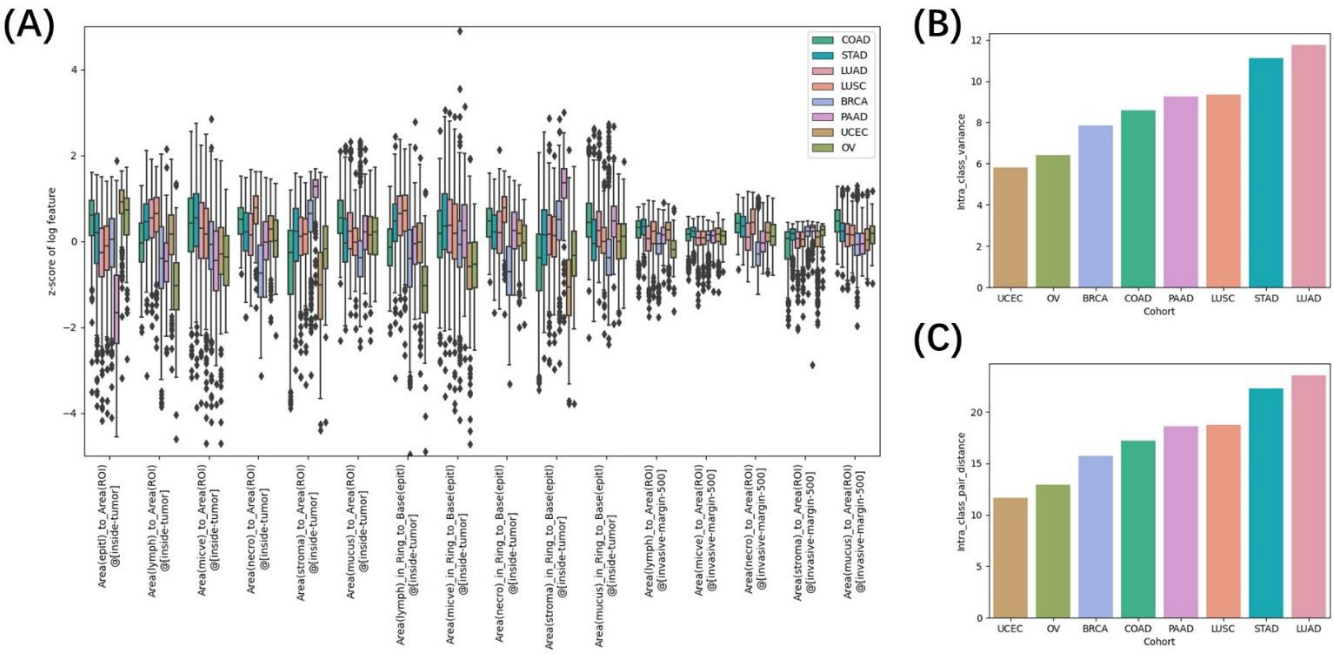

Figure S3-4 UMAP embedding and TME heterogeneity within each cancer type.

We used UMAP[17] to reduce the dimensionality of 16 representative features, resulting in a scatter plot embedded in a 2D plane. This process was implemented using UMAP in Python (https://github.com/lmcinnes/umap) with default parameter settings, such as n_neighbors set to 15 and using the Euclidean distance. The dispersion of the clusters on the UMAP plot can

reflect the heterogeneity of the cancer in the tumor microenvironment (Figure 3B, Figure S3-4 A). To quantify the heterogeneity, we calculated the data variance and the average (squared) distances between sample pairs within data from each cancer type (Figure S3-4 B, C). As shown, the two metrics get very similar results, where UCEC, OV, BRCA have less intra-cohort heterogeneity, and LUAD, STAD, LUSC have larger heterogeneity.

3.3 Survival analysis of tissue features

To elucidate the prognostic significance of aforementioned tissue features, we performed survival analyses on each cohort (of eight cancer types) for each tissue feature. Specifically, based on the numerical values of tissue features, patients were divided into two groups using a specific threshold (such as the median), and Kaplan-Meier survival curves were plotted for the two groups. The log-rank test was used to evaluate whether there was a significant difference in survival time between the two groups, with a p-value less than 0.05 considered significant. In addition, a Cox's proportional hazard model was established for the grouped data to obtain the relative risk and 95% confidence interval between the two groups. The survival analysis was performed using the lifelines library in Python.

We considered endpoints including overall survival (OS), disease-specific survival (DSS), disease-free interval (DFI), and progression-free interval (PFI), derived from Clinical Data Resource[18]. The observation endpoint for survival time is set at 5 years, and any endpoint time beyond this interval is marked as 0 (indicating no observation within the interval). To avoid interference from critically ill cases in survival analysis, we filtered out patients with a survival time less than 30 days. In order to improve the specificity of risk stratification, in cases where the two groups are not empty, we allow the threshold to adaptively adjust between the 25th and 75th percentiles, so as to obtain the optimal p-value in the log-rank test.

Considering the possible correlation between tissue features and pathological stages, we repeated the above analysis in stage subgroups (I, II, III, IV) using AJCC pathological stage. Under the stage-specific analysis, indeterminate stages (e.g., 'I/II NOS', 'Stage X', '[Discrepancy]', '[Not Applicable]', '[Not Available]', '[Unknown]') were excluded from the analysis. In the UCEC and OV cohorts, there was no AJCC stage key, so we turned to pathological staging. The summarized results of the survival analysis are shown in Figure S3-5 to Figure S3-8. Please note that in the survival analysis, there may be cases where the hazard ratio is larger than 1000, with a 95% CI ranging from 0 to infinity, but with a p-value less than 0.05. We have also excluded such data from the figures (using the criteria of CI lower bound < 0.001 and CI upper bound > 1000, no color is displayed). Taking OS as an example, the specific results of the survival analysis can be found in Table S3-1 to Table S3-8.

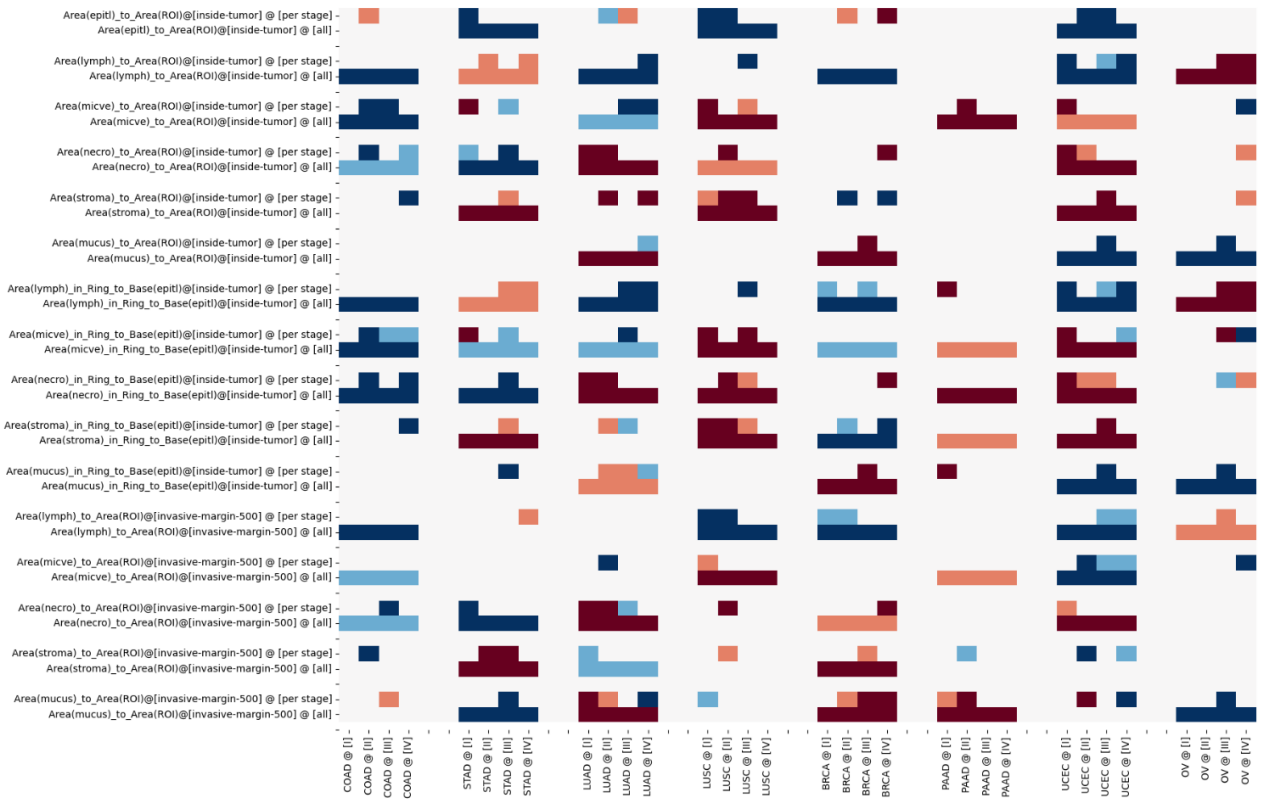

Figure S3-5. Summary of single-variate K-M analysis for overall survival. This figure corresponds to upper part of Figure 5 in main article. Each sub block represent hazard ratio and log-rank significancy in stage I~IV (upper 4 grids), and all stages (lower 4 grids).

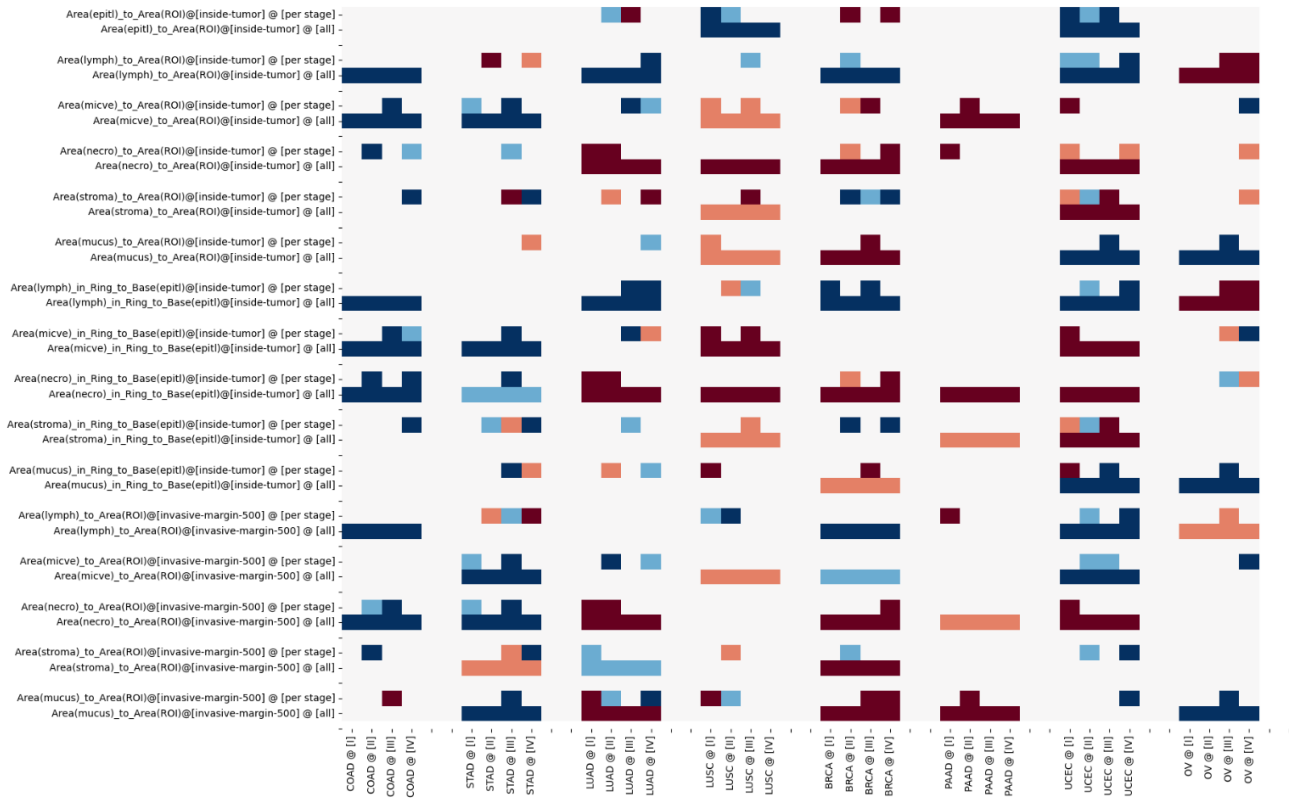

Figure S3-6. Summary of single-variate K-M analysis for disease-specific survival. Contents has similar meaning as that in Figure S3-4.

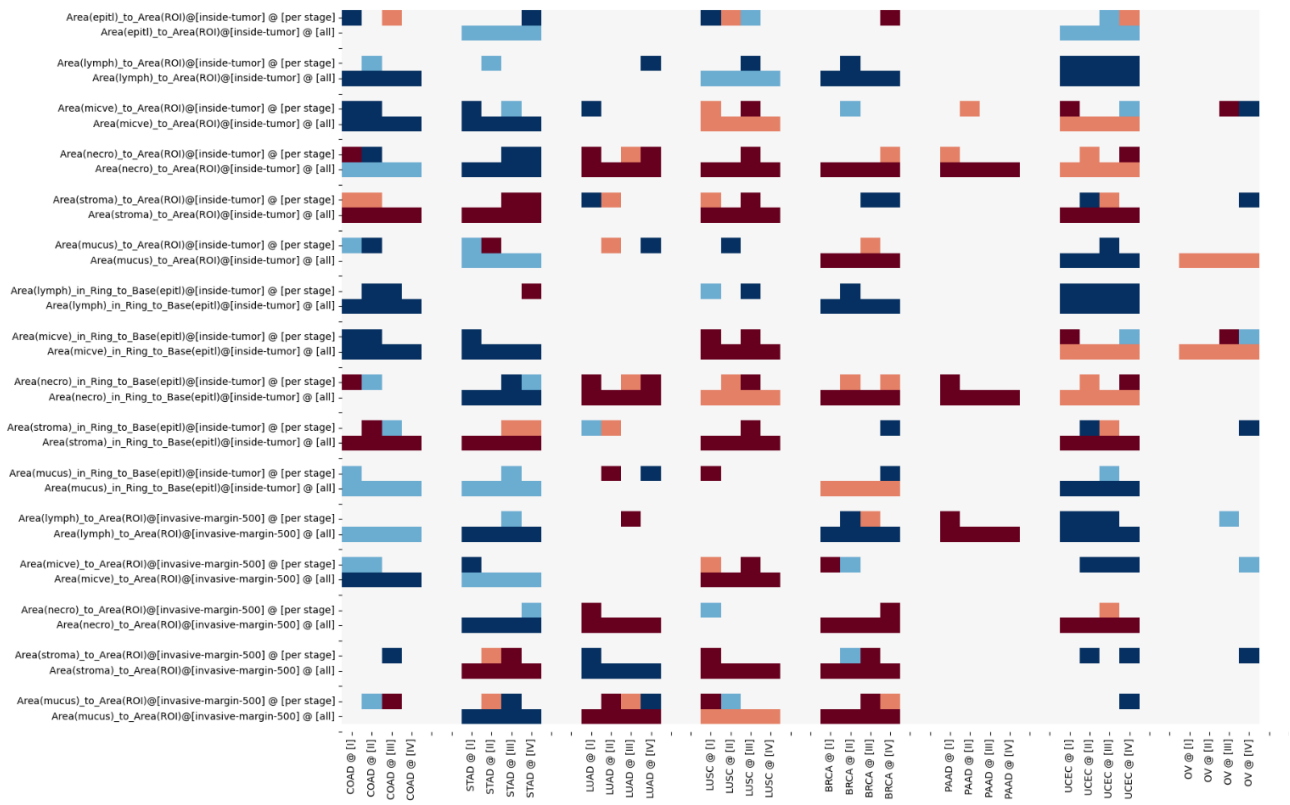

Figure S3-7. Summary of single-variate K-M analysis for disease-free interval. Contents has similar meaning as that in Figure S3-4.

Figure S3-8. Summary of single-variate K-M analysis for progression-free interval. Contents has similar meaning as that in Figure S3-4.

Table S3-1. Detailed results of overall survival K-M analysis in COAD cohort

	FeatureName	Stage	HazardRatio	pval	ZScoreThreshold	n_HighGroup	n_LowGroup
COAD	Area(epitl)_to_Area(ROI)@[inside-tumor]	All	1.38 (0.84~2.27)	0.204	1.084	99	294
		Stage I	'NaN' (0.00~inf)	0.149	0.899	29	41
		Stage II	2.66 (0.92~7.66)	0.061	1.082	36	106
		Stage III	0.62 (0.29~1.35)	0.227	-0.208	87	29
		Stage IV	1.90 (0.86~4.19)	0.109	0.398	28	26
	Area(lymph)_to_Area(ROI)@[inside-tumor]	All	0.50 (0.32~0.79)	0.002	-0.483	207	186
		Stage I	'NaN' (0.00~inf)	0.012	-0.446	45	25
		Stage II	1.57 (0.56~4.42)	0.388	-0.144	44	98
		Stage III	0.60 (0.29~1.25)	0.168	-0.491	61	55
		Stage IV	0.68 (0.30~1.52)	0.347	-0.575	20	34
	Area(micve)_to_Area(ROI)@[inside-tumor]	All	0.46 (0.29~0.71)	0.000	-0.097	229	164
		Stage I	'NaN' (0.00~inf)	0.120	0.923	25	45
		Stage II	0.24 (0.08~0.72)	0.006	-0.444	106	36
		Stage III	0.43 (0.20~0.92)	0.025	-0.423	87	29
		Stage IV	0.67 (0.31~1.48)	0.318	-0.063	23	31
	Area(necro)_to_Area(ROI)@[inside-tumor]	All	0.66 (0.41~1.07)	0.092	-0.369	295	98
		Stage I	0.19 (0.02~2.22)	0.146	-0.417	52	18
		Stage II	0.29 (0.11~0.82)	0.012	-0.351	106	36
		Stage III	1.27 (0.59~2.70)	0.537	-0.090	61	55
		Stage IV	0.49 (0.23~1.07)	0.069	-0.262	34	20
	Area(stroma)_to_Area(ROI)@[inside-tumor]	All	1.24 (0.79~1.94)	0.353	-0.343	142	251
		Stage I	'NaN' (0.00~inf)	0.040	-0.718	29	41
		Stage II	0.55 (0.19~1.56)	0.253	-0.672	75	67
		Stage III	1.60 (0.74~3.46)	0.228	0.132	29	87
		Stage IV	0.37 (0.17~0.81)	0.010	-0.929	40	14
	Area(mucus)_to_Area(ROI)@[inside-tumor]	All	0.78 (0.49~1.25)	0.295	-0.226	295	98
		Stage I	'NaN' (0.00~inf)	0.240	0.261	18	52
		Stage II	0.52 (0.19~1.43)	0.195	-0.187	106	36
		Stage III	0.63 (0.30~1.31)	0.211	-0.169	74	42
		Stage IV	1.80 (0.78~4.16)	0.162	-0.190	34	20
	Area(lymph)_in_Ring_to_Base(epitl)@[inside-tumor]	All	0.49 (0.31~0.77)	0.001	-0.487	229	164
		Stage I	'NaN' (0.00~inf)	0.007	-0.496	48	22
		Stage II	0.36 (0.08~1.61)	0.162	-0.192	36	106
		Stage III	0.56 (0.27~1.18)	0.123	-0.530	80	36
		Stage IV	0.63 (0.29~1.33)	0.225	-0.570	31	23
	Area(micve)_in_Ring_to_Base(epitl)@[inside-tumor]	All	0.38 (0.24~0.60)	0.000	-0.240	229	164
		Stage I	'NaN' (0.00~inf)	0.172	0.390	18	52
		Stage II	0.25 (0.09~0.74)	0.007	-0.415	106	36
		Stage III	0.53 (0.26~1.11)	0.087	-0.240	68	48
		Stage IV	0.48 (0.22~1.04)	0.057	-0.281	28	26
	Area(necro)_in_Ring_to_Base(epitl)@[inside-tumor]	All	0.63 (0.40~0.99)	0.045	-0.286	251	142
		Stage I	0.20 (0.02~2.33)	0.160	-0.420	52	18
		Stage II	0.25 (0.09~0.70)	0.004	-0.358	106	36
		Stage III	1.56 (0.75~3.24)	0.233	0.210	42	74
		Stage IV	0.44 (0.20~0.96)	0.035	-0.237	31	23
	Area(stroma)_in_Ring_to_Base(epitl)@[inside-tumor]	All	1.12 (0.71~1.76)	0.624	-0.408	142	251
		Stage I	'NaN' (0.00~inf)	0.068	-0.559	29	41
		Stage II	0.47 (0.17~1.36)	0.157	-0.561	75	67
		Stage III	1.64 (0.76~3.55)	0.203	-0.157	29	87
		Stage IV	0.45 (0.20~1.00)	0.046	-0.669	40	14
	Area(mucus)_in_Ring_to_Base(epitl)@[inside-tumor]	All	0.73 (0.46~1.15)	0.176	-0.103	186	207
		Stage I	0.36 (0.03~3.99)	0.386	-0.172	41	29
		Stage II	0.44 (0.15~1.28)	0.120	-0.119	83	59
		Stage III	0.69 (0.33~1.45)	0.326	-0.190	80	36
		Stage IV	1.56 (0.73~3.34)	0.254	-0.070	20	34
	Area(lymph)_to_Area(ROI)@[invasive-margin-500]	All	0.54 (0.30~0.98)	0.039	0.773	99	294
		Stage I	'NaN' (0.00~inf)	0.293	-0.303	48	22
		Stage II	2.18 (0.74~6.38)	0.145	0.293	67	75
		Stage III	2.17 (0.83~5.69)	0.108	-0.378	80	36
		Stage IV	1.51 (0.71~3.23)	0.279	-0.278	26	28
	Area(micve)_to_Area(ROI)@[invasive-margin-500]	All	0.67 (0.42~1.06)	0.086	0.160	164	229
		Stage I	'NaN' (0.00~inf)	0.235	-0.278	45	25
		Stage II	0.42 (0.12~1.48)	0.162	0.275	51	91
		Stage III	0.71 (0.34~1.50)	0.373	-0.292	74	42
		Stage IV	0.66 (0.29~1.46)	0.301	0.009	20	34
	Area(necro)_to_Area(ROI)@[invasive-margin-500]	All	0.63 (0.39~1.03)	0.062	-0.345	295	98
		Stage I	2.86 (0.18~45.66)	0.437	0.019	18	52
		Stage II	0.46 (0.16~1.29)	0.130	-0.330	106	36
		Stage III	0.43 (0.20~0.95)	0.033	-0.347	87	29
		Stage IV	1.64 (0.66~4.08)	0.283	-0.329	37	17
	Area(stroma)_to_Area(ROI)@[invasive-margin-500]	All	1.27 (0.80~2.00)	0.304	0.185	120	273
		Stage I	'NaN' (0.00~inf)	0.009	-0.005	18	52
		Stage II	0.24 (0.07~0.89)	0.022	0.021	51	91
		Stage III	1.55 (0.74~3.25)	0.243	0.359	36	80
		Stage IV	0.69 (0.31~1.51)	0.352	0.070	23	31
	Area(mucus)_to_Area(ROI)@[invasive-margin-500]	All	0.70 (0.39~1.25)	0.224	0.940	99	294
		Stage I	'NaN' (0.00~inf)	0.165	0.408	29	41
		Stage II	0.46 (0.16~1.34)	0.142	0.154	75	67
		Stage III	2.13 (0.98~4.59)	0.051	-0.046	61	55
		Stage IV	1.72 (0.80~3.73)	0.165	0.351	17	37

Table S3-2. Detailed results of overall survival K-M analysis in STAD cohort

	FeatureName	Stage	HazardRatio	pval	ZScoreThreshold	n_HighGroup	n_LowGroup
STAD	Area(epitl)_to_Area(ROI)@[inside-tumor]	All	0.68 (0.46~1.00)	0.046	0.322	119	210
		Stage I	0.15 (0.03~0.88)	0.017	0.134	28	12
		Stage II	1.67 (0.76~3.67)	0.195	-0.252	68	38
		Stage III	0.69 (0.43~1.12)	0.130	-0.366	84	60
		Stage IV	0.66 (0.27~1.62)	0.360	-0.367	21	10
	Area(lymph)_to_Area(ROI)@[inside-tumor]	All	1.40 (0.97~2.00)	0.067	0.549	101	228
		Stage I	5.18 (0.58~46.03)	0.103	-0.151	17	23
		Stage II	1.95 (0.95~4.00)	0.064	0.508	33	73
		Stage III	0.80 (0.47~1.36)	0.415	-0.283	108	36
		Stage IV	2.36 (0.92~6.03)	0.065	0.667	8	23
	Area(micve)_to_Area(ROI)@[inside-tumor]	All	0.83 (0.58~1.17)	0.288	0.131	174	155
		Stage I	5.75 (1.04~31.73)	0.024	1.754	10	30
		Stage II	1.83 (0.87~3.84)	0.105	0.407	50	56
		Stage III	0.64 (0.39~1.03)	0.066	-0.078	84	60
		Stage IV	1.71 (0.62~4.67)	0.292	-0.339	21	10
	Area(necro)_to_Area(ROI)@[inside-tumor]	All	0.65 (0.45~0.94)	0.020	-0.240	137	192
		Stage I	0.20 (0.03~1.31)	0.066	-0.340	28	12
		Stage II	1.37 (0.58~3.23)	0.471	-0.527	79	27
		Stage III	0.53 (0.31~0.89)	0.015	-0.151	52	92
		Stage IV	0.52 (0.20~1.40)	0.190	-0.508	23	8
	Area(stroma)_to_Area(ROI)@[inside-tumor]	All	1.48 (1.04~2.09)	0.028	0.090	137	192
		Stage I	'NaN' (0.00~inf)	0.053	-0.843	25	15
		Stage II	0.65 (0.26~1.58)	0.333	0.745	27	79
		Stage III	1.85 (0.99~3.47)	0.050	-0.732	108	36
		Stage IV	0.48 (0.19~1.20)	0.109	-0.646	23	8
	Area(mucus)_to_Area(ROI)@[inside-tumor]	All	0.70 (0.45~1.08)	0.104	-0.069	83	246
		Stage I	'NaN' (0.00~inf)	0.034	-0.026	17	23
		Stage II	1.58 (0.75~3.33)	0.226	-0.205	33	73
		Stage III	0.77 (0.48~1.25)	0.292	-0.313	84	60
		Stage IV	1.56 (0.66~3.69)	0.309	-0.271	15	16
	Area(lymph)_in_Ring_to_Base(epitl)@[inside-tumor]	All	1.40 (0.96~2.04)	0.081	0.503	83	246
		Stage I	4.23 (0.48~37.24)	0.159	-0.214	19	21
		Stage II	0.68 (0.33~1.42)	0.300	-0.145	62	44
		Stage III	1.63 (0.98~2.69)	0.057	0.514	44	100
		Stage IV	2.17 (0.85~5.54)	0.098	0.379	8	23
	Area(micve)_in_Ring_to_Base(epitl)@[inside-tumor]	All	0.71 (0.49~1.04)	0.080	0.319	119	210
		Stage I	6.12 (1.12~33.52)	0.017	0.964	10	30
		Stage II	1.36 (0.66~2.79)	0.401	0.081	50	56
		Stage III	0.60 (0.34~1.06)	0.077	0.613	44	100
		Stage IV	0.57 (0.21~1.57)	0.271	0.198	8	23
	Area(necro)_in_Ring_to_Base(epitl)@[inside-tumor]	All	0.64 (0.45~0.93)	0.017	-0.180	137	192
		Stage I	0.34 (0.07~1.71)	0.171	-0.321	28	12
		Stage II	0.75 (0.37~1.54)	0.437	-0.395	62	44
		Stage III	0.52 (0.31~0.86)	0.010	-0.177	60	84
		Stage IV	1.67 (0.70~3.98)	0.244	-0.341	16	15
	Area(stroma)_in_Ring_to_Base(epitl)@[inside-tumor]	All	1.50 (1.02~2.20)	0.040	-0.489	210	119
		Stage I	'NaN' (0.00~inf)	0.067	-0.668	28	12
		Stage II	2.29 (0.80~6.59)	0.113	-0.575	79	27
		Stage III	1.53 (0.93~2.52)	0.093	0.231	44	100
		Stage IV	0.48 (0.19~1.20)	0.109	-0.534	23	8
	Area(mucus)_in_Ring_to_Base(epitl)@[inside-tumor]	All	0.76 (0.50~1.17)	0.212	-0.090	83	246
		Stage I	'NaN' (0.00~inf)	0.125	0.063	10	30
		Stage II	1.39 (0.67~2.90)	0.371	-0.193	38	68
		Stage III	0.60 (0.37~0.96)	0.033	-0.234	84	60
		Stage IV	2.09 (0.76~5.73)	0.142	-0.230	21	10
	Area(lymph)_to_Area(ROI)@[invasive-margin-500]	All	0.91 (0.64~1.29)	0.595	0.205	155	174
		Stage I	2.55 (0.50~12.94)	0.242	0.795	10	30
		Stage II	1.82 (0.78~4.24)	0.162	-0.090	68	38
		Stage III	0.83 (0.51~1.34)	0.446	0.330	68	76
		Stage IV	2.12 (0.87~5.12)	0.089	0.289	10	21
	Area(micve)_to_Area(ROI)@[invasive-margin-500]	All	0.87 (0.61~1.23)	0.429	0.416	155	174
		Stage I	2.84 (0.56~14.32)	0.187	1.008	10	30
		Stage II	1.89 (0.86~4.15)	0.104	-0.049	62	44
		Stage III	0.76 (0.45~1.29)	0.310	-0.283	108	36
		Stage IV	1.82 (0.76~4.35)	0.175	-0.032	15	16
	Area(necro)_to_Area(ROI)@[invasive-margin-500]	All	0.64 (0.45~0.90)	0.011	-0.276	174	155
		Stage I	0.15 (0.03~0.85)	0.015	-0.225	28	12
		Stage II	0.70 (0.34~1.46)	0.340	-0.260	56	50
		Stage III	0.68 (0.42~1.09)	0.108	-0.314	76	68
		Stage IV	0.72 (0.27~1.91)	0.510	-0.391	23	8
	Area(stroma)_to_Area(ROI)@[invasive-margin-500]	All	1.65 (1.16~2.35)	0.005	0.230	155	174
		Stage I	3.50 (0.64~19.31)	0.125	0.036	15	25
		Stage II	2.07 (1.01~4.26)	0.043	0.560	38	68
		Stage III	1.76 (1.07~2.89)	0.024	0.208	76	68
		Stage IV	0.48 (0.19~1.20)	0.109	-0.856	23	8
	Area(mucus)_to_Area(ROI)@[invasive-margin-500]	All	0.67 (0.47~0.96)	0.028	-0.214	155	174
		Stage I	0.46 (0.09~2.33)	0.339	-0.223	25	15
		Stage II	1.62 (0.69~3.82)	0.265	-0.343	79	27
		Stage III	0.58 (0.34~0.97)	0.036	-0.361	108	36
		Stage IV	1.29 (0.54~3.07)	0.569	-0.323	18	13

Table S3-3. Detailed results of overall survival K-M analysis in LUAD cohort

	FeatureName	Stage	HazardRatio	pval	ZScoreThreshold	n_HighGroup	n_LowGroup
LUAD	Area(epitl)_to_Area(ROI)@[inside-tumor]	All	1.16 (0.83~1.62)	0.377	-0.515	228	204
		Stage I	0.74 (0.39~1.40)	0.357	0.093	60	179
		Stage II	0.53 (0.26~1.06)	0.067	-0.138	33	74
		Stage III	2.09 (0.96~4.56)	0.058	0.501	14	42
		Stage IV	0.48 (0.14~1.60)	0.222	-0.184	15	8
	Area(lymph)_to_Area(ROI)@[inside-tumor]	All	0.69 (0.48~0.99)	0.041	-0.361	324	108
		Stage I	0.72 (0.40~1.30)	0.269	-0.276	179	60
		Stage II	0.75 (0.41~1.39)	0.362	-0.353	74	33
		Stage III	0.65 (0.29~1.44)	0.286	-0.001	26	30
		Stage IV	0.16 (0.04~0.72)	0.007	-0.638	16	7
	Area(micve)_to_Area(ROI)@[inside-tumor]	All	0.67 (0.43~1.04)	0.073	0.750	108	324
		Stage I	1.33 (0.76~2.32)	0.314	-0.094	139	100
		Stage II	0.69 (0.33~1.43)	0.314	0.690	27	80
		Stage III	0.41 (0.17~0.98)	0.038	-0.067	23	33
		Stage IV	0.30 (0.09~0.95)	0.030	-0.666	16	7
	Area(necro)_to_Area(ROI)@[inside-tumor]	All	1.72 (1.22~2.44)	0.002	0.146	108	324
		Stage I	1.95 (1.07~3.56)	0.027	-0.439	126	113
		Stage II	2.16 (1.18~3.98)	0.011	0.682	27	80
		Stage III	0.60 (0.23~1.57)	0.290	0.380	14	42
		Stage IV	2.05 (0.69~6.15)	0.189	-0.294	12	11
	Area(stroma)_to_Area(ROI)@[inside-tumor]	All	1.18 (0.80~1.74)	0.395	-0.673	324	108
		Stage I	0.69 (0.39~1.23)	0.206	-0.183	113	126
		Stage II	2.25 (1.01~5.04)	0.042	-0.634	80	27
		Stage III	0.58 (0.27~1.25)	0.158	-0.730	42	14
		Stage IV	3.50 (1.05~11.63)	0.030	-0.412	8	15
	Area(mucus)_to_Area(ROI)@[inside-tumor]	All	1.47 (1.00~2.16)	0.046	-0.289	300	132
		Stage I	1.50 (0.84~2.69)	0.167	-0.256	139	100
		Stage II	1.27 (0.64~2.51)	0.488	-0.287	80	27
		Stage III	1.92 (0.84~4.38)	0.113	-0.238	33	23
		Stage IV	0.28 (0.06~1.26)	0.077	-0.056	7	16
	Area(lymph)_in_Ring_to_Base(epitl)@[inside-tumor]	All	0.67 (0.47~0.95)	0.025	-0.299	324	108
		Stage I	0.68 (0.38~1.21)	0.184	-0.212	179	60
		Stage II	1.29 (0.72~2.31)	0.385	0.115	51	56
		Stage III	0.38 (0.18~0.80)	0.008	-0.282	39	17
		Stage IV	0.21 (0.06~0.72)	0.007	-0.470	13	10
	Area(micve)_in_Ring_to_Base(epitl)@[inside-tumor]	All	0.69 (0.46~1.03)	0.065	0.356	132	300
		Stage I	1.54 (0.88~2.70)	0.129	-0.060	139	100
		Stage II	0.61 (0.29~1.27)	0.181	0.553	27	80
		Stage III	0.42 (0.20~0.88)	0.018	-0.281	36	20
		Stage IV	2.36 (0.70~7.91)	0.153	-0.299	10	13
	Area(necro)_in_Ring_to_Base(epitl)@[inside-tumor]	All	1.88 (1.33~2.66)	0.000	-0.344	228	204
		Stage I	2.52 (1.39~4.55)	0.002	-0.333	113	126
		Stage II	1.85 (0.99~3.43)	0.049	0.334	27	80
		Stage III	0.66 (0.27~1.63)	0.366	0.245	17	39
		Stage IV	2.23 (0.61~8.20)	0.215	-0.426	17	6
	Area(stroma)_in_Ring_to_Base(epitl)@[inside-tumor]	All	1.12 (0.80~1.57)	0.493	-0.336	252	180
		Stage I	1.29 (0.73~2.27)	0.377	-0.315	139	100
		Stage II	1.79 (0.93~3.46)	0.077	-0.352	68	39
		Stage III	0.51 (0.25~1.07)	0.068	-0.407	33	23
		Stage IV	2.28 (0.69~7.56)	0.167	-0.364	8	15
	Area(mucus)_in_Ring_to_Base(epitl)@[inside-tumor]	All	1.36 (0.97~1.92)	0.075	-0.060	132	300
		Stage I	1.63 (0.88~3.02)	0.115	-0.210	153	86
		Stage II	1.70 (0.95~3.04)	0.069	-0.050	39	68
		Stage III	1.92 (0.91~4.06)	0.083	-0.054	17	39
		Stage IV	0.28 (0.06~1.26)	0.077	-0.094	7	16
	Area(lymph)_to_Area(ROI)@[invasive-margin-500]	All	0.84 (0.60~1.17)	0.301	-0.339	180	252
		Stage I	1.19 (0.64~2.21)	0.572	0.243	60	179
		Stage II	0.80 (0.44~1.46)	0.464	-0.213	39	68
		Stage III	1.88 (0.77~4.57)	0.157	-0.587	39	17
		Stage IV	0.38 (0.11~1.29)	0.110	-0.582	10	13
	Area(micve)_to_Area(ROI)@[invasive-margin-500]	All	1.12 (0.79~1.59)	0.525	0.115	132	300
		Stage I	1.60 (0.91~2.83)	0.102	0.056	73	166
		Stage II	0.52 (0.29~0.94)	0.027	-0.375	51	56
		Stage III	1.33 (0.54~3.29)	0.528	-0.738	42	14
		Stage IV	0.45 (0.15~1.39)	0.157	-0.401	13	10
	Area(necro)_to_Area(ROI)@[invasive-margin-500]	All	1.57 (1.11~2.22)	0.010	-0.193	108	324
		Stage I	1.80 (1.03~3.15)	0.037	-0.300	60	179
		Stage II	2.32 (1.27~4.24)	0.005	0.405	27	80
		Stage III	0.42 (0.17~1.04)	0.053	-0.088	17	39
		Stage IV	0.68 (0.22~2.10)	0.503	-0.257	10	13
	Area(stroma)_to_Area(ROI)@[invasive-margin-500]	All	0.73 (0.52~1.03)	0.073	-0.981	300	132
		Stage I	0.48 (0.23~1.03)	0.055	0.238	60	179
		Stage II	0.74 (0.41~1.32)	0.302	-0.880	68	39
		Stage III	0.68 (0.29~1.59)	0.372	-0.508	39	17
		Stage IV	0.74 (0.25~2.17)	0.586	-1.041	15	8
	Area(mucus)_to_Area(ROI)@[invasive-margin-500]	All	2.12 (1.40~3.23)	0.000	-0.353	300	132
		Stage I	2.38 (1.02~5.58)	0.039	-0.391	179	60
		Stage II	1.87 (0.92~3.80)	0.077	-0.342	80	27
		Stage III	1.36 (0.65~2.84)	0.408	-0.252	26	30
		Stage IV	0.27 (0.09~0.84)	0.018	-0.242	13	10

Table S3-4. Detailed results of overall survival K-M analysis in LUSC cohort

	FeatureName	Stage	HazardRatio	pval	ZScoreThreshold	n_HighGroup	n_LowGroup
LUSC	Area(epitl)_to_Area(ROI)@[inside-tumor]	All	0.51 (0.35~0.75)	0.000	-0.080	155	275
		Stage I	0.36 (0.19~0.67)	0.001	-0.133	75	133
		Stage II	0.42 (0.21~0.85)	0.012	0.022	50	89
		Stage III	0.63 (0.31~1.28)	0.198	-0.080	31	42
		Stage IV	'NaN' (0.00~inf)	0.117	-0.331	3	3
	Area(lymph)_to_Area(ROI)@[inside-tumor]	All	0.83 (0.60~1.14)	0.253	0.306	203	227
		Stage I	0.72 (0.42~1.24)	0.231	0.559	75	133
		Stage II	0.67 (0.35~1.28)	0.222	-0.282	104	35
		Stage III	0.51 (0.26~0.99)	0.044	0.262	35	38
		Stage IV	'NaN' (0.00~inf)	0.480	0.299	2	4
	Area(micve)_to_Area(ROI)@[inside-tumor]	All	1.77 (1.14~2.74)	0.009	-0.580	322	108
		Stage I	2.27 (1.15~4.47)	0.015	-0.447	144	64
		Stage II	0.82 (0.46~1.46)	0.494	-0.050	66	73
		Stage III	2.01 (0.97~4.17)	0.056	-0.330	43	30
		Stage IV	0.47 (0.04~5.68)	0.549	0.192	2	4
	Area(necro)_to_Area(ROI)@[inside-tumor]	All	1.39 (1.00~1.93)	0.050	0.316	227	203
		Stage I	1.27 (0.76~2.12)	0.353	0.263	110	98
		Stage II	1.78 (0.99~3.18)	0.049	0.531	58	81
		Stage III	1.76 (0.88~3.53)	0.107	0.412	39	34
		Stage IV	'NaN' (0.00~inf)	0.480	0.496	2	4
	Area(stroma)_to_Area(ROI)@[inside-tumor]	All	1.66 (1.20~2.29)	0.002	-0.083	179	251
		Stage I	1.65 (0.99~2.73)	0.051	-0.164	98	110
		Stage II	1.80 (1.01~3.22)	0.044	-0.114	58	81
		Stage III	2.06 (1.06~4.00)	0.030	0.040	35	38
		Stage IV	0.39 (0.03~4.44)	0.433	-0.752	3	3
	Area(mucus)_to_Area(ROI)@[inside-tumor]	All	0.82 (0.59~1.14)	0.231	-0.303	275	155
		Stage I	0.79 (0.47~1.31)	0.359	-0.304	133	75
		Stage II	0.68 (0.37~1.24)	0.207	-0.254	58	81
		Stage III	0.74 (0.38~1.47)	0.394	-0.303	51	22
		Stage IV	'NaN' (0.00~inf)	0.480	-0.304	4	2
	Area(lymph)_in_Ring_to_Base(epitl)@[inside-tumor]	All	0.87 (0.62~1.20)	0.386	0.420	179	251
		Stage I	1.58 (0.82~3.03)	0.166	-0.203	156	52
		Stage II	1.35 (0.74~2.43)	0.325	0.158	73	66
		Stage III	0.47 (0.24~0.92)	0.024	0.267	35	38
		Stage IV	'NaN' (0.00~inf)	0.046	-0.219	4	2
	Area(micve)_in_Ring_to_Base(epitl)@[inside-tumor]	All	1.58 (1.14~2.19)	0.006	0.277	132	298
		Stage I	2.13 (1.11~4.10)	0.020	-0.311	144	64
		Stage II	0.74 (0.41~1.32)	0.300	-0.210	73	66
		Stage III	2.73 (1.31~5.69)	0.005	-0.229	39	34
		Stage IV	0.39 (0.03~4.44)	0.433	-0.216	3	3
	Area(necro)_in_Ring_to_Base(epitl)@[inside-tumor]	All	1.46 (1.02~2.10)	0.037	0.093	275	155
		Stage I	1.45 (0.87~2.44)	0.154	1.108	64	144
		Stage II	2.46 (1.19~5.10)	0.012	0.089	89	50
		Stage III	1.80 (0.93~3.50)	0.078	0.652	31	42
		Stage IV	'NaN' (0.00~inf)	0.480	0.503	2	4
	Area(stroma)_in_Ring_to_Base(epitl)@[inside-tumor]	All	1.58 (1.14~2.18)	0.005	-0.156	179	251
		Stage I	2.31 (1.17~4.55)	0.013	-0.430	144	64
		Stage II	1.86 (1.04~3.32)	0.033	-0.091	50	89
		Stage III	1.77 (0.91~3.45)	0.087	-0.169	35	38
		Stage IV	'NaN' (0.00~inf)	0.157	-0.617	4	2
	Area(mucus)_in_Ring_to_Base(epitl)@[inside-tumor]	All	1.27 (0.92~1.75)	0.152	-0.206	203	227
		Stage I	1.44 (0.86~2.42)	0.165	-0.169	64	144
		Stage II	0.72 (0.38~1.37)	0.308	-0.161	43	96
		Stage III	1.23 (0.64~2.37)	0.529	-0.202	31	42
		Stage IV	'NaN' (0.00~inf)	0.480	-0.231	4	2
	Area(lymph)_to_Area(ROI)@[invasive-margin-500]	All	0.67 (0.46~0.98)	0.036	0.362	132	298
		Stage I	0.52 (0.28~0.98)	0.039	0.293	64	144
		Stage II	0.50 (0.28~0.90)	0.019	-0.423	89	50
		Stage III	0.59 (0.28~1.26)	0.166	0.542	23	50
		Stage IV	'NaN' (0.00~inf)	0.157	-0.666	4	2
	Area(micve)_to_Area(ROI)@[invasive-margin-500]	All	1.45 (1.01~2.09)	0.042	-0.669	275	155
		Stage I	1.68 (0.99~2.85)	0.052	-0.551	110	98
		Stage II	0.71 (0.39~1.26)	0.236	-0.385	73	66
		Stage III	1.64 (0.85~3.16)	0.137	-0.158	31	42
		Stage IV	0.47 (0.04~5.68)	0.549	0.145	2	4
	Area(necro)_to_Area(ROI)@[invasive-margin-500]	All	1.30 (0.93~1.84)	0.127	0.298	132	298
		Stage I	0.80 (0.47~1.34)	0.393	-0.345	144	64
		Stage II	2.36 (1.19~4.65)	0.011	-0.286	89	50
		Stage III	1.58 (0.79~3.18)	0.195	0.441	19	54
		Stage IV	'NaN' (0.00~inf)	0.117	-0.278	3	3
	Area(stroma)_to_Area(ROI)@[invasive-margin-500]	All	1.27 (0.92~1.75)	0.152	-0.169	179	251
		Stage I	1.36 (0.82~2.28)	0.235	-0.537	110	98
		Stage II	1.70 (0.92~3.12)	0.085	0.535	35	104
		Stage III	0.67 (0.32~1.38)	0.273	-0.911	55	18
		Stage IV	0.47 (0.04~5.68)	0.549	-0.660	2	4
	Area(mucus)_to_Area(ROI)@[invasive-margin-500]	All	0.83 (0.59~1.16)	0.269	-0.186	155	275
		Stage I	0.61 (0.35~1.07)	0.082	-0.204	75	133
		Stage II	0.67 (0.35~1.29)	0.231	-0.366	104	35
		Stage III	1.51 (0.75~3.04)	0.242	-0.119	19	54
		Stage IV	'NaN' (0.00~inf)	0.046	-0.077	2	4

Table S3-5. Detailed results of overall survival K-M analysis in BRCA cohort

	FeatureName	Stage	HazardRatio	pval	ZScoreThreshold	n_HighGroup	n_LowGroup
BRCA	Area(epitl)_to_Area(ROI)@[inside-tumor]	All	1.33 (0.84~2.11)	0.224	0.455	244	730
		Stage I	0.66 (0.12~3.64)	0.635	-0.212	79	88
		Stage II	2.15 (0.98~4.71)	0.051	-0.402	351	198
		Stage III	0.81 (0.41~1.58)	0.529	-0.571	139	79
		Stage IV	4.47 (1.11~17.99)	0.024	-0.238	11	6
	Area(lymph)_to_Area(ROI)@[inside-tumor]	All	0.62 (0.41~0.94)	0.021	-0.683	568	406
		Stage I	0.20 (0.02~1.70)	0.101	-0.550	70	97
		Stage II	0.52 (0.22~1.25)	0.136	-0.052	138	411
		Stage III	0.68 (0.35~1.32)	0.249	-0.733	139	79
		Stage IV	0.74 (0.22~2.47)	0.619	-0.794	11	6
	Area(micve)_to_Area(ROI)@[inside-tumor]	All	0.75 (0.50~1.15)	0.186	-0.224	406	568
		Stage I	'NaN' (0.00~inf)	0.210	-0.674	125	42
		Stage II	1.60 (0.73~3.52)	0.236	-0.514	351	198
		Stage III	2.30 (0.81~6.52)	0.107	-0.730	163	55
		Stage IV	1.61 (0.47~5.54)	0.445	-0.104	5	12
	Area(necro)_to_Area(ROI)@[inside-tumor]	All	1.37 (0.89~2.12)	0.148	-0.494	244	730
		Stage I	0.28 (0.03~2.39)	0.213	-0.561	60	107
		Stage II	1.70 (0.87~3.33)	0.116	-0.488	138	411
		Stage III	1.25 (0.64~2.43)	0.510	-0.569	91	127
		Stage IV	4.40 (1.22~15.88)	0.014	-0.554	7	10
	Area(stroma)_to_Area(ROI)@[inside-tumor]	All	0.71 (0.47~1.07)	0.104	0.293	568	406
		Stage I	'NaN' (0.00~inf)	0.166	0.042	116	51
		Stage II	0.42 (0.18~0.96)	0.034	0.696	198	351
		Stage III	0.67 (0.34~1.33)	0.250	0.200	151	67
		Stage IV	0.21 (0.04~1.00)	0.033	1.169	5	12
	Area(mucus)_to_Area(ROI)@[inside-tumor]	All	1.56 (1.01~2.41)	0.044	-0.268	244	730
		Stage I	0.50 (0.09~2.72)	0.411	-0.320	79	88
		Stage II	1.61 (0.70~3.68)	0.255	-0.353	412	137
		Stage III	2.26 (1.16~4.43)	0.014	-0.320	91	127
		Stage IV	2.58 (0.74~9.01)	0.124	-0.272	5	12
	Area(lymph)_in_Ring_to_Base(epitl)@[inside-tumor]	All	0.58 (0.38~0.87)	0.008	-0.608	676	298
		Stage I	0.16 (0.02~1.37)	0.056	-0.470	79	88
		Stage II	0.51 (0.21~1.22)	0.124	-0.162	138	411
		Stage III	0.54 (0.28~1.05)	0.065	-0.596	139	79
		Stage IV	0.76 (0.22~2.64)	0.663	-0.653	12	5
	Area(micve)_in_Ring_to_Base(epitl)@[inside-tumor]	All	0.65 (0.39~1.08)	0.091	0.071	244	730
		Stage I	0.60 (0.11~3.31)	0.557	-0.081	70	97
		Stage II	1.49 (0.62~3.57)	0.373	-0.493	412	137
		Stage III	0.55 (0.26~1.15)	0.107	-0.057	79	139
		Stage IV	0.42 (0.11~1.69)	0.210	-0.526	13	4
	Area(necro)_in_Ring_to_Base(epitl)@[inside-tumor]	All	1.31 (0.84~2.02)	0.230	-0.461	244	730
		Stage I	0.24 (0.03~2.09)	0.163	-0.519	60	107
		Stage II	1.62 (0.81~3.25)	0.168	-0.545	290	259
		Stage III	1.20 (0.61~2.35)	0.594	-0.514	79	139
		Stage IV	4.40 (1.22~15.88)	0.014	-0.510	7	10
	Area(stroma)_in_Ring_to_Base(epitl)@[inside-tumor]	All	0.66 (0.44~1.00)	0.050	-0.153	622	352
		Stage I	'NaN' (0.00~inf)	0.204	-0.338	125	42
		Stage II	0.48 (0.22~1.06)	0.062	0.213	198	351
		Stage III	0.73 (0.36~1.48)	0.382	-0.091	151	67
		Stage IV	0.21 (0.04~1.00)	0.033	0.431	5	12
	Area(mucus)_in_Ring_to_Base(epitl)@[inside-tumor]	All	1.60 (1.05~2.43)	0.026	-0.214	298	676
		Stage I	2.00 (0.40~9.94)	0.386	-0.220	60	107
		Stage II	1.39 (0.68~2.82)	0.366	-0.208	138	411
		Stage III	2.01 (1.03~3.93)	0.037	-0.237	91	127
		Stage IV	0.44 (0.13~1.49)	0.176	-0.229	10	7
	Area(lymph)_to_Area(ROI)@[invasive-margin-500]	All	0.61 (0.40~0.92)	0.017	-0.616	514	460
		Stage I	0.17 (0.02~1.47)	0.068	-0.605	79	88
		Stage II	0.53 (0.28~1.02)	0.054	-0.631	320	229
		Stage III	1.42 (0.71~2.82)	0.317	-0.444	67	151
		Stage IV	0.53 (0.16~1.78)	0.295	-0.743	10	7
	Area(micve)_to_Area(ROI)@[invasive-margin-500]	All	0.74 (0.46~1.17)	0.189	-0.627	730	244
		Stage I	4.69 (0.55~40.19)	0.120	-0.009	79	88
		Stage II	0.80 (0.36~1.76)	0.578	0.291	138	411
		Stage III	1.53 (0.77~3.05)	0.219	0.182	55	163
		Stage IV	0.62 (0.16~2.38)	0.485	-0.101	5	12
	Area(necro)_to_Area(ROI)@[invasive-margin-500]	All	1.45 (0.96~2.18)	0.076	-0.407	352	622
		Stage I	0.37 (0.07~2.04)	0.237	-0.415	88	79
		Stage II	1.47 (0.76~2.82)	0.250	-0.407	198	351
		Stage III	1.49 (0.70~3.17)	0.301	-0.414	139	79
		Stage IV	5.64 (1.42~22.48)	0.006	-0.404	8	9
	Area(stroma)_to_Area(ROI)@[invasive-margin-500]	All	1.56 (1.03~2.35)	0.035	0.501	460	514
		Stage I	0.25 (0.03~2.17)	0.177	0.298	70	97
		Stage II	0.58 (0.30~1.15)	0.117	-0.156	412	137
		Stage III	1.84 (0.92~3.65)	0.078	1.249	55	163
		Stage IV	0.50 (0.14~1.74)	0.267	1.085	7	10
	Area(mucus)_to_Area(ROI)@[invasive-margin-500]	All	1.95 (1.28~2.95)	0.001	-0.358	460	514
		Stage I	'NaN' (0.00~inf)	0.148	-0.406	125	42
		Stage II	2.00 (0.91~4.39)	0.079	-0.396	381	168
		Stage III	2.15 (1.08~4.28)	0.026	-0.349	103	115
		Stage IV	3.53 (1.01~12.27)	0.035	-0.226	5	12

Table S3-6. Detailed results of overall survival K-M analysis in PAAD cohort

	FeatureName	Stage	HazardRatio	pval	ZScoreThreshold	n_HighGroup	n_LowGroup
PAAD	Area(epitl)_to_Area(ROI)@[inside-tumor]	All	0.66 (0.39~1.11)	0.111	-0.935	40	119
		Stage I	'NaN' (0.00~inf)	0.076	-0.963	4	12
		Stage II	1.43 (0.82~2.49)	0.203	-1.979	100	34
		Stage III	'NaN' (0.00~inf)	0.317	-1.924	2	1
		Stage IV	0.35 (0.02~5.89)	0.450	-1.640	4	1
	Area(lymph)_to_Area(ROI)@[inside-tumor]	All	1.34 (0.84~2.13)	0.222	-0.440	40	119
		Stage I	0.34 (0.07~1.70)	0.168	-0.750	12	4
		Stage II	0.84 (0.51~1.38)	0.496	-0.494	41	93
		Stage III	'NaN' (0.00~inf)	0.317	-0.778	2	1
		Stage IV	'NaN' (0.00~inf)	0.221	0.006	2	3
	Area(micve)_to_Area(ROI)@[inside-tumor]	All	1.79 (1.07~2.99)	0.024	-0.865	110	49
		Stage I	'NaN' (0.00~inf)	0.105	-0.745	11	5
		Stage II	1.81 (1.09~3.02)	0.021	-0.782	85	49
		Stage III	'NaN' (0.00~inf)	0.317	-0.955	2	1
		Stage IV	'NaN' (0.00~inf)	0.221	-0.453	2	3
	Area(necro)_to_Area(ROI)@[inside-tumor]	All	1.51 (0.90~2.55)	0.118	-0.555	119	40
		Stage I	3.37 (0.60~18.80)	0.142	-0.451	4	12
		Stage II	1.22 (0.71~2.10)	0.467	-0.550	100	34
		Stage III	'NaN' (0.00~inf)	0.317	-0.556	2	1
		Stage IV	'NaN' (0.00~inf)	0.117	0.102	3	2
	Area(stroma)_to_Area(ROI)@[inside-tumor]	All	1.36 (0.82~2.26)	0.229	1.216	119	40
		Stage I	2.87 (0.33~24.69)	0.316	1.195	11	5
		Stage II	1.37 (0.79~2.36)	0.257	1.288	100	34
		Stage III	'NaN' (0.00~inf)	0.317	1.630	2	1
		Stage IV	'NaN' (0.00~inf)	0.388	0.012	4	1
	Area(mucus)_to_Area(ROI)@[inside-tumor]	All	1.20 (0.76~1.90)	0.436	-0.095	49	110
		Stage I	'NaN' (0.00~inf)	0.150	-0.002	4	12
		Stage II	1.30 (0.77~2.19)	0.325	-0.304	100	34
		Stage III	'NaN' (0.00~inf)	0.317	-0.333	2	1
		Stage IV	'NaN' (0.00~inf)	0.281	-0.341	3	2
	Area(lymph)_in_Ring_to_Base(epitl)@[inside-tumor]	All	1.43 (0.92~2.23)	0.113	-0.202	49	110
		Stage I	5.48 (0.87~34.48)	0.043	-0.313	5	11
		Stage II	1.20 (0.74~1.93)	0.457	-0.200	41	93
		Stage III	'NaN' (0.00~inf)	0.317	-0.529	2	1
		Stage IV	'NaN' (0.00~inf)	0.221	-0.215	2	3
	Area(micve)_in_Ring_to_Base(epitl)@[inside-tumor]	All	1.51 (0.95~2.41)	0.081	-0.284	101	58
		Stage I	3.59 (0.70~18.27)	0.102	0.610	4	12
		Stage II	1.41 (0.86~2.31)	0.170	-0.295	85	49
		Stage III	'NaN' (0.00~inf)	0.317	-0.513	2	1
		Stage IV	'NaN' (0.00~inf)	0.281	-0.138	2	3
	Area(necro)_in_Ring_to_Base(epitl)@[inside-tumor]	All	1.76 (1.03~3.00)	0.037	-0.467	119	40
		Stage I	2.91 (0.53~15.98)	0.199	-0.517	8	8
		Stage II	0.72 (0.44~1.16)	0.174	-0.125	49	85
		Stage III	'NaN' (0.00~inf)	0.317	-0.497	2	1
		Stage IV	'NaN' (0.00~inf)	0.117	0.306	3	2
	Area(stroma)_in_Ring_to_Base(epitl)@[inside-tumor]	All	1.62 (0.96~2.74)	0.067	0.708	119	40
		Stage I	'NaN' (0.00~inf)	0.076	0.438	12	4
		Stage II	1.32 (0.77~2.27)	0.317	0.741	100	34
		Stage III	'NaN' (0.00~inf)	0.317	0.849	2	1
		Stage IV	'NaN' (0.00~inf)	0.388	-0.088	4	1
	Area(mucus)_in_Ring_to_Base(epitl)@[inside-tumor]	All	1.32 (0.86~2.02)	0.199	-0.104	75	84
		Stage I	7.92 (0.92~68.21)	0.026	-0.098	8	8
		Stage II	1.21 (0.77~1.91)	0.414	-0.104	63	71
		Stage III	'NaN' (0.00~inf)	0.317	-0.197	1	2
		Stage IV	'NaN' (0.00~inf)	0.281	-0.242	3	2
	Area(lymph)_to_Area(ROI)@[invasive-margin-500]	All	1.36 (0.87~2.14)	0.180	-0.490	101	58
		Stage I	3.76 (0.62~22.84)	0.123	0.076	4	12
		Stage II	1.30 (0.80~2.10)	0.287	-0.489	85	49
		Stage III	'NaN' (0.00~inf)	0.317	-0.506	2	1
		Stage IV	'NaN' (0.00~inf)	0.221	-0.380	2	3
	Area(micve)_to_Area(ROI)@[invasive-margin-500]	All	1.70 (0.98~2.93)	0.055	-0.760	119	40
		Stage I	2.76 (0.32~23.68)	0.335	-0.353	11	5
		Stage II	1.39 (0.88~2.18)	0.156	-0.001	56	78
		Stage III	'NaN' (0.00~inf)	0.317	-0.608	2	1
		Stage IV	'NaN' (0.00~inf)	0.221	-0.390	2	3
	Area(necro)_to_Area(ROI)@[invasive-margin-500]	All	1.35 (0.88~2.08)	0.170	-0.388	66	93
		Stage I	0.40 (0.08~1.98)	0.244	-0.410	12	4
		Stage II	1.35 (0.85~2.16)	0.206	-0.401	78	56
		Stage III	'NaN' (0.00~inf)	0.317	-0.413	2	1
		Stage IV	'NaN' (0.00~inf)	0.221	-0.184	2	3
	Area(stroma)_to_Area(ROI)@[invasive-margin-500]	All	0.74 (0.48~1.13)	0.160	0.919	84	75
		Stage I	2.61 (0.52~13.10)	0.228	1.210	5	11
		Stage II	0.68 (0.43~1.08)	0.098	1.042	63	71
		Stage III	'NaN' (0.00~inf)	0.317	0.427	2	1
		Stage IV	'NaN' (0.00~inf)	0.281	0.651	2	3
	Area(mucus)_to_Area(ROI)@[invasive-margin-500]	All	1.99 (1.28~3.09)	0.002	-0.362	84	75
		Stage I	3.93 (0.70~21.90)	0.094	-0.329	7	9
		Stage II	1.84 (1.14~2.97)	0.011	-0.373	78	56
		Stage III	'NaN' (0.00~inf)	0.317	-0.395	2	1
		Stage IV	'NaN' (0.00~inf)	0.281	-0.360	3	2

Table S3-7. Detailed results of overall survival K-M analysis in UCEC cohort

	FeatureName	Stage	HazardRatio	pval	ZScoreThreshold	n_HighGroup	n_LowGroup
UCEC	Area(epitl)_to_Area(ROI)@[inside-tumor]	All	0.47 (0.29~0.76)	0.002	0.626	347	116
		Stage I	0.70 (0.30~1.64)	0.409	0.995	171	122
		Stage II	0.10 (0.01~0.93)	0.012	0.724	32	11
		Stage III	0.31 (0.12~0.82)	0.012	1.010	43	59
		Stage IV	2.84 (0.76~10.53)	0.107	0.599	19	6
	Area(lymph)_to_Area(ROI)@[inside-tumor]	All	0.51 (0.31~0.83)	0.006	-0.585	347	116
		Stage I	0.11 (0.01~0.80)	0.008	0.048	90	203
		Stage II	0.29 (0.04~2.09)	0.194	-0.689	32	11
		Stage III	0.52 (0.24~1.13)	0.095	-0.495	71	31
		Stage IV	0.30 (0.09~1.01)	0.042	0.199	8	17
	Area(micve)_to_Area(ROI)@[inside-tumor]	All	1.54 (0.93~2.57)	0.091	0.002	116	347
		Stage I	3.54 (1.49~8.43)	0.002	-0.172	90	203
		Stage II	3.00 (0.31~28.99)	0.320	-0.413	23	20
		Stage III	1.28 (0.59~2.80)	0.535	-0.619	59	43
		Stage IV	0.37 (0.10~1.33)	0.113	0.136	7	18
	Area(necro)_to_Area(ROI)@[inside-tumor]	All	2.20 (1.36~3.54)	0.001	-0.063	142	321
		Stage I	2.51 (1.01~6.21)	0.040	-0.306	138	155
		Stage II	6.34 (0.66~60.95)	0.066	-0.158	13	30
		Stage III	1.83 (0.82~4.07)	0.135	0.011	26	76
		Stage IV	2.15 (0.80~5.79)	0.119	0.144	9	16
	Area(stroma)_to_Area(ROI)@[inside-tumor]	All	2.41 (1.49~3.89)	0.000	-0.621	116	347
		Stage I	1.97 (0.83~4.69)	0.117	-0.886	90	203
		Stage II	0.32 (0.05~2.29)	0.232	-1.300	32	11
		Stage III	2.61 (1.19~5.72)	0.012	-0.795	43	59
		Stage IV	0.56 (0.19~1.66)	0.289	-0.460	9	16
	Area(mucus)_to_Area(ROI)@[inside-tumor]	All	0.48 (0.30~0.78)	0.002	-0.267	270	193
		Stage I	1.81 (0.75~4.38)	0.179	-0.189	138	155
		Stage II	0.49 (0.05~4.71)	0.526	-0.203	18	25
		Stage III	0.23 (0.09~0.62)	0.001	-0.260	43	59
		Stage IV	1.69 (0.54~5.27)	0.361	-0.336	16	9
	Area(lymph)_in_Ring_to_Base(epitl)@[inside-tumor]	All	0.54 (0.33~0.88)	0.012	-0.543	347	116
		Stage I	0.18 (0.04~0.77)	0.009	-0.256	106	187
		Stage II	0.29 (0.04~2.09)	0.194	-0.610	32	11
		Stage III	0.52 (0.24~1.13)	0.091	-0.466	71	31
		Stage IV	0.20 (0.05~0.76)	0.011	0.259	7	18
	Area(micve)_in_Ring_to_Base(epitl)@[inside-tumor]	All	2.04 (1.25~3.33)	0.004	-0.274	116	347
		Stage I	3.82 (1.62~9.02)	0.001	-0.297	74	219
		Stage II	4.60 (0.48~44.40)	0.147	-0.394	18	25
		Stage III	1.78 (0.80~3.97)	0.153	-0.271	26	76
		Stage IV	0.41 (0.14~1.18)	0.090	-0.512	12	13
	Area(necro)_in_Ring_to_Base(epitl)@[inside-tumor]	All	2.17 (1.35~3.49)	0.001	-0.143	142	321
		Stage I	2.38 (1.00~5.65)	0.042	-0.113	74	219
		Stage II	6.34 (0.66~60.95)	0.066	-0.201	13	30
		Stage III	1.93 (0.90~4.17)	0.088	-0.139	31	71
		Stage IV	1.78 (0.66~4.80)	0.248	0.029	11	14
	Area(stroma)_in_Ring_to_Base(epitl)@[inside-tumor]	All	2.57 (1.59~4.14)	0.000	-0.559	116	347
		Stage I	2.25 (0.66~7.63)	0.182	-0.813	220	73
		Stage II	0.32 (0.05~2.29)	0.232	-0.808	32	11
		Stage III	2.45 (1.12~5.36)	0.020	-0.615	43	59
		Stage IV	0.41 (0.13~1.30)	0.119	-0.482	8	17
	Area(mucus)_in_Ring_to_Base(epitl)@[inside-tumor]	All	0.56 (0.35~0.91)	0.016	-0.232	296	167
		Stage I	1.99 (0.84~4.72)	0.112	-0.178	122	171
		Stage II	1.62 (0.23~11.54)	0.628	-0.196	18	25
		Stage III	0.38 (0.16~0.86)	0.016	-0.224	48	54
		Stage IV	0.41 (0.13~1.28)	0.114	-0.195	8	17
	Area(lymph)_to_Area(ROI)@[invasive-margin-500]	All	0.48 (0.30~0.77)	0.002	-0.322	296	167
		Stage I	'NaN' (0.00~inf)	0.003	0.576	74	219
		Stage II	0.26 (0.04~1.83)	0.143	-0.616	32	11
		Stage III	0.50 (0.23~1.10)	0.077	-0.464	76	26
		Stage IV	0.38 (0.13~1.10)	0.065	-0.654	19	6
	Area(micve)_to_Area(ROI)@[invasive-margin-500]	All	0.44 (0.27~0.73)	0.001	-0.676	347	116
		Stage I	0.54 (0.20~1.49)	0.227	0.602	90	203
		Stage II	0.11 (0.01~1.01)	0.017	-0.722	30	13
		Stage III	0.38 (0.13~1.09)	0.062	0.806	26	76
		Stage IV	0.38 (0.12~1.15)	0.077	0.063	11	14
	Area(necro)_to_Area(ROI)@[invasive-margin-500]	All	1.99 (1.22~3.24)	0.005	-0.180	116	347
		Stage I	2.25 (0.95~5.34)	0.059	-0.220	74	219
		Stage II	4.24 (0.44~40.79)	0.173	-0.296	18	25
		Stage III	1.68 (0.79~3.58)	0.176	-0.272	37	65
		Stage IV	0.56 (0.19~1.62)	0.275	-0.369	19	6
	Area(stroma)_to_Area(ROI)@[invasive-margin-500]	All	0.73 (0.44~1.20)	0.215	-0.829	321	142
		Stage I	0.56 (0.23~1.39)	0.207	-1.093	220	73
		Stage II	0.09 (0.01~0.86)	0.008	-1.113	32	11
		Stage III	1.35 (0.62~2.95)	0.450	0.566	31	71
		Stage IV	0.38 (0.13~1.13)	0.071	-0.416	15	10
	Area(mucus)_to_Area(ROI)@[invasive-margin-500]	All	0.77 (0.48~1.24)	0.287	-0.345	244	219
		Stage I	1.51 (0.64~3.59)	0.346	-0.227	90	203
		Stage II	7.58 (0.79~72.94)	0.039	-0.254	13	30
		Stage III	0.70 (0.31~1.56)	0.377	-0.380	71	31
		Stage IV	0.11 (0.02~0.50)	0.001	-0.289	12	13

Table S3-8. Detailed results of overall survival K-M analysis in OV cohort

	FeatureName	Stage	HazardRatio	pval	ZScoreThreshold	n_HighGroup	n_LowGroup
OV	Area(epitl)_to_Area(ROI)@[inside-tumor]	All	1.21 (0.73~1.99)	0.460	0.840	41	56
		Stage I	'NaN' (0.00~inf)	0.317	0.946	1	1
		Stage II	NaN				
		Stage III	0.84 (0.43~1.63)	0.594	-0.097	52	18
		Stage IV	0.72 (0.28~1.86)	0.499	1.047	10	11
	Area(lymph)_to_Area(ROI)@[inside-tumor]	All	1.75 (1.02~3.01)	0.041	-0.802	62	35
		Stage I	'NaN' (0.00~inf)	0.317	-0.097	1	1
		Stage II	NaN				
		Stage III	2.18 (1.09~4.36)	0.024	-0.779	45	25
		Stage IV	6.03 (1.58~23.03)	0.004	-0.804	11	10
	Area(micve)_to_Area(ROI)@[inside-tumor]	All	0.67 (0.37~1.22)	0.191	-0.159	25	72
		Stage I	'NaN' (0.00~inf)	0.317	0.212	1	1
		Stage II	NaN				
		Stage III	1.48 (0.78~2.78)	0.229	-0.663	41	29
		Stage IV	0.19 (0.06~0.66)	0.004	-0.571	12	9
	Area(necro)_to_Area(ROI)@[inside-tumor]	All	0.70 (0.42~1.16)	0.162	-0.469	51	46
		Stage I	'NaN' (0.00~inf)	0.317	-0.544	1	1
		Stage II	NaN				
		Stage III	0.66 (0.35~1.23)	0.181	-0.462	41	29
		Stage IV	2.88 (0.81~10.21)	0.088	-0.575	16	5
	Area(stroma)_to_Area(ROI)@[inside-tumor]	All	1.29 (0.78~2.13)	0.320	-0.333	41	56
		Stage I	'NaN' (0.00~inf)	0.317	-1.151	1	1
		Stage II	NaN				
		Stage III	1.43 (0.78~2.64)	0.240	-0.582	37	33
		Stage IV	2.69 (0.89~8.15)	0.068	-0.337	7	14
	Area(mucus)_to_Area(ROI)@[inside-tumor]	All	0.41 (0.25~0.69)	0.000	-0.286	62	35
		Stage I	'NaN' (0.00~inf)	0.317	-0.338	1	1
		Stage II	NaN				
		Stage III	0.48 (0.26~0.89)	0.018	-0.266	45	25
		Stage IV	0.46 (0.18~1.23)	0.116	-0.302	10	11
	Area(lymph)_in_Ring_to_Base(epitl)@[inside-tumor]	All	1.88 (1.08~3.25)	0.023	-0.656	62	35
		Stage I	'NaN' (0.00~inf)	0.317	-0.240	1	1
		Stage II	NaN				
		Stage III	2.29 (1.09~4.79)	0.025	-0.652	48	22
		Stage IV	6.03 (1.58~23.03)	0.004	-0.662	11	10
	Area(micve)_in_Ring_to_Base(epitl)@[inside-tumor]	All	1.36 (0.81~2.28)	0.246	-0.549	57	40
		Stage I	'NaN' (0.00~inf)	0.317	-0.264	1	1
		Stage II	NaN				
		Stage III	1.97 (1.03~3.77)	0.037	-0.556	41	29
		Stage IV	0.19 (0.04~0.87)	0.018	-0.426	6	15
	Area(necro)_in_Ring_to_Base(epitl)@[inside-tumor]	All	0.66 (0.40~1.10)	0.110	-0.479	57	40
		Stage I	'NaN' (0.00~inf)	0.317	-0.526	1	1
		Stage II	NaN				
		Stage III	0.57 (0.30~1.08)	0.077	-0.484	45	25
		Stage IV	2.88 (0.81~10.21)	0.088	-0.542	16	5
	Area(stroma)_in_Ring_to_Base(epitl)@[inside-tumor]	All	1.34 (0.73~2.48)	0.344	-0.674	73	24
		Stage I	'NaN' (0.00~inf)	0.317	-0.754	1	1
		Stage II	NaN				
		Stage III	1.51 (0.78~2.91)	0.213	-0.111	18	52
		Stage IV	2.01 (0.67~6.08)	0.201	-0.428	6	15
	Area(mucus)_in_Ring_to_Base(epitl)@[inside-tumor]	All	0.44 (0.26~0.73)	0.001	-0.235	67	30
		Stage I	'NaN' (0.00~inf)	0.317	-0.255	1	1
		Stage II	NaN				
		Stage III	0.41 (0.22~0.76)	0.004	-0.176	37	33
		Stage IV	0.51 (0.20~1.29)	0.152	-0.242	12	9
	Area(lymph)_to_Area(ROI)@[invasive-margin-500]	All	1.61 (0.97~2.68)	0.062	-0.691	51	46
		Stage I	'NaN' (0.00~inf)	0.317	0.383	1	1
		Stage II	NaN				
		Stage III	1.78 (0.95~3.34)	0.070	-0.706	41	29
		Stage IV	0.70 (0.27~1.82)	0.452	-0.726	13	8
	Area(micve)_to_Area(ROI)@[invasive-margin-500]	All	0.86 (0.52~1.42)	0.562	-0.182	46	51
		Stage I	'NaN' (0.00~inf)	0.317	0.036	1	1
		Stage II	NaN				
		Stage III	1.37 (0.65~2.88)	0.403	0.199	18	52
		Stage IV	0.28 (0.09~0.88)	0.020	-0.769	16	5
	Area(necro)_to_Area(ROI)@[invasive-margin-500]	All	1.34 (0.75~2.40)	0.320	-0.395	67	30
		Stage I	'NaN' (0.00~inf)	0.317	-0.338	1	1
		Stage II	NaN				
		Stage III	1.75 (0.84~3.66)	0.134	-0.389	48	22
		Stage IV	1.28 (0.42~3.93)	0.666	-0.401	16	5
	Area(stroma)_to_Area(ROI)@[invasive-margin-500]	All	1.23 (0.74~2.03)	0.423	0.529	51	46
		Stage I	'NaN' (0.00~inf)	0.317	-0.618	1	1
		Stage II	NaN				
		Stage III	1.33 (0.67~2.66)	0.408	0.188	48	22
		Stage IV	1.83 (0.71~4.73)	0.207	0.733	10	11
	Area(mucus)_to_Area(ROI)@[invasive-margin-500]	All	0.54 (0.32~0.89)	0.013	-0.309	57	40
		Stage I	'NaN' (0.00~inf)	0.317	-0.336	1	1
		Stage II	NaN				
		Stage III	0.49 (0.25~0.99)	0.040	-0.184	25	45
		Stage IV	0.60 (0.24~1.54)	0.287	-0.309	9	12

3.4 CORRELATION WITH MOLECULAR FEATURES

3.4.1 Spearman correlation

Based on the correlation between tissue features and molecular features described in the main article, we noticed that some cases exhibit extremely high Spearman correlation coefficients (with absolute value exceeding 0.5). These cases are presented in Table S3-9 and visualized in scatter plot form in Figure S3-9.

Table S3-9. Tissue feature- molecular feature pairs with high Spearman correlation

Cohort	Tissue feature	Molecular feature	Spearman Corr
BRCA	Area(lymph)_in_Ring_to_Base(epitl)@[inside-tumor]	Leukocyte Fraction	0.543
BRCA	Area(lymph)_in_Ring_to_Base(epitl)@[inside-tumor]	Lymphocyte Infiltration Signature Score	0.584
BRCA	Area(lymph)_in_Ring_to_Base(epitl)@[inside-tumor]	TCR Shannon	0.518
BRCA	Area(lymph)_in_Ring_to_Base(epitl)@[inside-tumor]	TCR Richness	0.545
BRCA	Area(lymph)_to_Area(ROI)@[inside-tumor]	Leukocyte Fraction	0.509
BRCA	Area(lymph)_to_Area(ROI)@[inside-tumor]	Lymphocyte Infiltration Signature Score	0.544
BRCA	Area(lymph)_to_Area(ROI)@[inside-tumor]	TCR Richness	0.515
LUAD	Area(lymph)_in_Ring_to_Base(epitl)@[inside-tumor]	Lymphocyte Infiltration Signature Score	0.556
LUAD	Area(lymph)_to_Area(ROI)@[inside-tumor]	Lymphocyte Infiltration Signature Score	0.553
LUAD	Area(necro)_to_Area(ROI)@[inside-tumor]	Proliferation	0.513
STAD	Area(stroma)_in_Ring_to_Base(epitl)@[inside-tumor]	Proliferation	-0.528
STAD	Area(stroma)_in_Ring_to_Base(epitl)@[inside-tumor]	Wound Healing	-0.501

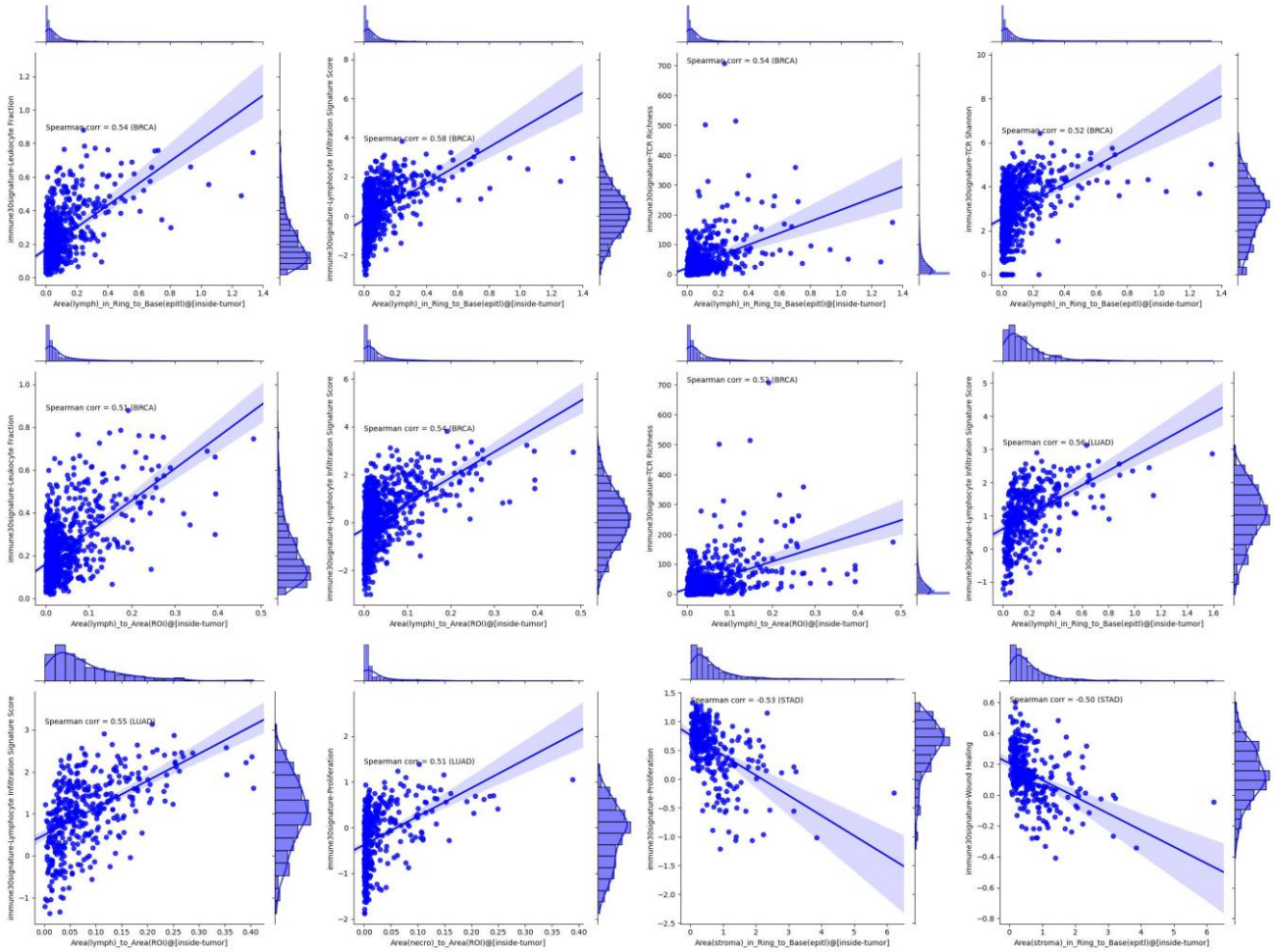

Figure S3-9. Scatter plots for high Spearman correlated cases. The figure shows 7, 3, 2 cases from BRCA, LUAD, and STAD cohort respectively, with the order from top to bottom, and from left to right.

Similar to the approach described in the main article to obtain Figure 6, we investigated the correlation between a total of 160 immune signatures[19] and the 16 representative tissue features. We identified numerous variable pairs that exhibited significant Spearman correlation, as shown in Figures S3-10. Overall, COAD and BRCA demonstrated a higher number of significant correlated pairs.

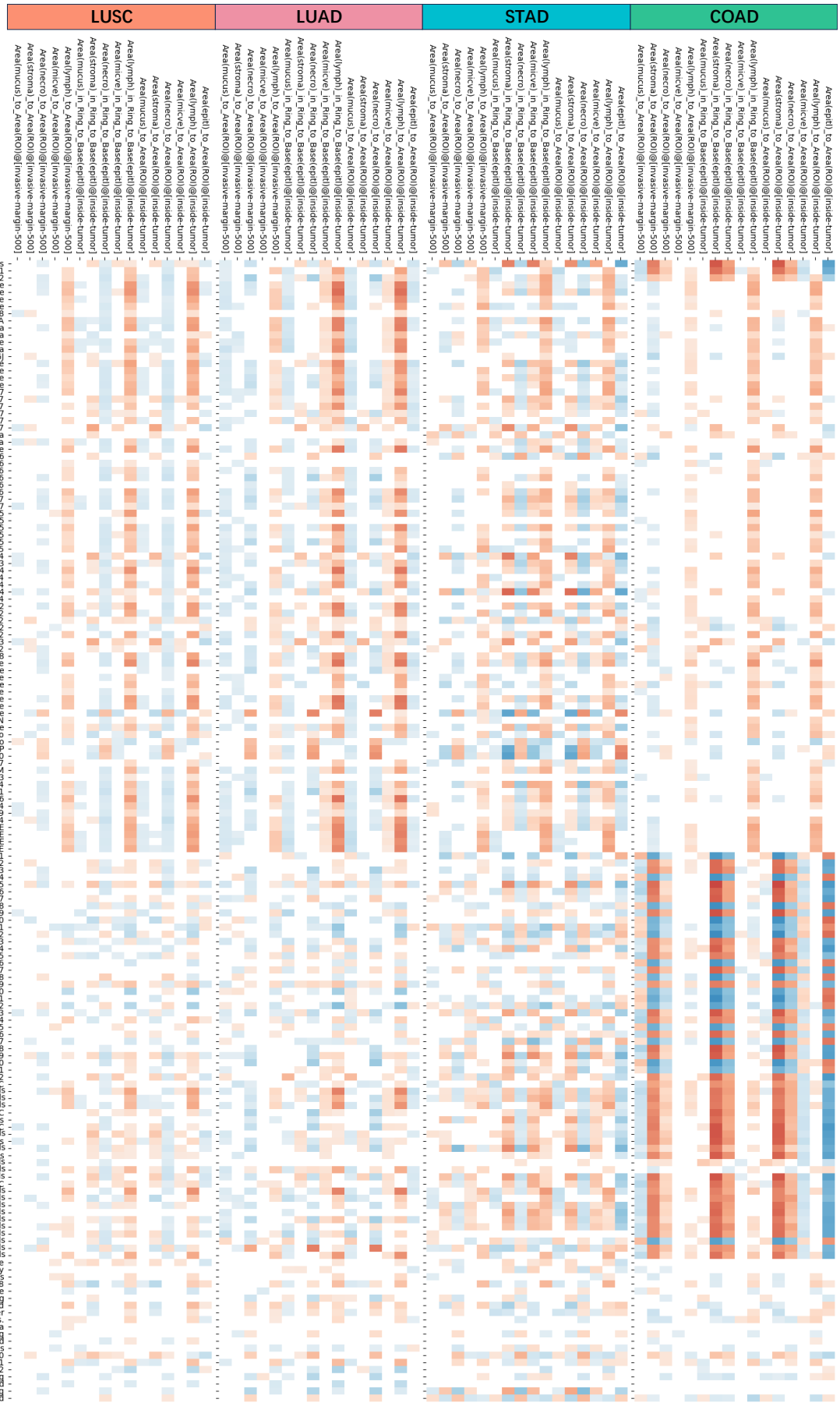

Figure S3-10. Spearman correlation between 16 representative tissue features and 160 immune signatures

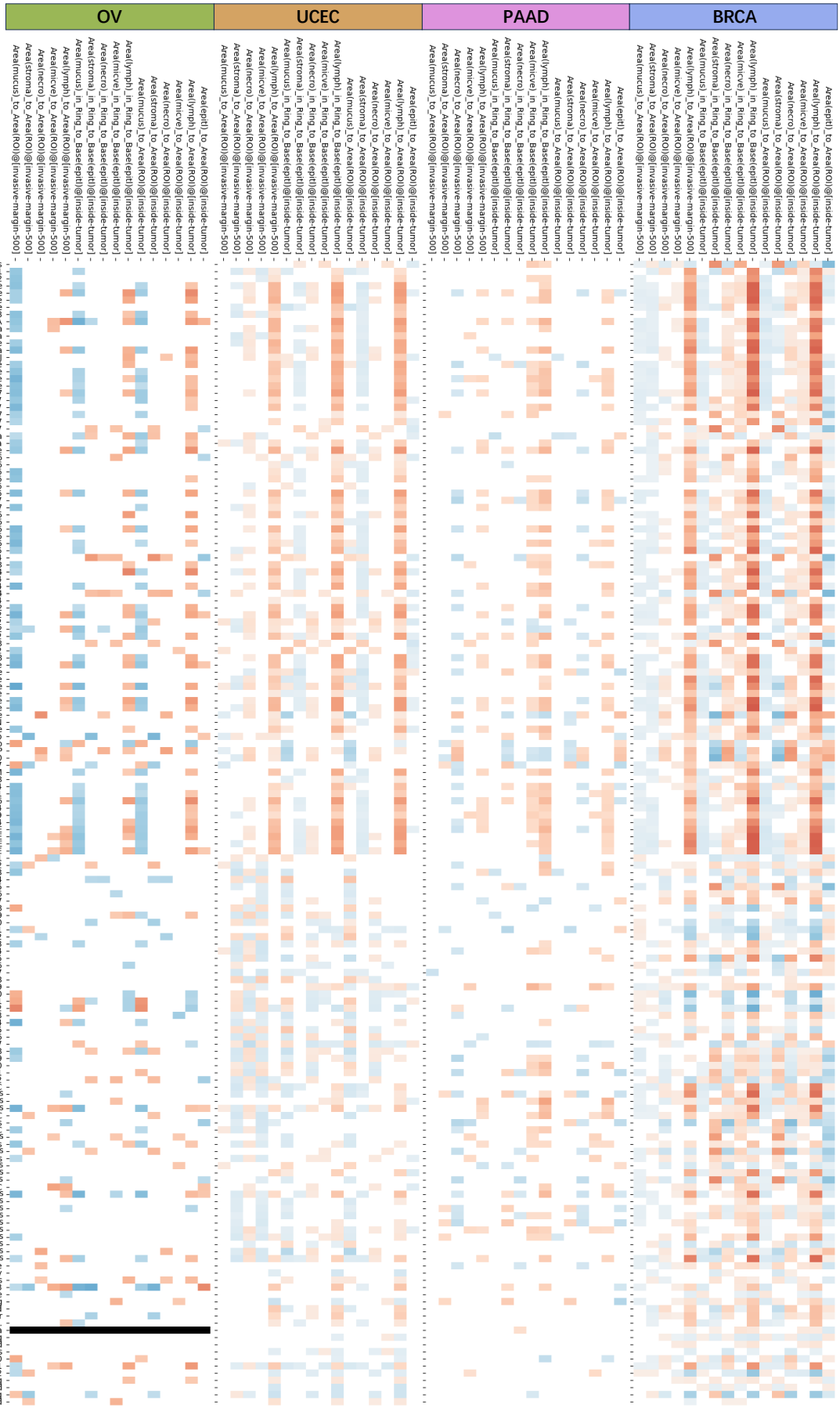

Figure S3-10. *(Continue)*

3.4.2 Mann-Whitney U Test for immune subtypes

We also investigated the differences in tissue features among the six immune subtypes[19] in each cohort. The corresponding boxplots are shown in Figure S3-11. Paired Mann-Whitney U tests were used to compare the medians of tissue characteristics among up to six immune subtypes. The results are summarized in Table S3-9.

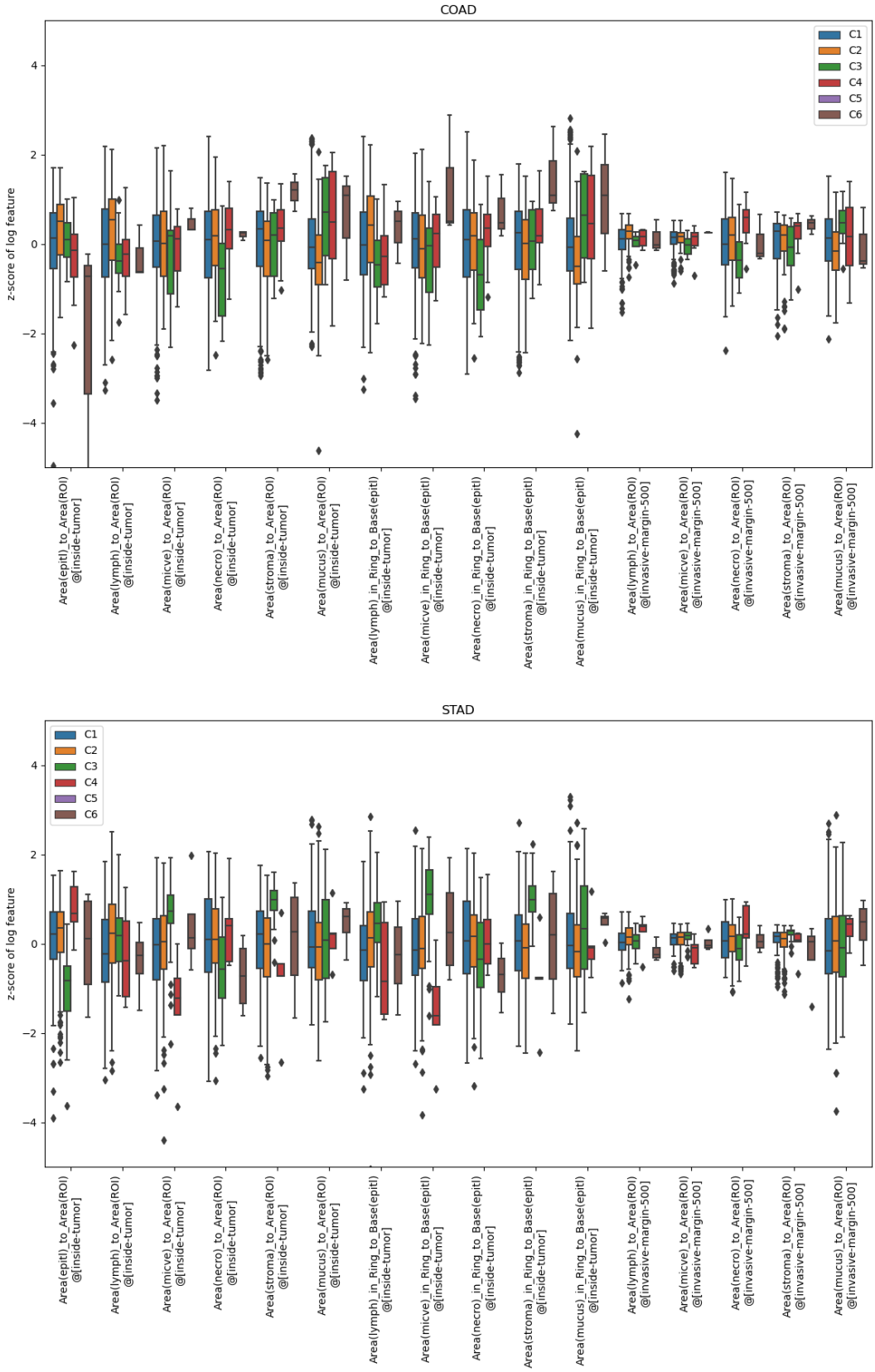

Figure S3-11. Boxplot of tissue features among 6 immune subtypes.

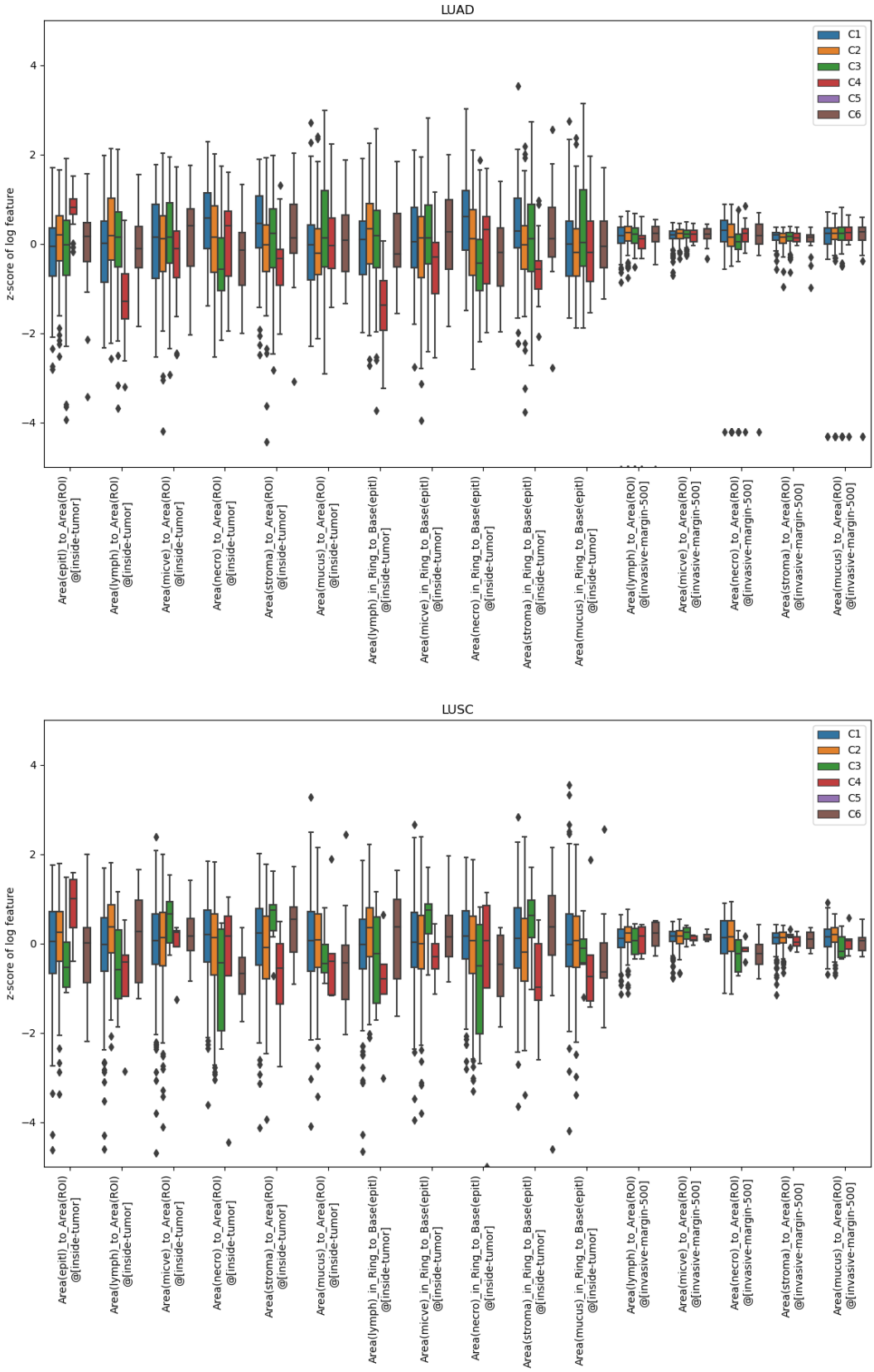

Figure S3-11. *(Continue)*

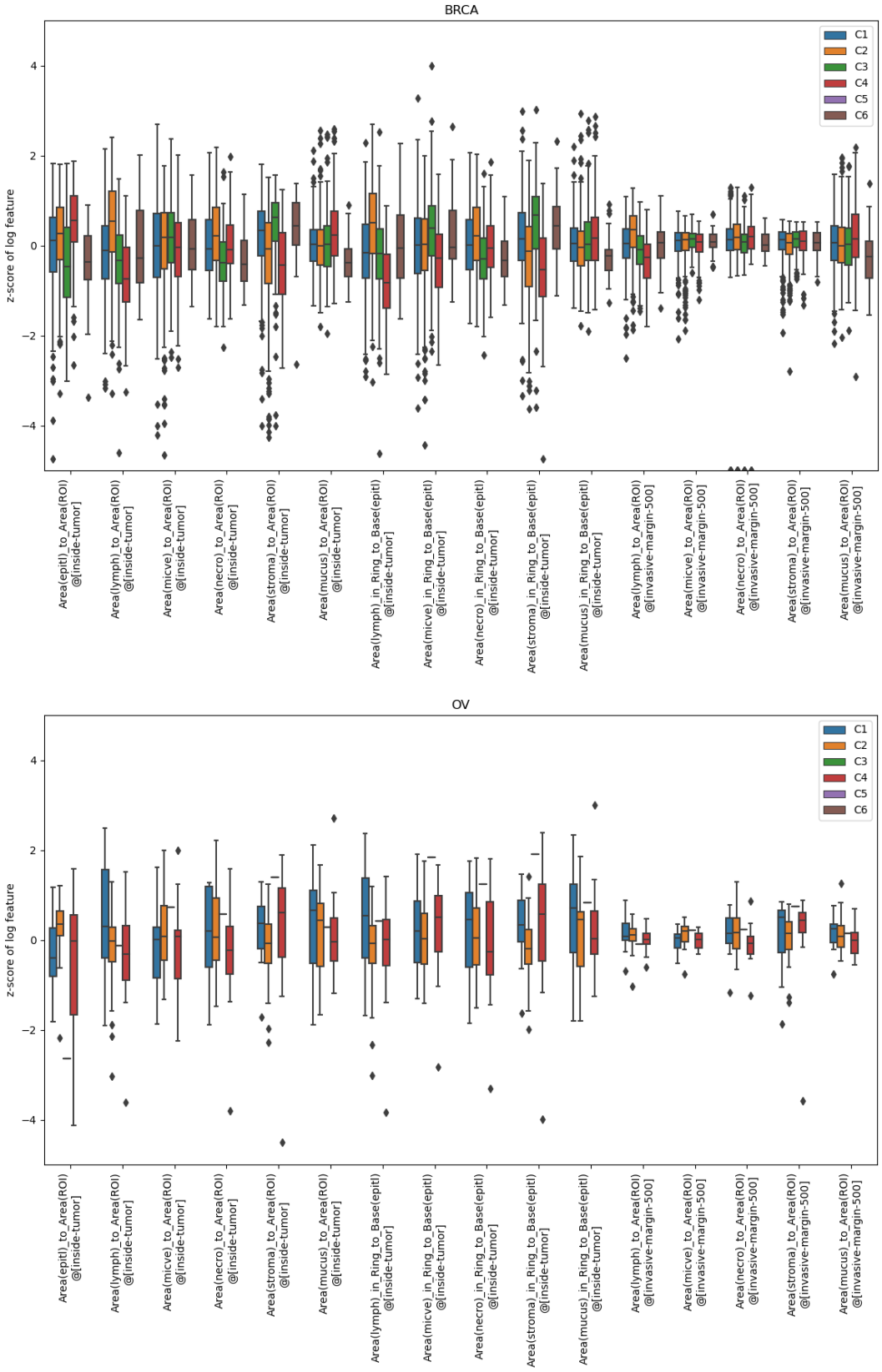

Figure S3-11. *(Continue)*

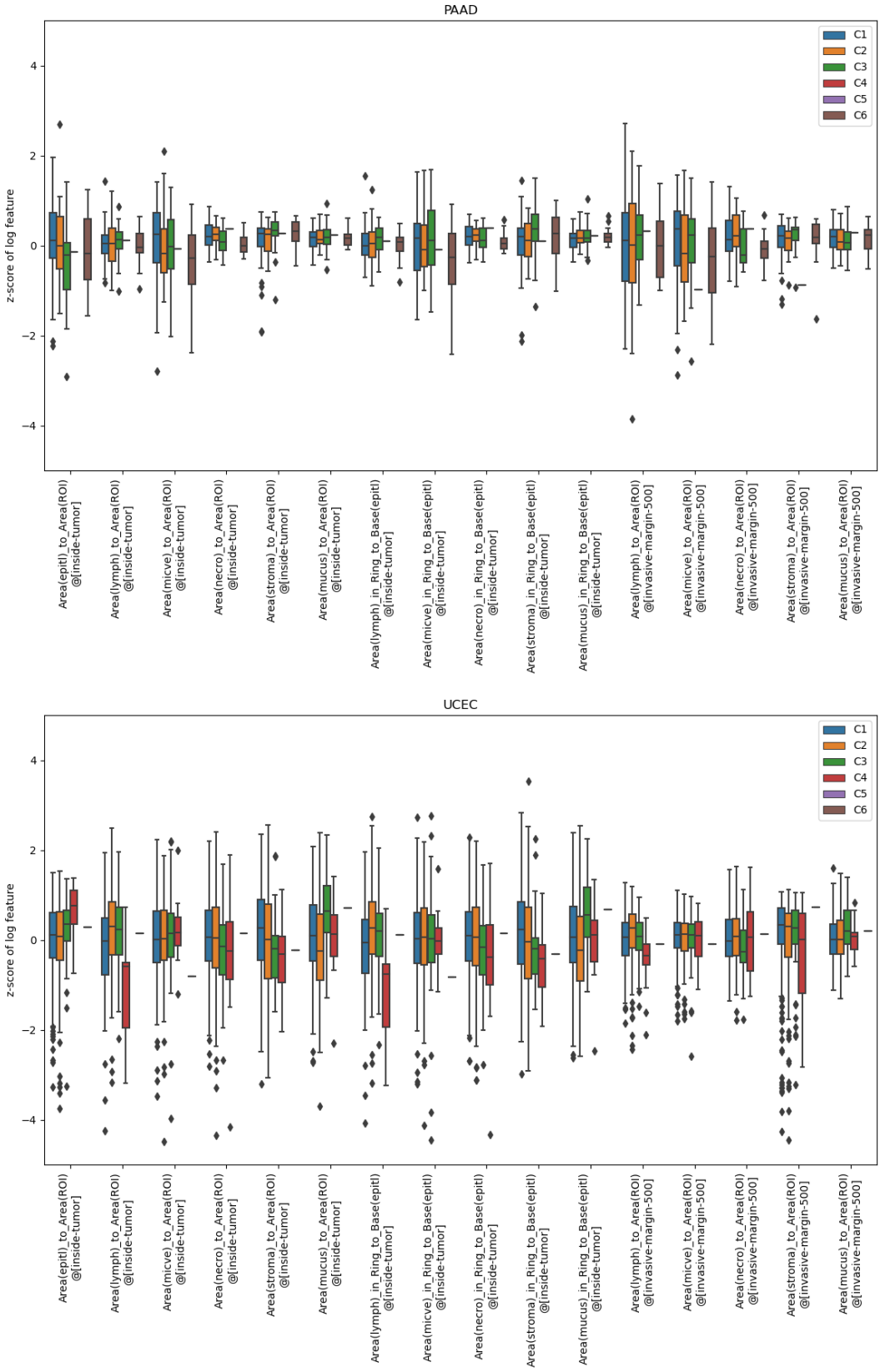

Figure S3-11. *(Continue)*

Table S3-9. Summary of Mann-Whitney U Test for tissue features among immune subtypes. n_sig in the table means the number of immune subcluster pairs that have significant different median in corresponding tissue feature.

	Cohort	COAD	STAD	LUAD	LUSC	BRCA	PAAD	UCEC	OV
Immune subtype	C1	304	110	75	251	338	53	219	12
	C2	77	167	129	167	370	29	175	31
	C3	8	31	154	6	170	35	49	1
	C4	12	5	19	5	82	1	16	15
	C5	0	0	0	0	0	0	0	0
	C6	3	4	23	14	36	18	1	0
	n_subtype_pairs	10	10	10	10	10	10	10	6
Mann-Whitney U	n_sig Area(epitl)_to_Area(ROI)@[inside-tumor]	3	3	6	0	9	1	3	1
	n_sig Area(lymph)_to_Area(ROI)@[inside-tumor]	2	1	5	2	7	0	4	0
	n_sig Area(micve)_to_Area(ROI)@[inside-tumor]	0	6	0	0	3	0	0	0
	n_sig Area(necro)_to_Area(ROI)@[inside-tumor]	1	2	5	2	8	1	1	0
	n_sig Area(stroma)_to_Area(ROI)@[inside-tumor]	3	3	5	1	8	2	3	0
	n_sig Area(mucus)_to_Area(ROI)@[inside-tumor]	3	0	2	1	7	0	4	0
	n_sig Area(lymph)_in_Ring_to_Base(epitl)@[inside-tumor]	1	3	5	2	7	0	4	0
	n_sig Area(micve)_in_Ring_to_Base(epitl)@[inside-tumor]	0	5	4	0	6	0	0	0
	n_sig Area(necro)_in_Ring_to_Base(epitl)@[inside-tumor]	0	2	5	2	7	2	1	0
	n_sig Area(stroma)_in_Ring_to_Base(epitl)@[inside-tumor]	4	3	6	1	8	2	3	1
	n_sig Area(mucus)_in_Ring_to_Base(epitl)@[inside-tumor]	3	1	2	1	7	0	4	0
	n_sig Area(lymph)_to_Area(ROI)@[invasive-margin-500]	2	1	2	1	8	0	5	0
	n_sig Area(micve)_to_Area(ROI)@[invasive-margin-500]	1	4	0	0	0	0	0	2
	n_sig Area(necro)_to_Area(ROI)@[invasive-margin-500]	2	2	5	2	5	4	2	0
	n_sig Area(stroma)_to_Area(ROI)@[invasive-margin-500]	0	3	0	0	2	0	0	0
	n_sig Area(mucus)_to_Area(ROI)@[invasive-margin-500]	2	0	0	2	5	0	2	0

3.4.3 Predict molecular feature by tissue features

To assess the predictability from tissue features to molecular-level features, we established LASSO models for each of the 33 immunological signatures as the prediction targets. Specifically, we first removed data with NaN labels, then converted continuous labels into binary labels using the median value. Subsequently, we evaluated the predictive performance of the models via five-fold cross-validation. During each cross-validation fold, a logistic regression model was trained using the LogisticRegressionCV method from sklearn libraray (https://scikit-learn.org/), inside which the hyperparameters are tuned inner 5-fold cross-validation. The model used an 'l1' penalty and the 'liblinear' solver. Once the model was fine-tuned, it was applied to the outer cross-validation test set to record the false positive rate (FPR) and true positive rate (TPR), which were then used to calculate the area under the receiver operating characteristic curve (AUROC). The average AUROC results for each predicted molecular features are reported in Table S3-10. It can be observed that there are numerous items with AUC ⩾ 0.6. Even without considering the feature obtained from the calculation of TIL Regional Fraction (7th row), some immune signatures still had AUC values exceeding 0.75.

Table S3-10. AUC of LASSO models to classify molecular signatures. Cases that AUC∈[0.6,0.7), AUC∈[0.7,0.75), and AUC⩾0.75 are marked with blue, orange, and pink, respectively.

Signature\Cohort	COAD	STAD	LUAD	LUSC	BRCA	PAAD	UCEC	OV	PAN-CAN
hrd&tp53-HRD_Score	0.657	0.612	0.665	0.648	0.711	0.514	0.613	0.500	0.668
hrd&tp53-tp53_score	0.722	0.617	0.660	0.627	0.773	0.482	0.695	0.417	0.721
tmb-TMB	0.648	0.664	0.619	0.554	0.628	0.522	0.693	0.476	0.760
immune30signature-Leukocyte Fraction	0.709	0.707	0.704	0.713	0.750	0.597	0.645	0.585	0.771
immune30signature-Stromal Fraction	0.692	0.654	0.676	0.621	0.717	0.500	0.622	0.433	0.751
immune30signature-Intratumor Heterogeneity	0.622	0.622	0.615	0.468	0.672	0.500	0.564	0.474	0.652
immune30signature-TIL Regional Fraction	0.819	0.853	0.872	0.838	0.873	0.751	0.792		0.866
immune30signature-Proliferation	0.613	0.750	0.739	0.629	0.788	0.460	0.620	0.434	0.776
immune30signature-Wound Healing	0.657	0.721	0.727	0.662	0.759	0.602	0.645	0.697	0.785
immune30signature-Macrophage Regulation	0.607	0.723	0.694	0.656	0.730	0.601	0.629	0.621	0.746
immune30signature-Lymphocyte Infiltration Signature Score	0.682	0.717	0.751	0.740	0.762	0.524	0.666	0.634	0.770
immune30signature-IFN-gamma Response	0.595	0.509	0.611	0.523	0.652	0.403	0.491	0.444	0.617
immune30signature-TGF-beta Response	0.672	0.716	0.667	0.692	0.733	0.483	0.567	0.478	0.758
immune30signature-SNV Neoantigens	0.579	0.408	0.655	0.548	0.645	0.562	0.686	0.683	0.773
immune30signature-Indel Neoantigens	0.656		0.582	0.497	0.573	0.465	0.658		0.659
immune30signature-Silent Mutation Rate	0.583	0.682	0.663	0.474	0.645	0.479	0.729	0.390	0.772
immune30signature-Nonsilent Mutation Rate	0.515	0.709	0.672	0.542	0.659	0.550	0.681	0.429	0.776
immune30signature-Fraction Altered (Copy number burden score)	0.653	0.664	0.634	0.619	0.654	0.644	0.668	0.534	0.640
immune30signature-Aneuploidy Score	0.581	0.589	0.591	0.553	0.581	0.514	0.665	0.699	0.537
immune30signature-Homologous Recombination Defects	0.673	0.572	0.668	0.626	0.712	0.626	0.644	0.461	0.664
immune30signature-BCR Evenness	0.500	0.471	0.487	0.615	0.554	0.553	0.581	0.639	0.510
immune30signature-BCR Shannon	0.660	0.593	0.647	0.668	0.738	0.682	0.551	0.509	0.718
immune30signature-BCR Richness	0.586	0.578	0.649	0.666	0.742	0.456	0.367	0.591	0.721
immune30signature-TCR Shannon	0.573	0.648	0.668	0.652	0.742	0.573	0.575	0.569	0.694
immune30signature-TCR Richness	0.619	0.655	0.689	0.665	0.755	0.483	0.683	0.611	0.707
immune30signature-TCR Evenness	0.565	0.573	0.504	0.500	0.486	0.462	0.420	0.437	0.500
immune30signature-CTA Score	0.528	0.574	0.604	0.491	0.623	0.491	0.565	0.388	0.668
immune30signature-Lymphocytes	0.618	0.653	0.672	0.669	0.709	0.565	0.608	0.595	0.698
immune30signature-Neutrophils	0.502	0.572	0.582	0.464	0.527	0.504	0.504	0.486	0.504
immune30signature-Eosinophils	0.472	0.500	0.500	0.500	0.500	0.500	0.500	0.500	0.500
immune30signature-Mast Cells	0.603	0.656	0.626	0.547	0.721	0.459	0.520	0.512	0.668
immune30signature-Dendritic Cells	0.607	0.528	0.532	0.496	0.517	0.414	0.519	0.490	0.519
immune30signature-Macrophages	0.561	0.594	0.640	0.570	0.670	0.574	0.514	0.595	0.634

Similarly, we considered the full 160 immune signature using same modeling pipeline. The AUC values are summarized in Figure S3-11, from which a large number of signatures can be predicted by tissue feature accurately.

Table S3-11. AUC of LASSO models to classify 160 immune signatures. Cases that AUC∈[0.6,0.7), AUC∈[0.7,0.75), and AUC⩾0.75 are marked with blue, orange, and pink, respectively.

	COAD	STAD	LUAD	LUSC	BRCA	PAAD	UCEC	OV	PAN-CAN
160signature-Angiogenesis	0.799	0.784	0.609	0.602	0.735	0.606	0.604	0.494	0.807
160signature-APM1	0.782	0.618	0.706	0.653	0.736	0.395	0.618	0.650	0.689
160signature-APM2	0.719	0.686	0.662	0.654	0.746	0.450	0.588	0.512	0.745
160signature-ICS5_score	0.683	0.700	0.726	0.710	0.769	0.537	0.681	0.537	0.758
160signature-LIexpression_score	0.682	0.717	0.751	0.740	0.762	0.524	0.666	0.634	0.770
160signature-Chemokine12_score	0.549	0.615	0.713	0.681	0.782	0.522	0.667	0.500	0.751
160signature-NHI_5gene_score	0.649	0.649	0.706	0.674	0.765	0.514	0.621	0.526	0.680
160signature-CD68	0.546	0.562	0.601	0.604	0.649	0.494	0.631	0.728	0.683
160signature-CD8A	0.659	0.672	0.717	0.710	0.766	0.460	0.677	0.510	0.738
160signature-PD1_data	0.677	0.677	0.763	0.705	0.751	0.588	0.681	0.661	0.747
160signature-PDL1_data	0.649	0.584	0.657	0.553	0.679	0.526	0.607	0.567	0.717
160signature-PD1_PDL1_score	0.704	0.651	0.735	0.657	0.778	0.502	0.663	0.650	0.758
160signature-CTLA4_data	0.638	0.651	0.716	0.678	0.794	0.572	0.683	0.476	0.752
160signature-Bcell_mg_IGJ	0.649	0.623	0.584	0.597	0.701	0.458	0.639	0.468	0.725
160signature-Bcell_receptors_score	0.645	0.700	0.738	0.705	0.768	0.586	0.661	0.464	0.751
160signature-STAT1_score	0.659	0.694	0.710	0.682	0.752	0.592	0.637	0.541	0.723
160signature-CSF1_response	0.607	0.723	0.694	0.656	0.730	0.601	0.629	0.621	0.746
160signature-TcClassII_score	0.700	0.730	0.695	0.679	0.767	0.448	0.628	0.561	0.737
160signature-IL12_score_21050467	0.685	0.693	0.689	0.661	0.791	0.541	0.670	0.642	0.764
160signature-IL4_score_21050467	0.571	0.695	0.651	0.670	0.696	0.433	0.593	0.628	0.713
160signature-IL2_score_21050467	0.619	0.657	0.717	0.633	0.753	0.615	0.650	0.477	0.732
160signature-IL13_score_21050467	0.587	0.567	0.664	0.612	0.693	0.531	0.512	0.687	0.652
160signature-IFNG_score_21050467	0.614	0.596	0.683	0.630	0.706	0.447	0.583	0.627	0.691
160signature-TGFB_score_21050467	0.672	0.716	0.667	0.692	0.733	0.483	0.567	0.478	0.758
160signature-TREM1_data	0.604	0.596	0.534	0.549	0.622	0.562	0.550	0.452	0.680
160signature-DAP12_data	0.569	0.658	0.612	0.651	0.630	0.451	0.601	0.673	0.689
160signature-Tcell_receptors_score	0.719	0.668	0.751	0.703	0.768	0.483	0.711	0.738	0.757
160signature-IL8_21978456	0.619	0.645	0.544	0.471	0.660	0.439	0.593	0.634	0.764
160signature-IFN_21978456	0.554	0.478	0.568	0.537	0.641	0.465	0.516	0.444	0.601
160signature-MHC1_21978456	0.579	0.577	0.604	0.635	0.671	0.436	0.539	0.616	0.646
160signature-MHC2_21978456	0.654	0.666	0.618	0.660	0.737	0.471	0.595	0.512	0.702
160signature-Bcell_21978456	0.499	0.458	0.551	0.525	0.554	0.482	0.524	0.476	0.500
160signature-Tcell_21978456	0.672	0.703	0.708	0.672	0.748	0.534	0.660	0.651	0.757
160signature-CD103pos_mean_25446897	0.657	0.732	0.679	0.637	0.727	0.521	0.650	0.500	0.755
160signature-CD103neg_mean_25446897	0.639	0.658	0.637	0.569	0.636	0.473	0.597	0.567	0.706
160signature-IgG_19272155	0.673	0.665	0.686	0.701	0.754	0.511	0.655	0.389	0.769
160signature-Interferon_19272155	0.558	0.512	0.604	0.536	0.646	0.476	0.528	0.444	0.603
160signature-LCK_19272155	0.651	0.704	0.704	0.692	0.756	0.508	0.685	0.660	0.763
160signature-MHC.I_19272155	0.584	0.509	0.623	0.659	0.672	0.421	0.608	0.527	0.646
160signature-MHC.II_19272155	0.633	0.651	0.677	0.632	0.731	0.552	0.620	0.512	0.725
160signature-STAT1_19272155	0.634	0.658	0.737	0.689	0.780	0.468	0.613	0.523	0.707
160signature-Troester_WoundSig_19887484	0.607	0.752	0.664	0.652	0.743	0.507	0.574	0.586	0.746
160signature-MDACC.FNA.1_20805453	0.635	0.713	0.634	0.654	0.748	0.614	0.651	0.408	0.739
160signature-IGG_Cluster_21214954	0.622	0.660	0.713	0.726	0.779	0.480	0.676	0.459	0.775
160signature-Minterferon_Cluster_21214954	0.615	0.631	0.670	0.630	0.726	0.427	0.573	0.667	0.664
160signature-Immune_cell_Cluster_21214954	0.679	0.645	0.703	0.678	0.757	0.498	0.651	0.683	0.751
160signature-MCD3_CD8_21214954	0.618	0.805	0.645	0.605	0.756	0.513	0.529	0.583	0.796
160signature-Interferon_Cluster_21214954	0.594	0.531	0.539	0.561	0.664	0.478	0.536	0.474	0.617
160signature-B_cell_PCA_16704732	0.675	0.698	0.745	0.678	0.775	0.549	0.686	0.496	0.772
160signature-CD8_PCA_16704732	0.699	0.685	0.697	0.712	0.765	0.405	0.690	0.659	0.742
160signature-GRANS_PCA_16704732	0.602	0.668	0.576	0.592	0.704	0.538	0.612	0.590	0.769
160signature-LYMPHS_PCA_16704732	0.602	0.521	0.515	0.592	0.604	0.519	0.571	0.621	0.500
160signature-T_cell_PCA_16704732	0.711	0.655	0.737	0.683	0.790	0.531	0.677	0.492	0.763
160signature-TGFB_PCA_17349583	0.651	0.666	0.663	0.654	0.709	0.607	0.541	0.456	0.778
160signature-Rotterdam_ERneg_PCA_15721472	0.646	0.506	0.626	0.501	0.645	0.503	0.600	0.661	0.690
160signature-HER2_Immune_PCA_18006808	0.644	0.726	0.708	0.686	0.766	0.482	0.660	0.660	0.764
160signature-IR7_score	0.715	0.702	0.745	0.718	0.767	0.553	0.646	0.528	0.756
160signature-Buck14_score	0.547	0.494	0.596	0.520	0.633	0.594	0.615	0.381	0.652
160signature-TAMsurr_score	0.525	0.635	0.641	0.608	0.780	0.470	0.609	0.473	0.699
160signature-Immune_NSCLC_score	0.669	0.691	0.663	0.606	0.745	0.504	0.648	0.680	0.753
160signature-Module3_IFN_score	0.595	0.509	0.611	0.523	0.652	0.403	0.491	0.444	0.617
160signature-Module4_TcellBcell_score	0.674	0.712	0.766	0.702	0.785	0.478	0.694	0.422	0.776
160signature-Module5_TcellBcell_score	0.686	0.671	0.732	0.704	0.786	0.553	0.652	0.574	0.766
160signature-Module11_Prolif_score	0.613	0.750	0.739	0.629	0.788	0.460	0.620	0.434	0.776
160signature-GP11_Immune_IFN	0.623	0.490	0.555	0.566	0.642	0.454	0.548	0.447	0.612
160signature-GP2_ImmuneTcellBcell_score	0.655	0.724	0.684	0.666	0.753	0.444	0.625	0.484	0.762
160signature-CD8_CD68_ratio	0.599	0.651	0.685	0.612	0.621	0.599	0.486	0.692	0.642
160signature-TAMsurr_TcClassII_ratio	0.622	0.700	0.640	0.609	0.658	0.465	0.630	0.539	0.647
160signature-CHANG_CORE_SERUM_RESPONSE_UP	0.657	0.721	0.727	0.662	0.759	0.602	0.645	0.697	0.785
160signature-CSR_Activated_15701700	0.650	0.754	0.704	0.650	0.743	0.458	0.664	0.660	0.802
160signature-CD103pos_CD103neg_ratio_25446897	0.585	0.627	0.623	0.527	0.643	0.570	0.539	0.643	0.534
160signature-LYM	0.644	0.711	0.671	0.668	0.719	0.527	0.647	0.573	0.747
160signature-IFIT3	0.462	0.504	0.628	0.528	0.632	0.476	0.538	0.467	0.622
160signature-G_GIMAP4	0.627	0.726	0.672	0.650	0.719	0.529	0.642	0.760	0.742
160signature-G_HLA.DPA1	0.649	0.678	0.673	0.616	0.731	0.470	0.583	0.398	0.706
160signature-G_SLAMF6	0.645	0.680	0.734	0.746	0.773	0.516	0.670	0.619	0.773
160signature-G_LILRB4	0.621	0.667	0.652	0.622	0.702	0.473	0.609	0.558	0.707
160signature-G_SIGLEC9	0.605	0.693	0.614	0.610	0.665	0.492	0.536	0.667	0.698
160signature-G_CYTH4	0.634	0.692	0.703	0.676	0.729	0.526	0.646	0.594	0.747
160signature-G_CD3E	0.692	0.679	0.726	0.698	0.776	0.496	0.677	0.738	0.762

Table S3-11. *(Continue)*

	COAD	STAD	LUAD	LUSC	BRCA	PAAD	UCEC	OV	PAN-CAN
160signature-ICR_SCORE	0.669	0.710	0.715	0.707	0.791	0.427	0.681	0.617	0.762
160signature-ICR_INHIB_SCORE	0.641	0.659	0.716	0.700	0.797	0.485	0.644	0.548	0.765
160signature-ICR_ACT_SCORE	0.679	0.715	0.731	0.712	0.784	0.458	0.696	0.617	0.750
160signature-C7_Atom_1	0.834	0.633	0.569	0.489	0.632	0.443	0.636	0.692	0.729
160signature-C7_Atom_2	0.809	0.501	0.552	0.579	0.642	0.593	0.498	0.611	0.678
160signature-C7_Atom_3	0.819	0.587	0.603	0.616	0.604	0.491	0.613	0.567	0.722
160signature-C7_Atom_4	0.811	0.593	0.557	0.487	0.593	0.477	0.685	0.451	0.712
160signature-C7_Atom_5	0.833	0.705	0.674	0.653	0.761	0.444	0.599	0.374	0.803
160signature-C7_Atom_6	0.823	0.527	0.544	0.584	0.640	0.551	0.548	0.579	0.678
160signature-C7_Atom_7	0.831	0.533	0.605	0.573	0.680	0.572	0.570	0.597	0.708
160signature-C7_Atom_8	0.806	0.537	0.524	0.617	0.659	0.568	0.637	0.619	0.711
160signature-C7_Atom_9	0.819	0.541	0.692	0.495	0.525	0.509	0.698	0.483	0.758
160signature-C7_Atom_10	0.825	0.492	0.571	0.641	0.633	0.457	0.594	0.781	0.733
160signature-C7_Atom_11	0.785	0.689	0.656	0.623	0.685	0.646	0.598	0.446	0.690
160signature-C7_Atom_12	0.858	0.664	0.619	0.645	0.692	0.503	0.657	0.626	0.705
160signature-C7_Atom_13	0.798	0.633	0.582	0.510	0.630	0.499	0.610	0.581	0.708
160signature-C7_Atom_14	0.828	0.702	0.634	0.583	0.621	0.495	0.598	0.597	0.747
160signature-C7_Atom_15	0.801	0.589	0.559	0.594	0.767	0.514	0.652	0.419	0.688
160signature-C7_Atom_16	0.819	0.495	0.539	0.590	0.600	0.562	0.516	0.383	0.720
160signature-C7_Atom_17	0.830	0.604	0.555	0.560	0.629	0.404	0.588	0.441	0.709
160signature-C7_Atom_18	0.778	0.499	0.527	0.587	0.584	0.459	0.638	0.513	0.733
160signature-C7_Atom_19	0.800	0.598	0.610	0.623	0.675	0.599	0.624	0.528	0.662
160signature-C7_Atom_20	0.815	0.600	0.675	0.657	0.741	0.433	0.586	0.473	0.731
160signature-C7_Atom_21	0.791	0.500	0.538	0.566	0.640	0.497	0.701	0.633	0.740
160signature-C7_Atom_22	0.795	0.647	0.704	0.649	0.735	0.457	0.660	0.532	0.778
160signature-C7_Atom_23	0.838	0.656	0.631	0.501	0.666	0.566	0.571	0.544	0.726
160signature-C7_Atom_24	0.781	0.677	0.622	0.621	0.548	0.557	0.617	0.618	0.729
160signature-C7_Atom_25	0.786	0.656	0.538	0.576	0.605	0.524	0.663	0.500	0.647
160signature-C7_Atom_26	0.816	0.554	0.560	0.628	0.675	0.490	0.640	0.592	0.675
160signature-C7_Atom_27	0.814	0.677	0.568	0.577	0.646	0.621	0.652	0.530	0.716
160signature-C7_Atom_28	0.821	0.651	0.571	0.525	0.630	0.490	0.654	0.622	0.747
160signature-C7_Atom_29	0.800	0.735	0.650	0.682	0.710	0.579	0.626	0.544	0.787
160signature-C7_Atom_30	0.807	0.544	0.633	0.593	0.602	0.489	0.629	0.404	0.665
160signature-C7_Atom_31	0.775	0.625	0.575	0.561	0.672	0.549	0.603	0.559	0.521
160signature-C7_Atom_32	0.814	0.702	0.641	0.669	0.661	0.444	0.592	0.647	0.771
160signature-aDC	0.751	0.591	0.632	0.539	0.729	0.487	0.612	0.554	0.710
160signature-B cells	0.808	0.645	0.730	0.692	0.778	0.585	0.620	0.646	0.744
160signature-CD8 T cells	0.815	0.699	0.692	0.675	0.702	0.510	0.598	0.418	0.681
160signature-Cytotoxic cells	0.781	0.691	0.699	0.678	0.736	0.469	0.647	0.643	0.737
160signature-DC	0.803	0.672	0.617	0.537	0.708	0.553	0.619	0.551	0.719
160signature-Eosinophils	0.805	0.689	0.586	0.561	0.738	0.633	0.581	0.677	0.749
160signature-iDC	0.810	0.567	0.657	0.618	0.673	0.477	0.587	0.704	0.721
160signature-Lymph vessels	0.794	0.648	0.552	0.577	0.703	0.566	0.606	0.429	0.749
160signature-Macrophages	0.804	0.637	0.620	0.626	0.665	0.531	0.617	0.527	0.774
160signature-Mast cells	0.740	0.798	0.634	0.569	0.755	0.541	0.507	0.490	0.800
160signature-Neutrophils	0.779	0.544	0.618	0.538	0.625	0.516	0.610	0.652	0.732
160signature-NK CD56bright cells	0.626	0.600	0.516	0.551	0.610	0.556	0.535	0.474	0.500
160signature-NK CD56dim cells	0.556	0.539	0.684	0.664	0.733	0.462	0.590	0.461	0.630
160signature-NK cells	0.815	0.707	0.650	0.653	0.760	0.447	0.588	0.470	0.787
160signature-pDC	0.763	0.651	0.564	0.637	0.638	0.525	0.544	0.760	0.675
160signature-T cells	0.789	0.662	0.747	0.699	0.780	0.432	0.619	0.538	0.743
160signature-T helper cells	0.808	0.682	0.634	0.647	0.599	0.505	0.590	0.676	0.657
160signature-Tcm cells	0.819	0.692	0.652	0.569	0.587	0.504	0.543	0.353	0.754
160signature-Tem cells	0.793	0.674	0.541	0.457	0.673	0.478	0.584	0.466	0.740
160signature-Tfh cells	0.797	0.612	0.638	0.619	0.634	0.529	0.600	0.661	0.780
160signature-Tgd cells	0.791	0.699	0.593	0.504	0.605	0.587	0.587	0.541	0.687
160signature-Th1 cells	0.804	0.544	0.665	0.629	0.717	0.484	0.632	0.473	0.698
160signature-Th17 cells	0.812	0.561	0.624	0.597	0.621	0.522	0.564	0.503	0.681
160signature-Th2 cells	0.800	0.719	0.753	0.612	0.642	0.434	0.697	0.467	0.685
160signature-Treg cells	0.755	0.671	0.722	0.699	0.785	0.386	0.634	0.668	0.699
160signature-B.cells.naive	0.489	0.515	0.557	0.575	0.598	0.415	0.476	0.443	0.604
160signature-B.cells.memory	0.511	0.569	0.493	0.487	0.613	0.423	0.461	0.496	0.500
160signature-Plasma.cells	0.588	0.542	0.551	0.504	0.582	0.504	0.536	0.494	0.622
160signature-T.cells.CD8	0.574	0.637	0.643	0.641	0.637	0.530	0.624	0.687	0.635
160signature-T.cells.CD4.naive	0.539			0.529	0.500		0.500		0.500
160signature-T.cells.CD4.memory.resting	0.528	0.520	0.630	0.481	0.621	0.466	0.577	0.428	0.592
160signature-T.cells.CD4.memory.activated	0.516	0.704	0.569	0.656	0.634	0.500	0.589		0.713
160signature-T.cells.follicular.helper	0.589	0.569	0.584	0.593	0.625	0.386	0.593	0.676	0.638
160signature-T.cells.regulatory..Tregs.	0.655	0.530	0.492	0.597	0.632	0.462	0.599	0.672	0.500
160signature-T.cells.gamma.delta	0.500	0.500	0.542	0.500	0.500	0.500	0.500		0.500
160signature-NK.cells.resting	0.575	0.620	0.562	0.510	0.516	0.487	0.500	0.500	0.541
160signature-NK.cells.activated	0.509	0.501	0.480	0.543	0.590	0.476	0.496	0.494	0.500
160signature-Monocytes	0.537	0.563	0.511	0.461	0.510	0.465	0.551	0.440	0.500
160signature-Macrophages.M0	0.588	0.699	0.675	0.650	0.614	0.481	0.471	0.473	0.621
160signature-Macrophages.M1	0.614	0.561	0.674	0.639	0.718	0.513	0.653	0.584	0.625
160signature-Macrophages.M2	0.490	0.597	0.614	0.639	0.684	0.555	0.511	0.638	0.654
160signature-Dendritic.cells.resting	0.524	0.614	0.638	0.523	0.558	0.479	0.470	0.500	0.600
160signature-Dendritic.cells.activated	0.500	0.506	0.605	0.538	0.526	0.386	0.596	0.467	0.500
160signature-Mast.cells.resting	0.500	0.728	0.626	0.504	0.715	0.455	0.601	0.509	0.730
160signature-Mast.cells.activated	0.639	0.695	0.516	0.558	0.500	0.500	0.545	0.587	0.690

REFERENCES

1. Litjens, G. *et al.* 1399 H&E-stained sentinel lymph node sections of breast cancer patients: the CAMELYON dataset. *GigaScience* **7**, giy065 (2018).

2. Ronneberger, O., Fischer, P. & Brox, T. U-Net: Convolutional networks for biomedical image segmentation. in *International Conference on Medical image computing and computer-assisted intervention* 234–241 (Springer, 2015).

3. Simonyan, K. & Zisserman, A. Very Deep Convolutional Networks for Large-Scale Image Recognition. *arXiv:1409.1556 [cs]* (2015).

4. Hou, Q., Zhou, D. & Feng, J. Coordinate Attention for Efficient Mobile Network Design. in *2021 IEEE/CVF Conference on Computer Vision and Pattern Recognition (CVPR)* 13708–13717 (IEEE, 2021). doi:10.1109/CVPR46437.2021.01350.

5. Tellez, D. *et al.* Quantifying the effects of data augmentation and stain color normalization in convolutional neural networks for computational pathology. *Medical Image Analysis* **58**, 101544 (2019).

6. Mormont, R., Geurts, P. & Maree, R. Comparison of Deep Transfer Learning Strategies for Digital Pathology. in *2018 IEEE/CVF Conference on Computer Vision and Pattern Recognition Workshops (CVPRW)* 2343–234309 (IEEE, 2018). doi:10.1109/CVPRW.2018.00303.

7. Kingma, D. P. & Ba, J. Adam: A method for stochastic optimization. *arXiv:1412.6980v9 [cs.LG]* (2014).

8. Beck, A. H. *et al.* Systematic Analysis of Breast Cancer Morphology Uncovers Stromal Features Associated with Survival. *Science Translational Medicine* **3**, 108ra113-108ra113 (2011).

9. Saltz, J. *et al.* Spatial organization and molecular correlation of tumor-infiltrating lymphocytes using deep learning on pathology images. *Cell reports* **23**, 181–193 (2018).

10. Zhao, K. *et al.* Artificial intelligence quantified tumour-stroma ratio is an independent predictor for overall survival in resectable colorectal cancer. *EBioMedicine* **61**, 103054 (2020).

11. Jiao, Y., Li, J., Qian, C. & Fei, S. Deep learning-based tumor microenvironment analysis in colon adenocarcinoma histopathological whole-slide images. *Computer Methods and Programs in Biomedicine* **204**, 106047 (2021).

12. Zhu, J.-Y., Park, T., Isola, P. & Efros, A. A. Unpaired image-to-image translation using cycle-consistent adversarial networks. *arXiv:1703.10593 [cs]* (2020).

13. Long, J., Shelhamer, E. & Darrell, T. Fully convolutional networks for semantic segmentation. in *Proceedings of the IEEE conference on computer vision and pattern recognition* 3431–3440 (2015).

14. Li, Z. *et al.* Deep Learning Methods for Lung Cancer Segmentation in Whole-slide Histopathology Images - the ACDC@LungHP Challenge 2019. *IEEE J. Biomed. Health Inform.* **25**, 429–440 (2020).

15. Wang, S. *et al.* Comprehensive analysis of lung cancer pathology images to discover tumor shape and boundary features that predict survival outcome. *Sci Rep* **8**, 10393 (2018).

16. Diao, J. A. *et al.* Human-interpretable image features derived from densely mapped cancer pathology slides predict diverse molecular phenotypes. *Nat Commun* **12**, 1613 (2021).

17. McInnes, L., Healy, J. & Melville, J. UMAP: Uniform Manifold Approximation and Projection for Dimension Reduction. *arXiv:1802.03426 [cs, stat]* (2020).

18. Liu, J. *et al.* An Integrated TCGA Pan-Cancer Clinical Data Resource to Drive High-Quality Survival Outcome Analytics. *Cell* **173**, 400-416.e11 (2018).

19. Thorsson, V. *et al.* The Immune Landscape of Cancer. *Immunity* **48**, 812-830.e14 (2018).